

INFORMATION TO USERS

This manuscript has been reproduced from the microfilm master. UMI films the text directly from the original or copy submitted. Thus, some thesis and dissertation copies are in typewriter face, while others may be from any type of computer printer.

The quality of this reproduction is dependent upon the quality of the copy submitted. Broken or indistinct print, colored or poor quality illustrations and photographs, print bleedthrough, substandard margins, and improper alignment can adversely affect reproduction.

In the unlikely event that the author did not send UMI a complete manuscript and there are missing pages, these will be noted. Also, if unauthorized copyright material had to be removed, a note will indicate the deletion.

Oversize materials (e.g., maps, drawings, charts) are reproduced by sectioning the original, beginning at the upper left-hand corner and continuing from left to right in equal sections with small overlaps. Each original is also photographed in one exposure and is included in reduced form at the back of the book.

Photographs included in the original manuscript have been reproduced xerographically in this copy. Higher quality 6" x 9" black and white photographic prints are available for any photographs or illustrations appearing in this copy for an additional charge. Contact UMI directly to order.

UMI

A Bell & Howell Information Company
300 North Zeeb Road, Ann Arbor, MI 48106-1346 USA
313/761-4700 800/521-0600

**Low temperature epitaxial silicon growth
using electron cyclotron resonance plasma deposition**

by

Scott Jeffrey DeBoer

**A Dissertation Submitted to the
Graduate Faculty in Partial Fulfillment of the
Requirements for the Degree of
DOCTOR OF PHILOSOPHY**

**Department: Electrical Engineering and Computer Engineering
Major: Electrical Engineering (Microelectronics)**

Approved:

Signature was redacted for privacy.

In Charge of Major Work

Signature was redacted for privacy.

For the Major Department

Signature was redacted for privacy.

For the Graduate College

**Iowa State University
Ames, Iowa**

1995

UMI Number: 9531731

UMI Microform 9531731
Copyright 1995, by UMI Company. All rights reserved.

**This microform edition is protected against unauthorized
copying under Title 17, United States Code.**

UMI
300 North Zeeb Road
Ann Arbor, MI 48103

**To my wife, Jennifer DeBoer
and my parents,
George and Beverly DeBoer**

TABLE OF CONTENTS

ABSTRACT	v
I. INTRODUCTION	1
1.1 Fundamentals of Epitaxial Silicon Growth	1
1.2 Previous Research	3
1.3 Project Objectives	9
II. SYSTEM DESIGN	11
2.1 Fundamentals of the ECR Process	11
2.2 Gas System Design	14
2.3 Deposition Chamber Design	17
III. SYSTEM CHARACTERIZATION	23
3.1 Magnetic Field and Three Stub Tuner Optimization	23
3.2 Plasma Characterization	25
3.3 Wafer Temperature Measurements	42
IV. MATERIAL CHARACTERIZATION TECHNIQUES	44
4.1 UV Reflectance	44
4.2 Raman Spectroscopy	45
4.3 Spreading Resistance Profiling	48
4.4 Film Thickness	49
4.5 Four-Point Probe	49
4.6 Van der Pauw	50

4.7	Hall Mobility	51
4.8	Electron Microscopy	52
V.	WAFER CLEANING PROCEDURE	55
5.1	Wet Cleaning Process	55
5.2	Hydrogen Plasma Cleaning	56
VI.	EPITAXIAL SILICON GROWTH AND CHARACTERIZATION	60
6.1	Growth Model	60
6.2	Microwave Power Effects	62
6.3	Growth Pressure Effects	66
6.4	Substrate Bias Effects	69
6.5	Growth Temperature Effects	75
6.6	Effect of the $H_2:SiH_4$ Ratio	86
6.7	Growth of Doped Films	89
6.8	Helium Dilution Effects	92
VII.	CONCLUSIONS	95
	REFERENCES	99
	ACKNOWLEDGMENTS	101
	APPENDIX A. ELECTRON MOTION IN A STATIC MAGNETIC FIELD	102
	APPENDIX B. MAGNET DESIGN	105
	APPENDIX C. STANDARD OPERATING PROCEDURE	108
	APPENDIX D. PAPER ACCEPTED FOR PUBLICATION IN APPLIED PHYSICS LETTERS	111

ABSTRACT

The development of a process for the low temperature ($< 600^{\circ}\text{C}$) growth of epitaxial silicon is an important technological issue. Conventional growth processes involve temperatures in excess of 1000°C . At these temperatures autodoping and impurity redistribution limit the feature size achievable in VLSI fabrication. As the typical feature sizes move into the submicron region, new processes for epitaxial silicon deposition will be needed. Another application for a low temperature growth process is the fabrication of solar cells on inexpensive metallurgical grade silicon wafers. Impurity diffusion from the wafer during conventional epitaxial silicon growth limits the quality of the solar cells if expensive high purity wafers are not used. We have used electron cyclotron resonance (ECR) plasma deposition to grow high quality epitaxial silicon films on silicon wafers. This growth technique relies on the deposition of silicon from a highly energetic hydrogen and silane plasma. The presence of the hydrogen in the plasma provides reactive etching of the silicon surface during growth. This reduces the oxygen and carbon contamination in the film as well as increasing the number of available growth sites on the surface by displacing the adsorbed hydrogen. By optimizing the growth pressure, substrate temperature, microwave power, substrate bias and silane to hydrogen ratio we have developed a process which provides enhanced growth rates and good uniformity at temperatures ($425\text{-}575^{\circ}\text{C}$) significantly below those used in conventional processes. The structural and electrical properties of the films have been characterized using SEM, TEM, Raman spectroscopy, UV reflectance, spreading resistance profiles, Hall mobility measurements, and both four-point probe and van der Pauw resistivity measurements.

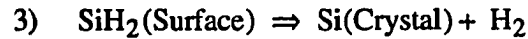
I. INTRODUCTION

1.1 Fundamentals of Epitaxial Silicon Growth

Epitaxy is defined as the ordered growth of one crystal on another crystal, such that the two crystals have the same orientation. When the two crystals are the same material, the process is referred to as homoepitaxy. The growth of silicon films on silicon substrates, referred to as epi silicon, is an extremely important technological use of homoepitaxy. Single crystal films with thicknesses of 0.1 to 20 μm can easily be deposited on single crystal silicon substrates [1]. The most commonly used process for the growth of epitaxial silicon is chemical vapor deposition (CVD). A wide variety of CVD processes exist. These processes differ from one another in terms of the growth temperature, pressure, the gases involved, and in whether or not an additional energy source assists in the deposition process. The two basic steps of a CVD process are the same regardless of the specific process parameters.

The first step is the removal of the native oxide which forms on bare silicon wafers. In conventional CVD reactors, this is done by heating the wafer to the temperature where the oxide desorbs from the surface ($>800^\circ\text{C}$) leaving the bare silicon exposed. Other techniques have been developed for oxide removal in low temperature growth processes. These techniques are described in the next section.

The second step is the transport of a silicon-containing gas (SiCl_4 , SiH_4 , Si_2H_6) to the surface of the wafer where chemical reactions involving the gas are induced. These reactions are induced either thermally or by a combination of thermal and some other energy source such as a plasma. An example of these chemical reactions is shown below for a CVD process using silane.



In the first reaction, energy is transferred to the silane molecule and it is separated into hydrogen gas and an SiH_2 molecule. This reaction can be the growth limiting step if the silane near the wafer becomes depleted, or the SiH_4 dissociation rate is low due to a lack of energy input. Actually, it is still unclear whether SiH_2 or SiH_3 dominates in the growth process [2]. It is likely that both species are involved, and the dominance of one or the other depends on the specific growth conditions. The second reaction involves the adsorption of the SiH_2 onto the wafer surface. This reaction limits the growth rate when the number of available surface sites is low. In the third reaction, the adsorbed SiH_2 molecule is incorporated into the lattice at a kink site. This step can limit the growth process when the surface diffusion rate is low.

A model for the three step process is shown in Figure 1.1. The adsorbed molecules diffuse along the surface until they reach an atomic surface step. The molecules then diffuse along the step to a kink site, where they are incorporated into the lattice.

An important consideration in the growth of epitaxial silicon is that as long as the surface diffusion rate (reaction 3) remains higher than the adsorption rate (reaction 2), little interaction among adsorbed molecules takes place before they are incorporated into the lattice. However, when the adsorption rate is much greater than the surface diffusion rate, the adsorbed molecules may interact with each other and form regions of three dimensional growth. This results in the roughening of the film surface and the films appear hazy [1].

Thermally induced CVD has been used by the semiconductor industry for epitaxial silicon wafer production for over 20 years. Typical industrial processes involve growth using SiCl_4 at

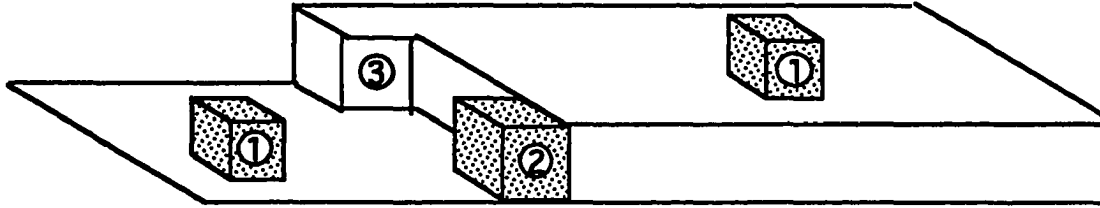


Figure 1.1: The epitaxial growth process is depicted by the boxes which represent silicon atoms on the wafer surface. The steps are; 1) adsorption at a surface site, 2) Diffusion along surface to an atomic step, 3) Diffusion along step and incorporation at a kink site.

substrate temperatures greater than 1150°C. Deposition of silicon can also be obtained by the pyrolytic decomposition of silane which can occur at temperatures as low as 600°C.

1.2 Previous Research

The low temperature growth of epitaxial silicon has several potential applications. As the feature sizes of devices are reduced to the sub-micrometer range, conventional high temperature CVD processes will not work due to impurity redistribution and auto doping. The diffusion length of dopants out of the substrate is on the order of a micron for standard high temperature CVD growth. This puts a lower limit on the device size, since the dimensions of the device must be greater than the dopant diffusion length.

A great deal of research has been done in the last ten years on developing a low temperature ($< 600^{\circ}\text{C}$) growth process for epitaxial silicon. Some of the first work was done by B. Meyerson at IBM. In 1986, Meyerson was able to grow high quality epitaxial silicon films between 750°C and 850°C using silane [3]. The depositions were done in a UHV/CVD system with a base pressure of 10^{-9} Torr. Meyerson found that the films which were deposited at temperatures below 750°C had a high density of crystalline defects. Spreading resistance profiles of the films grown at 800°C determined the active carrier levels to be 10^{14} cm^{-3} in undoped films.

In 1987, Meyerson verified that epitaxial silicon could be grown at temperatures as low as 550°C [4]. The 3000 \AA thick films grown in this work showed a wide range of boron doping levels ($5 \times 10^{14} - 1 \times 10^{20} \text{ cm}^{-3}$). Good quality p-n junctions were formed using ion implantation.

In later work, Meyerson identified hydrogen passivation of the silicon wafer surface as the key to low temperature epitaxy [5]. The hydrogen passivation was accomplished by dipping the wafers in a dilute HF solution just prior to growth. The HF treatment completely removes the oxide from the surface and leaves it terminated primarily by hydrogen. This hydrogen passivation of the wafer surface was found to result in bistable temperature conditions for epitaxial growth. This behavior can be understood from the desorption spectra for hydrogen from a silicon (100) wafer shown in Figure 1.2. Epitaxial growth is possible between 425°C and 650°C because the hydrogen desorption rate is low and there is an excess of silicon-containing molecules waiting to adsorb in the positions left by the desorbing hydrogen. In the temperature region between 650°C and 750°C , epitaxial growth fails due to the rapid desorption of hydrogen. This rapid desorption results in a large amount of the silicon being exposed to contamination before epitaxial growth begins. At temperatures above 750°C , the desorption of oxygen occurs, so the surface remains clean despite the lack of hydrogen termination. When the temperature is reduced below 425°C , the growth rate becomes too low

to be practical. The extremely slow desorption of hydrogen results in there being very few available sites for silicon adsorption.

Work on low temperature epitaxy was also done by R. Reif, J. Comfort and T. Donahue starting in 1984. In 1984, Donahue and Reif did some of the first work on low temperature crystalline silicon growth [6]. They were able to grow silicon epi-layers between 650°C and 850°C. This research identified the problem of excessive oxygen incorporation in the films as the growth temperature is decreased. The oxygen level in the epitaxial silicon films increases from $\sim 10^{18} \text{ cm}^{-3}$ at 800°C to $\sim 10^{20} \text{ cm}^{-3}$ at 700°C. This high oxygen content causes the undoped films to be n-type with resistivities as low as 0.01 W-cm ($> 10^{18} \text{ cm}^{-3}$ free carriers). This is due to the 0.16 eV donor level arising from the oxygen [7]. The lowest free carrier concentration achieved for epitaxial films grown on boron doped wafers was $\sim 10^{16} \text{ cm}^{-3}$.

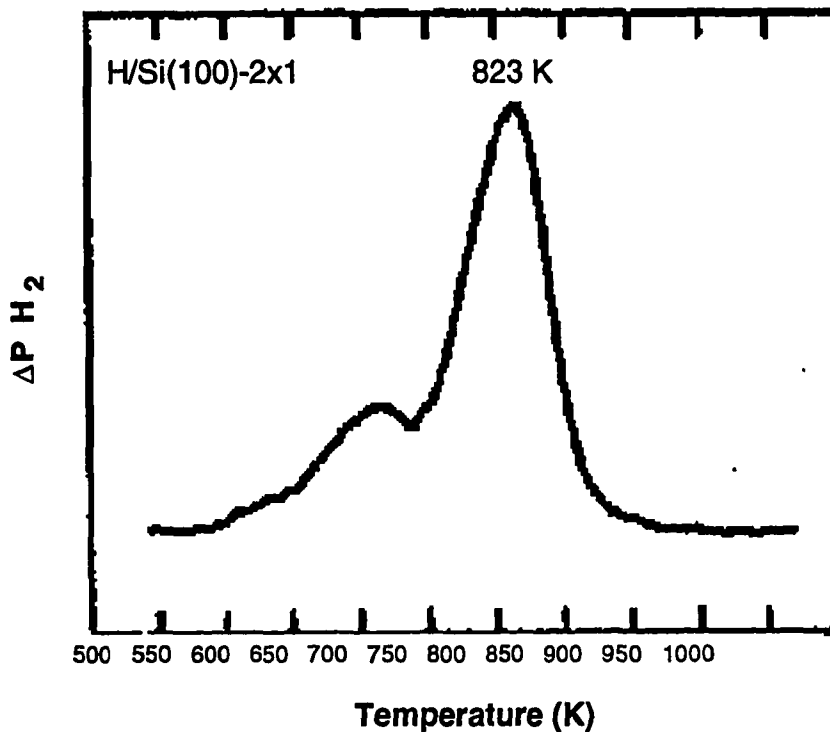


Figure 1.2: Temperature programmed desorption spectra for hydrogen evolution from the silicon surface [5].

In 1988, Reif and Comfort studied both low temperature CVD and low temperature plasma enhanced chemical vapor deposition (PECVD) in a high vacuum system with a base pressure of 10^{-7} Torr [8,9]. In the PECVD process, an RF power (0-20W) is used to generate a plasma. The plasma enhanced deposition operates in parallel with the thermal deposition process. Epitaxial films were deposited at temperatures from 600-800°C. They determined that there was no fundamental temperature limit to epitaxial growth, at least down to 550°C. However, at temperatures below 600°C, the growth rates for CVD are prohibitively low (< 30 Å/min). This group also relates the low growth rate to the lack of adsorption sites for silicon due to hydrogen surface coverage. They found that by using plasma enhanced chemical vapor deposition (PECVD) the growth rate could be increased. They were able to get a growth rate of approximately 170 Å/min at 600°C. A correlation was found between increased growth rate and good film quality. For a constant level of background contamination (carbon and oxygen) in the growth chamber, the contamination which is incorporated into the film will be reduced as the growth rate is increased. No mention was made of the quality of the films deposited at temperatures below 750°C.

A study done by M. Liehr in 1990 provided more evidence that the fundamental limitation for epitaxial growth at temperatures below 600°C is the hydrogen desorption from the wafer surface [10]. In this work the hydrogen coverage of the wafer surface during growth was determined. The result shown in Figure 1.3 indicates that the surface hydrogen termination remains even during growth at low temperatures. The CVD growth rate for epitaxial silicon from SiH_4 is shown in Figure 1.4.

Another promising growth process for epitaxial silicon is electron cyclotron resonance chemical vapor deposition (ECR-CVD). This process uses a reactive plasma to deposit high quality silicon films. The specifics of this growth process will be discussed in the next chapter. The growth of amorphous [11] and polycrystalline [12] films has been previously reported. The growth of epitaxial silicon in an ECR-CVD system was reported by D. Mui in

1991 [2] and by H. Tae in 1994 [13]. Both of the reactors used were UHV systems with base pressures of 10^{-9} Torr.

In the work done by Mui, good quality epitaxial films were grown at 460°C by using a He and SiH_4 plasma. The growth rate at 460°C was found to be less than $5 \text{ \AA}/\text{min}$, so the low base pressure was very important. The pressure during deposition was 5×10^{-4} Torr in this research. The undoped epi-Si layers grown in this work were found to be n-type with carrier concentrations less than $5 \times 10^{16} \text{ cm}^{-3}$.

H. Tae et al investigated the effects of substrate biasing on film quality. A silane and hydrogen plasma was used with growth pressures in the 10^{-4} to 10^{-3} Torr range. Their research indicated that good quality epitaxial films could be grown at 560°C only when a

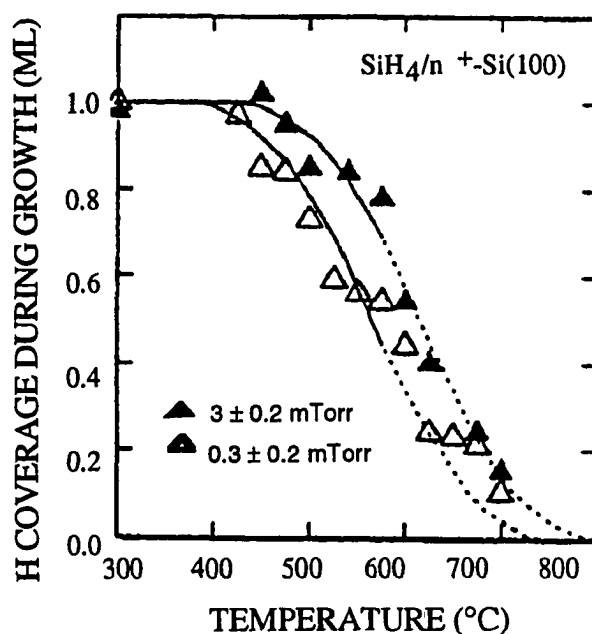


Figure 1.3: Hydrogen coverage of Si(100) surface during growth for two different growth pressures [2].

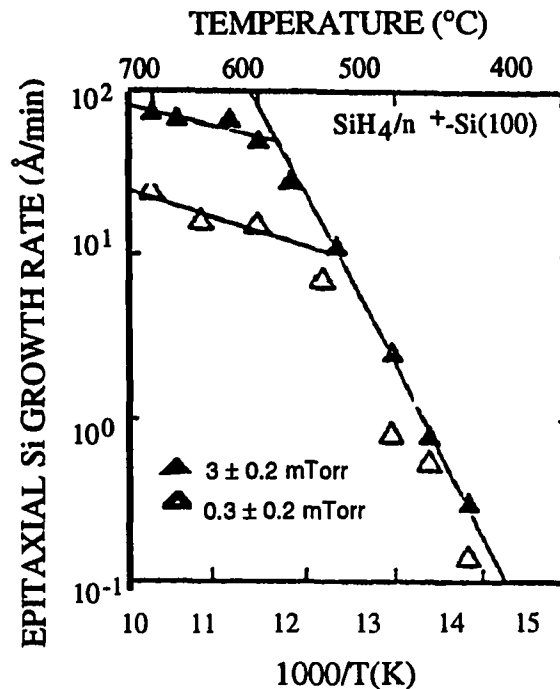


Figure 1.4: Growth rate for epitaxial silicon from SiH₄ at low temperatures [2].

positive bias of greater than 10V was applied to the substrate. This positive bias was used to reduce the energy of the ions from the plasma before they hit the wafer. Their work also showed that when negative biases of greater than 50V were applied, the resulting films were completely polycrystalline. The growth rate for the good films grown in this work was again less than 5 Å/min. No mention is made of the resistivity of the undoped films.

Overall, there are two main conclusions that can be drawn from the previous research done on low temperature silicon epitaxy ($T < 650^{\circ}\text{C}$):

- 1) The growth rates for the processes developed so far are extremely low. This is important for some applications, but it is not practical when thicker epi layers are needed as in the case of solar cell growth.

2) The dominant mechanism for growth at temperatures below 650°C is the desorption of hydrogen from the wafer surface. The hydrogen termination will prevent epitaxial silicon growth if a method is not devised to displace it.

1.3 Project Objectives

The goal of this research is to develop a process for the growth of high quality epitaxial silicon at temperatures below 550°C. Some of the potential applications for such a growth process were described at the beginning of this chapter. We believe that such a process may also be important for the growth of inexpensive epitaxial silicon solar cells on metallurgical-grade (MG) silicon substrates. This could significantly reduce the cost of silicon solar cells due to the price difference between MG silicon (~ \$1.50/kg) and high quality semiconductor-grade silicon (~ \$80.00/kg) [14].

The first step in accomplishing this goal is the choice of a suitable growth method. We have chosen to use a high vacuum ECR-CVD system. The ECR-CVD system offers several features which are compatible with low temperature growth. In an ECR-CVD system, the energy and density of the ions impinging on the substrate can be controlled. This can be used to increase the surface mobility of the adsorbed species which in turn will reduce the necessary growth temperature. The interaction between the energetic plasma species and the hydrogen terminated wafer surface also causes the removal of some of the hydrogen atoms. This results in larger growth rates at low temperatures due to the increased number of adsorption sites. The operation of the ECR-CVD system in a different pressure range (5-25 mTorr) also allows a much higher growth rate to be achieved than was seen in previous research.

There are five major components to this research: 1) System design and construction, 2) System characterization, 3) Identification of the necessary material characterization techniques, 4) Development of a suitable wafer cleaning procedure and 5) Silicon film growth and characterization. Each of these components will be described in the following chapters.

II. SYSTEM DESIGN

A high vacuum (HV) electron cyclotron resonance plasma deposition system was designed and constructed for this research. The two main components of the deposition system are the gas handling system and the deposition chamber. Each of these components was a major engineering project. The total construction time for the laboratory was almost exactly 1 year.

2.1 Fundamentals of the ECR Process

The first step in the design of an ECR plasma deposition system is an understanding of the plasma source. There are several different possible arrangements for ECR sources. Variations occur in system size and shape, method of microwave introduction, and the number, position, and type of the magnets [15]. The most commonly used arrangement is the Hitachi/NTT type ECR source shown in Figure 2.1. The plasma source is a stainless steel tube with two coils around it which are used to generate a uniform DC magnetic field. Microwaves are introduced through a quartz window on one end of the tube. The plasma is extracted from the other end of the tube.

In order to understand the plasma generation process, it is best to start with an overly simplified model. Free electrons in the plasma generation region spiral around the static magnetic field lines due to the Lorentz force. In Appendix A, it is shown that the frequency of the rotation (gyrotron frequency) is given by

$$\omega_o = \frac{qB_z}{m_e} \quad (2.1)$$

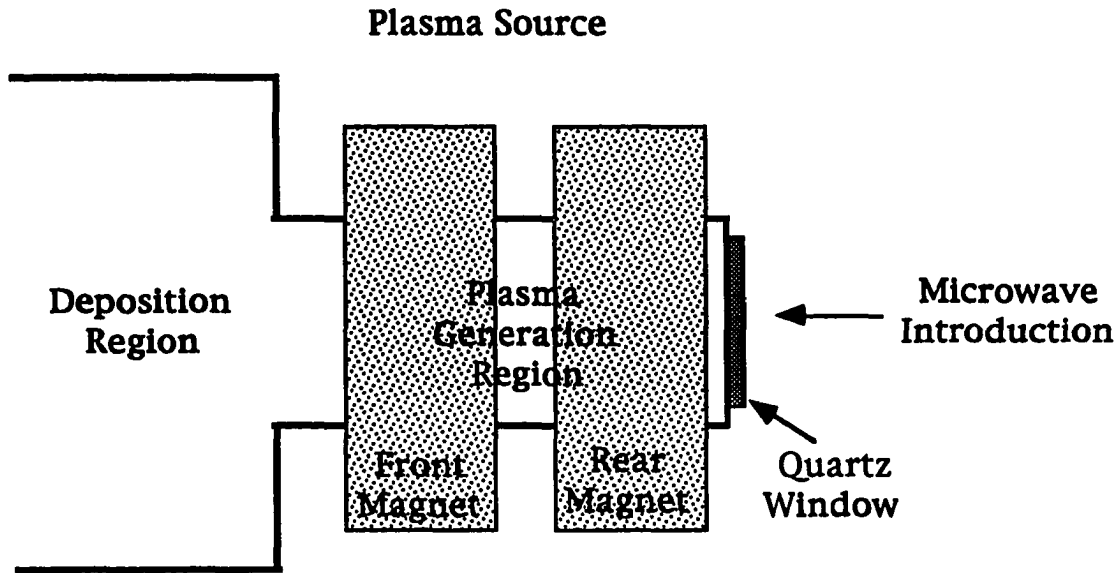


Figure 2.1: Typical arrangement for a Hitachi/NTT type ECR source.

and the radius of the spiral is given by

$$R = \left(\frac{m_e}{qB_z} \right) \sqrt{v_x^2 + v_y^2}. \quad (2.2)$$

Linearly polarized microwaves enter the region propagating along the axis of the static magnetic field. Linearly polarized plane waves may be equivalently expressed as two circularly polarized waves rotating in opposite directions. For example, the electric field of the linearly polarized microwaves, which can be expressed as

$$\mathbf{E} = E_0 \cos(\omega t) \mathbf{a}_y, \quad (2.3)$$

may also be written as

$$\mathbf{E} = \text{Re} \left[\frac{E_0}{2} (\mathbf{a}_y + j\mathbf{a}_x) e^{j\omega t} + \frac{E_0}{2} (\mathbf{a}_y - j\mathbf{a}_x) e^{j\omega t} \right] \quad (2.4)$$

where the first component in the bracket is a wave with right-hand circular polarization (RCP) and the second term is a wave with left-hand circular polarization (LCP).

When the gyrotron frequency and the frequency of the microwaves are the same, the electrons and the electric field vector of the RCP waves are rotating in phase with each other. This is the electron cyclotron resonance condition. The energy of the RCP microwaves goes into accelerating the electrons. The electrons then collide with neutral gas molecules, causing ionization and the formation of free radicals. Since the electrons and the LCP electric field vector are rotating in opposite directions, electron cyclotron resonance can not be the method of microwave power absorption for the LCP waves. Other possible energy loss mechanisms must be looked into for the LCP microwaves. There are many rather complex theories regarding the absorption of the LCP waves. The important result that comes out of the theories is that when the plasma density gets large enough, the LCP waves are almost completely absorbed. The point where this occurs is called the critical density, N_{cr} . When the density of the plasma exceeds N_{cr} , the microwaves are no longer able to propagate through the plasma (the amplitude decreases exponentially). By solving Maxwell's equations [16], the critical density is determined to be

$$N_{cr} = \frac{\omega^2 \epsilon_0 m_e}{q^2} \quad (2.5)$$

which results in a critical density of $7.5 \times 10^{10} \text{ cm}^{-3}$ for the 2.45 GHz used in this work.

2.2 Gas System Design

The design of the gas handling system was based on the NREL guidelines. These guidelines include the relevant regulations of the Fire Code, the Building Code, and additional safety regulations used by NREL [17]. The hazardous production materials (HPMs) that the system was designed for are hydrogen, methane, silane, disilane, 100 ppm phosphine, and 1% diborane. The design standards for the construction of the gas delivery system are shown in Table 2.1. The components of a gas line for an HPM gas are shown in Figure 2.2.

A safety interlock is built into the control system for the gases to provide automatic closure of all the pneumatic valves under certain conditions. The interlock is activated by sensors which monitor the exhaust ventilation, flow of the safety nitrogen, overpressure in the

Table 2.1: Gas system design standards.

- No sharing of HPM gas lines.
- Components compatible with gases used.
- Flow limiting orifices on all HPM gas cylinders.
- Excess flow valves installed on all HPM gas cylinders.
- Normally closed pneumatic valve installed on high pressure side.
- Purging assemblies installed on HPM gas lines.
- Check valve installed on purge gas side of the purging assembly.
- Manual packless valves are used for the purge assembly.
- Only compatible HPMs may have common purge assemblies.
(Compatible HPMs have identical classification under the codes).
- Purge gas cylinders are contained in the gas cabinet.
- Regulators are high purity, positive-seal stainless steel with tied diaphragm design.
- Gas delivery valves are NC air operated bellows valves.
- Tubing is 1/4" x .035" .316L stainless steel.
- Only VCR metal gasket face seal fittings are used. No compression fittings.
- Red panic button is present which stops all gas flow.
- Gas lines leak tested using both a helium leak detector and a hydrogen leak detector.

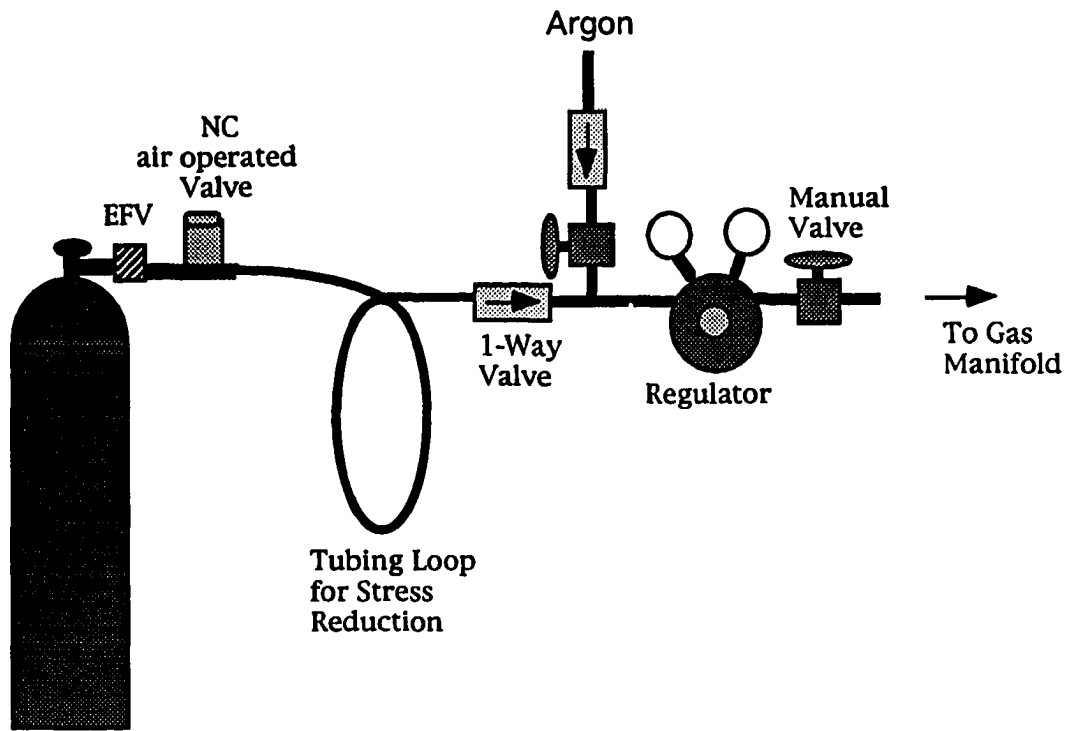


Figure 2.2: Components used in HPM gas lines.

chamber, emergency-off button, and the TELOS toxic gas detector. The TELOS system provides continuous toxic gas detection in the gas cabinets, the gas distribution manifold, and the area near the reactor.

There are three separate gas manifolds for the system. The manifolds are shown in Figure 2.3. The gas passes through a filter and then the flow rate is set by a Unit Instruments mass flow controller (MFC). After leaving the MFC, the gas enters whichever manifold is open. The plasma manifold runs to the plasma generation region. Only the plasma gases, H_2 and He, pass through this line. Separate manifolds are provided for intrinsic and dopant gases in order to eliminate cross-contamination. The electrical control system for the manifolds is wired so that these two manifolds can never both be open at the same time. When

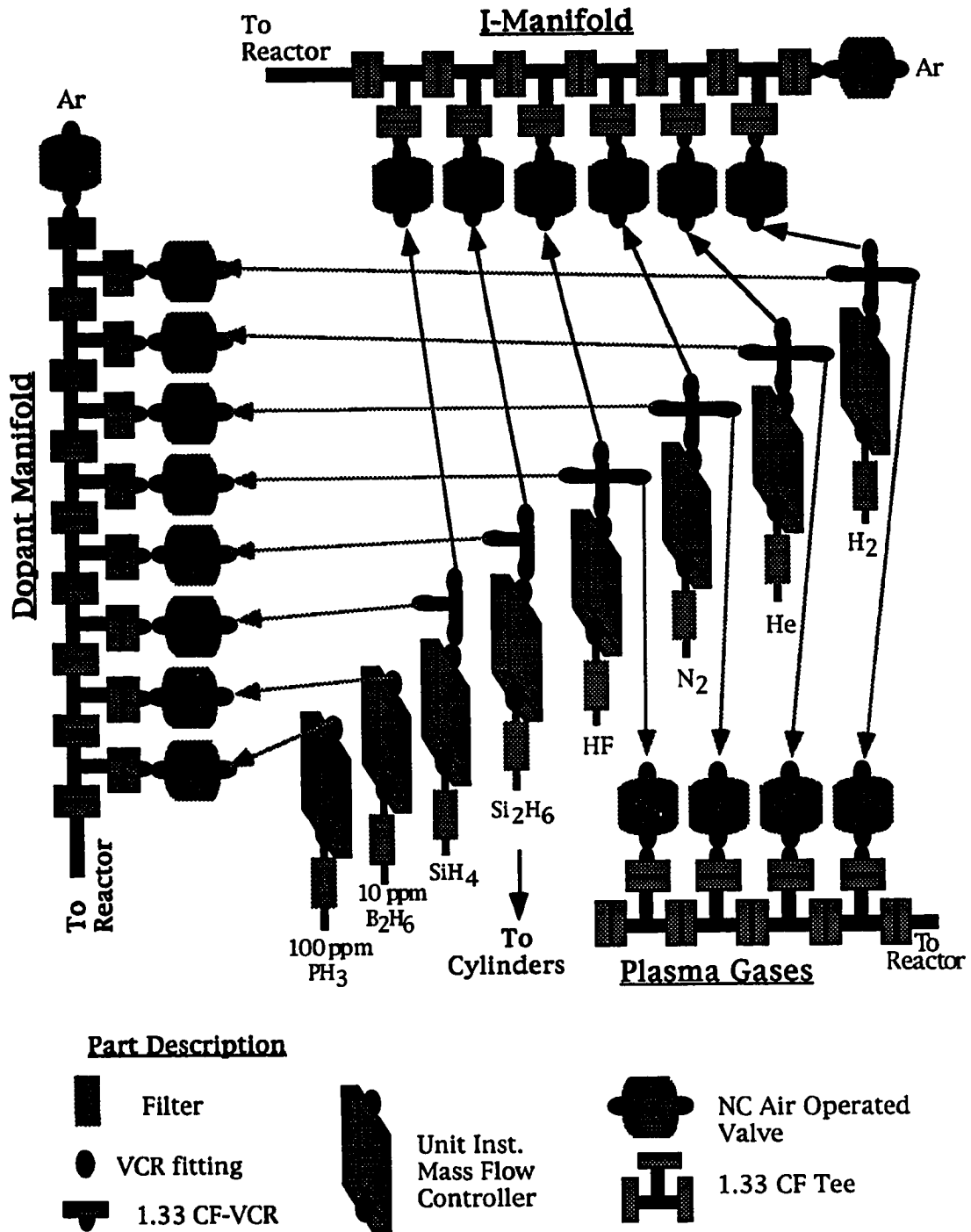


Figure 2.3: Diagram of the gas manifolds.

doped/intrinsic films are grown, the dopant/intrinsic line is used to transfer the process gases to the deposition chamber. Both the intrinsic and the dopant manifolds enter the chamber right behind the substrate heater.

2.3 Deposition Chamber Design

A diagram of the deposition system is shown in Figure 2.4. The system was designed and constructed between the Fall of 1992 and the Fall of 1993. Unlike most of the ultra-high vacuum ECR systems previously used for epitaxial silicon growth [2,13], this apparatus is a standard high vacuum system which is much more representative of a production environment. A microwave generator with a frequency of 2.45 GHz serves as the power source. This is the frequency used in most commercial ECR deposition systems. The microwaves from the generator travel through a shielded coaxial cable to a three stub tuner on WR340 waveguide. The microwaves then enter the plasma chamber through a quartz window which is pressed against a silicon o-ring to provide the vacuum seal. The tuner allows impedance matching between the waveguide, the quartz window, and the plasma. The plasma gases, H₂ and He, are introduced uniformly around the quartz window by a gas distribution ring.

The magnetic field needed for ECR resonance is determined by Equation 2.6 to be

$$B = \frac{m_e \omega_0}{q} = 875 \text{ Gauss} \quad (2.6)$$

for 2.45 GHz microwaves. The design and construction of the magnets is described in Appendix B. Two DC power supplies (100V, 20A) are used to power the magnets.

The main chamber consists of a 6-way cross on top of a 4-way cross. All of the flanges

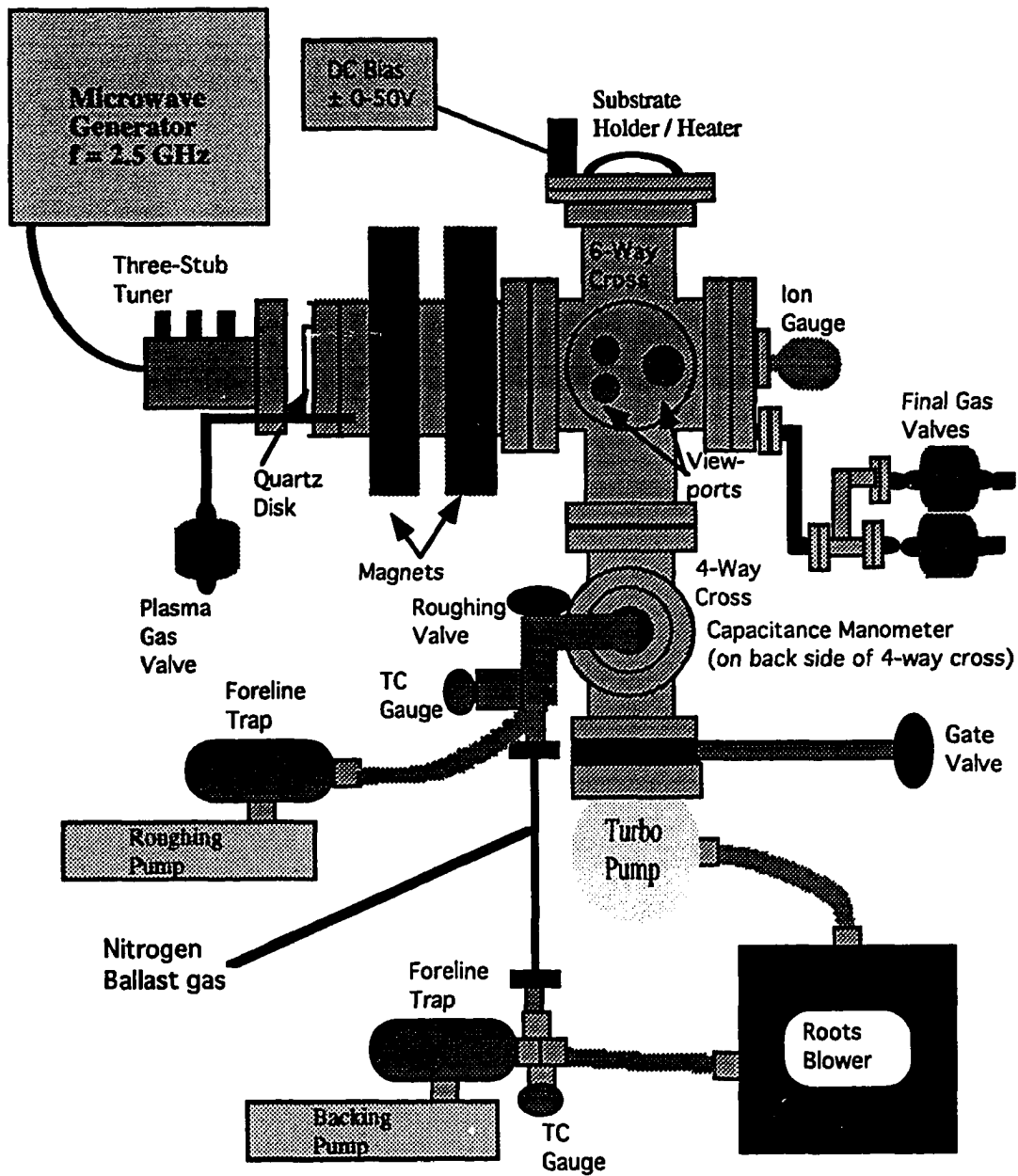


Figure 2.4: Diagram of the ECR-CVD system.

are of the knife-edge copper-sealed variety. The pump arrangement shown in Figure 2.4, allows a base pressure of less than 10^{-7} Torr to be achieved in the chamber. Two rotary vane pumps, a Roots blower, and a turbo pump are used to achieve this pressure. The system is pumped down from atmospheric pressure by first opening the roughing valve and allowing the roughing pump to lower the chamber pressure to about 500 mTorr. Nitrogen ballast gas and a foreline trap are used to avoid backstreaming of oil from the roughing pump to the chamber. Once the chamber pressure is below 500 mTorr, the roughing valve is closed and the gate valve over the turbo pump is opened. The system then pumps down to its base pressure. Under typical operating conditions, the pressure will be at 4×10^{-7} Torr in less than 10 minutes.

The Roots pump on the outlet of the turbo is used to increase the flow rate. A rotary vane pump backs the Roots blower. This is required to keep the Roots blower from overheating. The exhaust from the pumps is then diluted to a safe level with nitrogen and run into the duct. The deposition chamber is pumped continuously when not in use to avoid adsorption of water vapor on the chamber walls.

A large flow of nitrogen is left on during the time the system is open for sample loading or unloading (typically five seconds). As soon as the sample is loaded, the nitrogen is turned off and the roughing valve is opened. Venting of the chamber for sample loading is done with filtered dry nitrogen. A blank ASA flange is used to seal off the system when the sample holder is not loaded. Nitrogen is only weakly bonded to stainless steel, so it desorbs quickly as the system is pumped back down.

There are three different types of pressure gauges used on the system. Thermocouple (TC) gauges are used to monitor the pressure at the inlets of the rotary vane pumps. TC gauges operate in the range (10 mT to 2000 mT) where the thermal conductivity of a gas is proportional to the gas pressure. In a TC gauge, a constant current is passed through a hot filament and the filament temperature is monitored by a thermocouple as the gas pressure changes.

An ion gauge is used to measure the base pressure in the system. Ion gauges are reliable in the 10^{-2} to 10^{-11} Torr range. They have three components (shown in Figure 2.5); the filament, a positively biased grid-anode, and an ion collector at ground potential. During operation, electrons are emitted from the heated filament and accelerated towards the grid. Some of the accelerated electrons will ionize gas molecules before being collected at the grid. The positively charged ions will then travel to the collector. The operation of ion gauges is based on the fact that the ion current measured at the collector is proportional to the pressure.

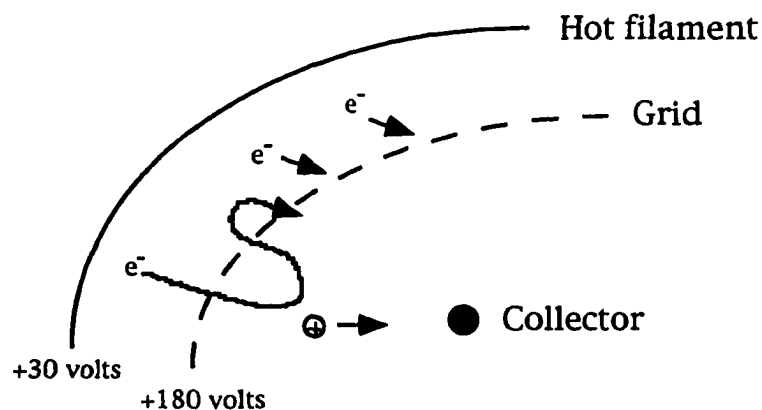


Figure 2.5: Ion gauge operation.

The third type of pressure gauge used on the system is a capacitance manometer. This gauge operates in the 1 mT to 1 Torr range and is used to monitor the pressure during the film growth process. This type of pressure gauge is basically a variable parallel plate capacitor. One of the plates is an elastic metal diaphragm which is exposed to the vacuum chamber. As the chamber pressure varies, the diaphragm is deflected resulting in a change in the capacitance. This dependence of capacitance on pressure is the operating principle for this type of pressure gauge.

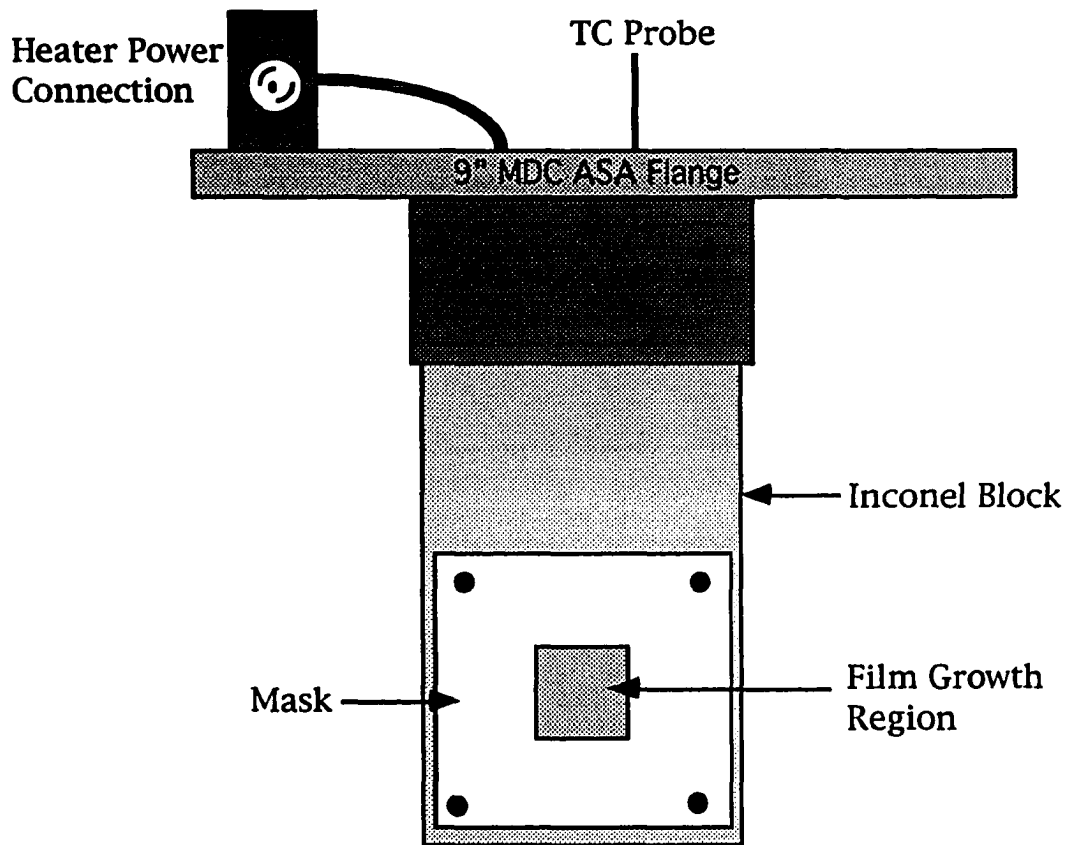


Figure 2.6: Substrate heater used in ECR-CVD system.

In order to allow high temperature operation, the substrate holder was fabricated from inconel. Inconel is a nickel alloy which is stable at temperatures above 1000°C. The substrate heater is shown in Figure 2.6. It is heated by nine high temperature cartridge heaters, which are outside the vacuum chamber to avoid outgassing. The operational temperature range for the sample holder is 0-900°C. The temperature is sensed with a type K thermocouple and controlled with a Watlow temperature controller. The sample holder is welded onto an ASA flange as shown. When the holder is lowered into the chamber, the ASA flange seals down on a silicon o-ring. This o-ring also provides electrical isolation between the sample holder and

the chamber. A DC bias of up to $\pm 50V$ can be applied to the substrate holder with respect to the rest of the chamber. The sample holder surface is polished to a finish of 32 micro-inches in order to get the best possible thermal contact with the substrates. A high purity graphite mask is tightened down evenly to hold the substrate in place against the heater.

III. SYSTEM CHARACTERIZATION

After the construction of the system was completed, work began on characterizing the operating conditions of the system. The ECR system inherently contains a large number of variables. The substrate temperature, microwave power, chamber pressure, magnetic field, gas flows, substrate bias, and three stub tuner can all be varied. This is an advantage in that it gives the system great flexibility. However, it is important to eliminate some of the variables in order to gain an understanding of the system and to ensure reproducibility.

3.1 Magnetic Field and Three Stub Tuner Optimization

It was determined that the most difficult aspect of the system to control was the plasma. The plasma parameters are affected by the magnetic field, the three stub tuner, the pressure, the substrate bias and the microwave power. Small variations in these system variables, especially the magnetic field and the tuner, drastically alter the plasma properties. Only one arrangement of magnetic field profile and three stub tuner adjustment was found to be suitable.

In this arrangement, the reflected microwave power remains less than one percent of the incident power independently of the system pressure and incident power level. This is an important result in that it eliminates the magnetic field and three stub tuner settings from the list of variables, and it increases the reproducibility of plasma conditions. The latter follows from the extreme sensitivity of the plasma parameters on these two variables. By never having to alter the settings on the magnet power supplies or the tuner dials, we ensure reproducible plasma conditions. The position of the magnets and the magnetic field profile used are shown in Figures 3.1 and 3.2 respectively.

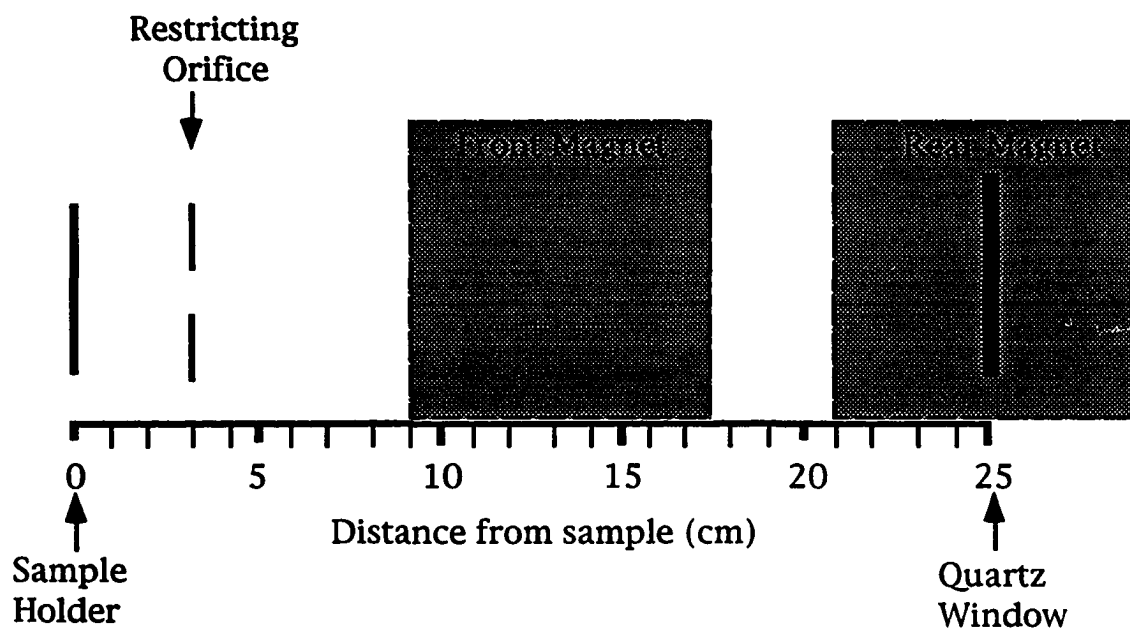


Figure 3.1: Axial position of the system elements.

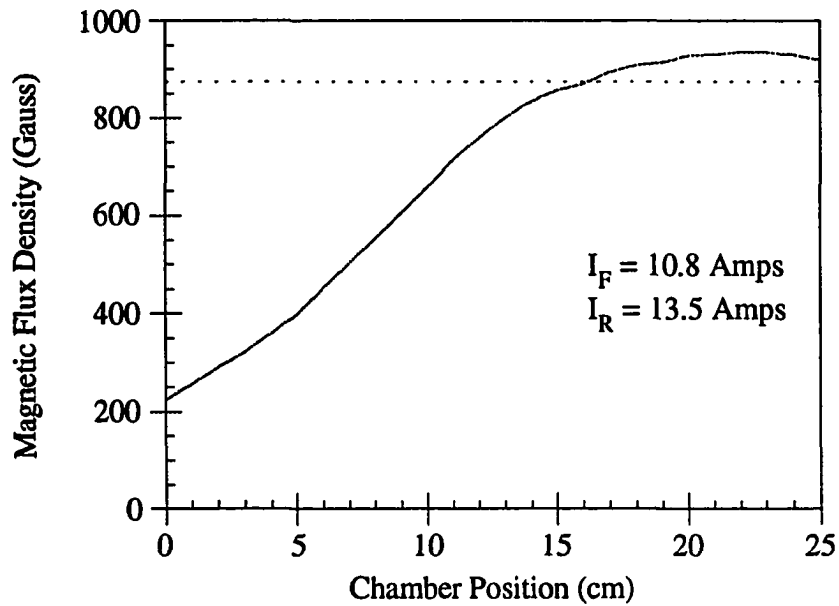


Figure 3.2: Magnetic field profile present in the system during growth. The dotted line indicates the resonance condition.

3.2 Plasma Characterization

3.2.1 Langmuir Probe Theory

An important step in characterization of the ECR system is the understanding of the plasma parameters and the dependence of these parameters on the other system variables (microwave power and chamber pressure).

A plasma is defined as [18] "A conglomeration of positively and negatively charged particles which is on the average neutral due to the equal number density of the positive and negative charges. A plasma may contain neutral particles or it may be fully ionized. The ions may be singly or multiply charged and they also may be atomic or molecular." The fact that the plasma is neutral on the average is usually referred to as quasi-neutrality.

Langmuir probes are the simplest and most commonly used technique for determining the important plasma parameters. The procedure simply involves placing a metal probe in the plasma, and measuring the I-V curve between the probe and the vacuum chamber (ground potential). The setup for the Langmuir probe measurement is shown in Figure 3.3. Langmuir probe theory depends on the plasma being relatively unaffected by the insertion of the probe. When the probe is placed in the plasma, a region called the sheath forms around it. In this region the quasi-neutrality condition is not valid (excess charge densities build up). The size of the sheath for a given probe bias depends on the Debye shielding length in the plasma,

$$\lambda_D = \left(\frac{kT_e}{4\pi N_e e^2} \right) \quad (3.1)$$

where T_e is the electron temperature and N_e is the plasma density [19]. One assumption used in the plasma parameter calculations is that the sheath width is small compared to the probe

dimensions. This assumes that all the particles entering the sheath will be collected by the probe.

The other conditions on the Langmuir theory are: the electron velocity distribution must be Maxwellian, magnetic fields present must be below approximately 200 Gauss, and the mean free path is much larger than probe dimensions [19].

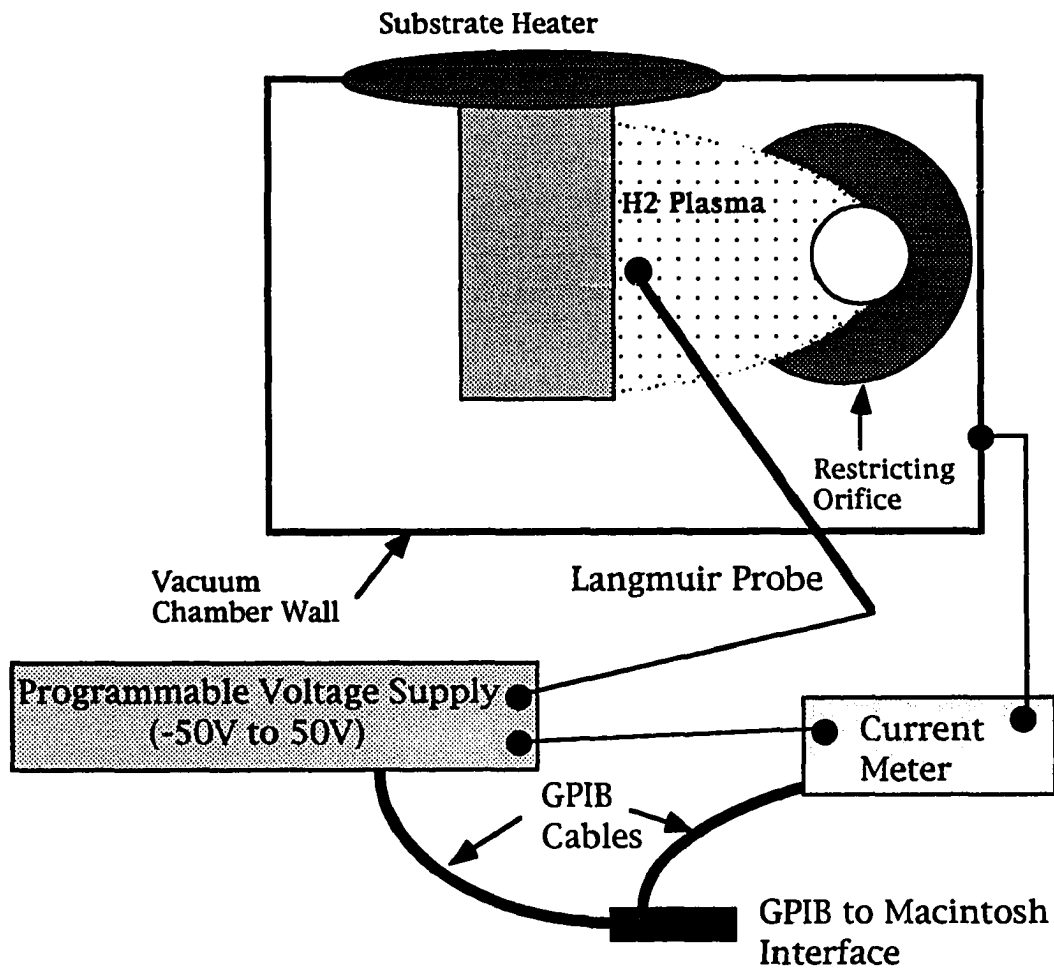


Figure 3.3: Setup for Langmuir probe measurement.

3.2.2 I-V Curve Generation and Interpretation

The setup for the Langmuir probe measurement is shown in Figure 3.3. A BASIC program on the Macintosh is used to control a DC voltage supply via the IEEE 488 interface. The current is measured by a HP DMM and sent back to the Macintosh on the GPIB. The I-V data is sent to an Excel spreadsheet which calculates the plasma parameters.

The probe used in these measurements is a disk with an area of 0.512 cm^2 . The back of the disk is insulated with boron nitride so that the only part of the probe that is exposed to the plasma is the front face. A typical plasma I-V curve is shown in Figure 3.4.

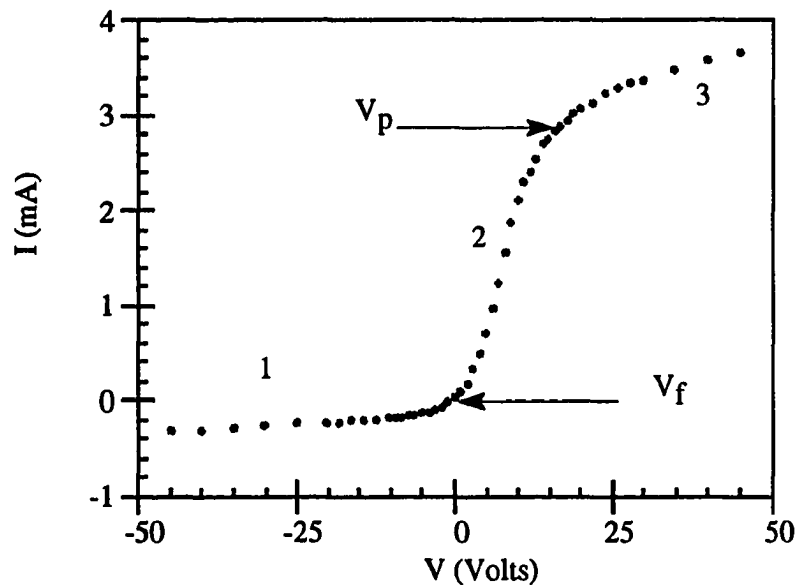


Figure 3.4: Raw data from a Langmuir probe measurement.

The three regions which have been labeled in the figure are:

- 1) Ionic region
- 2) Transition region
- 3) Electronic region

At large negative voltages (region 1), almost all of the electrons are repelled and the ions are attracted, causing the current in this region to be due purely to ions. A layer of positive charge due to the ions builds up until it has the same magnitude as the negative charge on the probe. This layer of charge is the sheath that was described previously. Outside of this sheath, there is very little electric field, so the plasma is not disturbed. The current is due to the random thermal motion of the ions carrying them into the sheath. Ideally, if the area of the sheath remained perfectly constant, region 1 would be flat. In practice, it turns out that the ionic region is linear with a very small slope.

At large positive voltages (region 3), the ions will be repelled and the current will be due primarily to electrons. In this case, a negatively charged sheath, due to the attracted electrons, forms around the probe.

Region 2 is called the transition region since it connects the region where ion current dominates to the region where the current is purely due to electrons. The division between the electronic region and the transition region occurs at the plasma potential, V_p , which is defined as the voltage at the knee of the curve.

When the probe is at the same potential as the plasma, no electric fields are present due to the probe. This potential is called the plasma potential. The plasma potential is often used as an estimate of the ion energy. The current at V_p is due to the particles which hit the probe as a result of random thermal motion. The thermal velocity of electrons is much larger than the thermal velocity of the ions due to the electrons smaller mass. This results in the majority of the current collected at the space potential being due to electrons.

Another physically meaningful point in the transition region is the floating potential, V_f . The floating potential is the voltage where the current goes to zero. At this point, the voltage has been decreased from the plasma potential and enough electrons have been repelled to allow the ionic and electronic components of the current to exactly cancel.

3.2.3 Determination of Plasma Parameters

Once the plasma I-V curve has been generated, several useful plasma parameters can be extracted. The electron temperature, electron density, plasma potential, and ion current density are all easily determined [11]. The electron current can be isolated from the ion current by fitting a line to the ion current in region 1 and subtracting it from the total current ($I_e = I_T - I_i$) in all three regions. If we assume that the electron distribution is Maxwellian, the velocity is given by

$$\bar{v} = \sqrt{\frac{8kT_e}{\pi m_e}} \quad (3.2)$$

and the electron current is given by

$$I_e = \frac{AqN\bar{v}}{4} = \frac{AqN_0\bar{v}}{4} e^{\left(\frac{-qV_B}{kT_e}\right)} \quad (3.3)$$

where N_0 is the electron density in the undisturbed plasma, V_B is the potential barrier seen by the electrons, T_e is the electron temperature, and A is the area of the probe [19]. As the potential is reduced from V_P towards V_f , the potential barrier, V_B , increases and fewer electrons make it to the probe. The electron temperature can now be determined by plotting $\ln(I_e)$ vs. V as shown in Figure 3.5. The graph is linear in the transition region with a slope = $1/T_e(\text{eV})$.

The determination of the plasma potential can be a large source of error. In order to be consistent, we have developed a standard procedure for determining V_P from the $\ln(I_e)$ vs. V graph. First a linear fit is made to the transition region without including the knee and to the electronic region without including the knee. The intersection of these two lines is the plasma

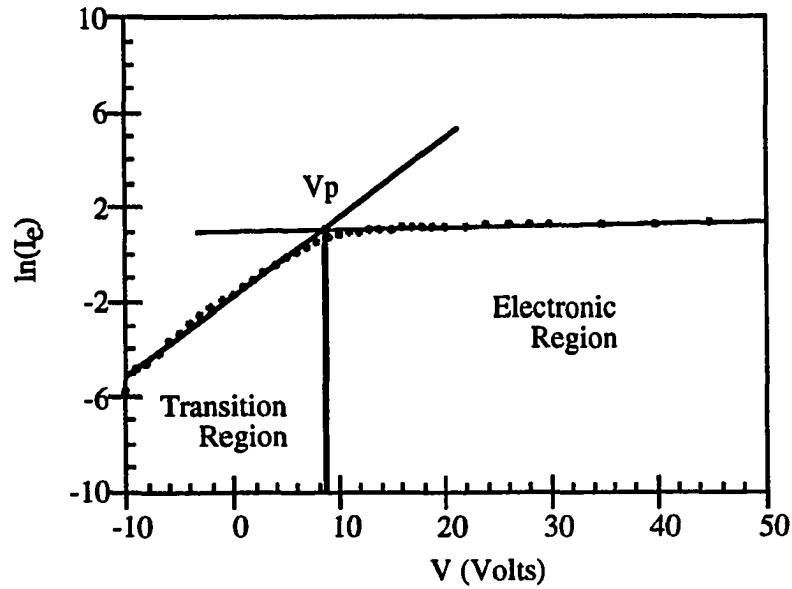


Figure 3.5: Langmuir probe data with the ionic component subtracted out.

potential. This procedure is illustrated in Figure 3.5.

The electron density in the plasma can be determined by using Equation 3.3 at the plasma potential (Area Sheath = Area Probe, $V=V_p$, $I=I_{eo}$). This results in the expression for the electron density given in Equation 3.4.

$$N_e(\text{cm}^{-3}) = \frac{I_{eo}}{qA} \sqrt{\frac{2\pi m_e}{k_B T_e}} = 3.73 \times 10^8 \left[\frac{I_{eo}(\text{mA})}{A(\text{cm}^2) \sqrt{T_e(\text{eV})}} \right] \quad (3.4)$$

The ion current density is determined by using the current at zero volts and the probe area.

$$J_i = \frac{I_i(V=0)}{A} \quad (3.5)$$

3.2.4 Plasma Characterization Results

Langmuir probe measurements have been used to look at the variation of the plasma parameters as a function of the chamber pressure and incident microwave power. The study has been limited to the range of pressures (2 - 25 mTorr) and powers (50 - 250 Watts) which will be used during film deposition. Most of the measurements were done using hydrogen plasmas. Some measurements were done on helium plasmas for comparison. The three stub tuner settings and magnet field profile were the same for all the measurements.

When film growths are done using a plasma which contains silane (SiH_4), the walls of the ECR source become coated with silicon. This silicon is sputtered from the walls during plasma measurements and results in the probe being coated with silicon. This can lead to large errors in the calculated plasma parameters if care is not taken. In Figure 3.6, five measurements were done without cleaning the probe in between. The current collected by the probe is significantly reduced as the probe gets coated. This decrease in current is due to the

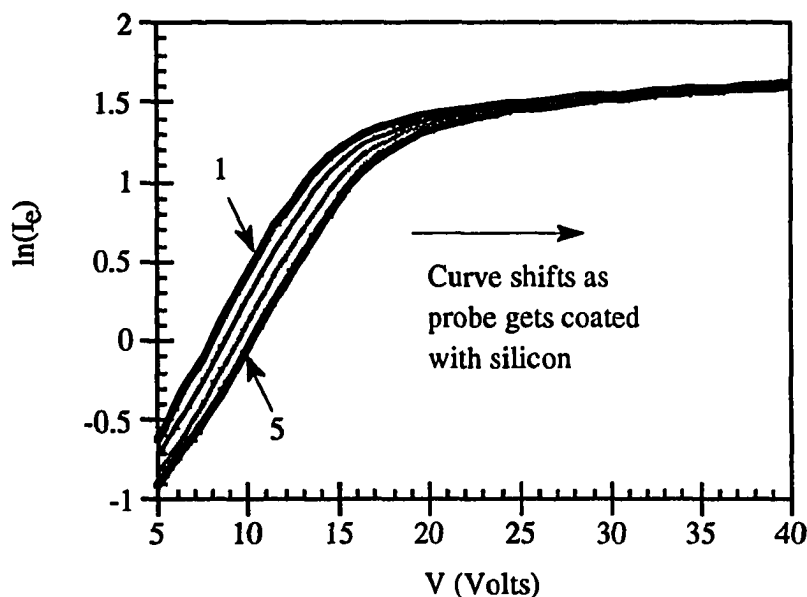


Figure 3.6: Results of 5 consecutive measurements. The sputtering of silicon from the chamber walls results in the coating of the probe.

barrier caused by the silicon film.

All of the measurements of hydrogen plasma parameters versus microwave power were done after the chamber walls were covered with silicon. The slope of the transition region and the current at the plasma potential remains approximately constant, so the determination of the electron temperature and density are relatively unaffected by the probe coating. However, the magnitudes of the electron temperature and electron density may be changed by the presence of the silicon atoms in the plasma. The plasma potential, which is the knee of the curve, is obviously shifted to higher voltages. The ion current is also strongly affected. Anytime we wish to determine these parameters, the probe must be cleaned between each I-V measurement.

The measurements reported here for the variation of the hydrogen plasma parameters with pressure were done in a clean chamber so no probe coating took place. All of the helium plasma results were also obtained when the system was clean.

The assumptions and simplifications made in the Langmuir theory result in the calculated plasma parameters differing from the actual plasma conditions by as much as a factor of two. This is not really a problem in our case, since we are more interested in the dependence of the plasma on our system variables than we are in knowing exact values for the plasma parameters. We have found the measured results to be reproducible to within approximately $\pm 10\%$.

The variation of the ion current density with pressure is shown in Figure 3.7. The fairly linear decrease in the ion current is due to the decreasing mean free path as the pressure is increased.

Figure 3.8 shows that there is no definite dependence of the ion current on the incident microwave power in this range. This behavior is similar to the results found in oxygen and argon plasmas at low powers [15]. If the power were increased further, the current density would eventually increase rapidly.

The electron density as a function of pressure is shown in Figure 3.9 for two different incident microwave power levels. Each of the curves shows a maximum in the density

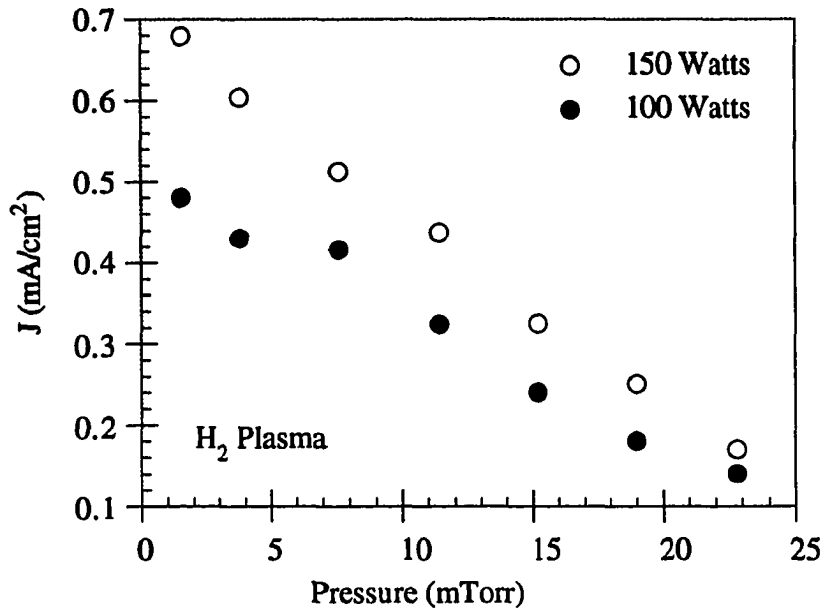


Figure 3.7: Dependence of the ion current on pressure.

occurring at about 7.5 mTorr. This effect has been noted before. The saturation pressure has been found to shift slightly to higher pressures as the microwave power is increased [15].

In Figure 3.10, the plasma density is shown to increase linearly with microwave power in the region of interest. As the power absorbed in the plasma goes up, the degree of ionization increases in the plasma. This results in an increased plasma density.

The dependence of the plasma potential on pressure is shown in Figure 3.11 and the measured variation of the plasma potential with power is shown in Figure 3.12. The plasma potential is important in that it determines the ion energy and the amount of sputtering that occurs from the chamber walls. The data in Figure 3.11 was taken before the system had been exposed to a SiH_4 plasma, so there was no silicon present during the measurement. The presence of silicon in the system resulted in the measured values of the plasma potential in

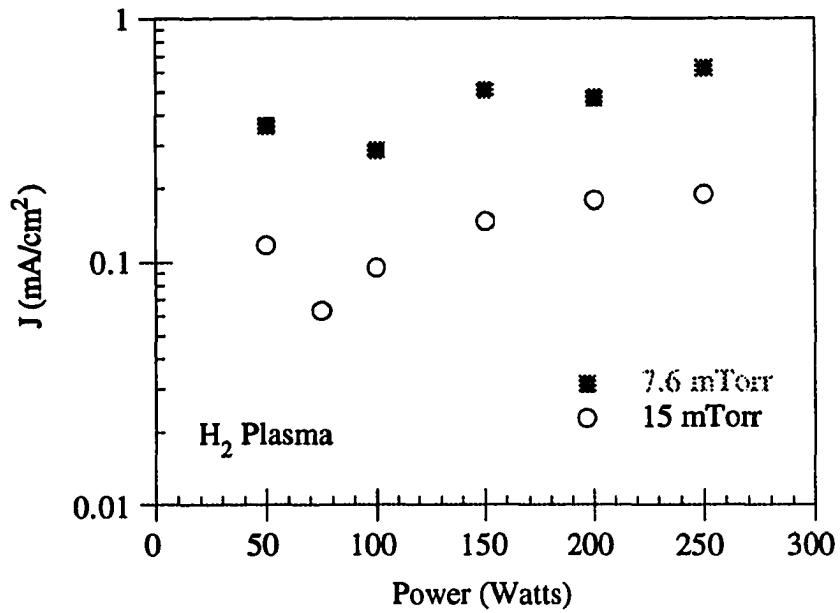


Figure 3.8: Variation of the ion current with microwave power.

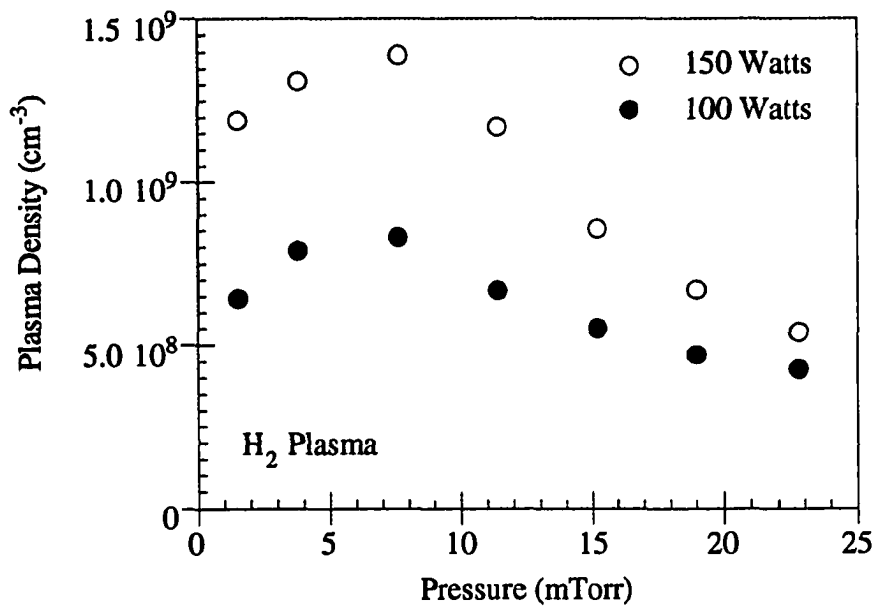


Figure 3.9: Variation of the plasma density with chamber pressure.

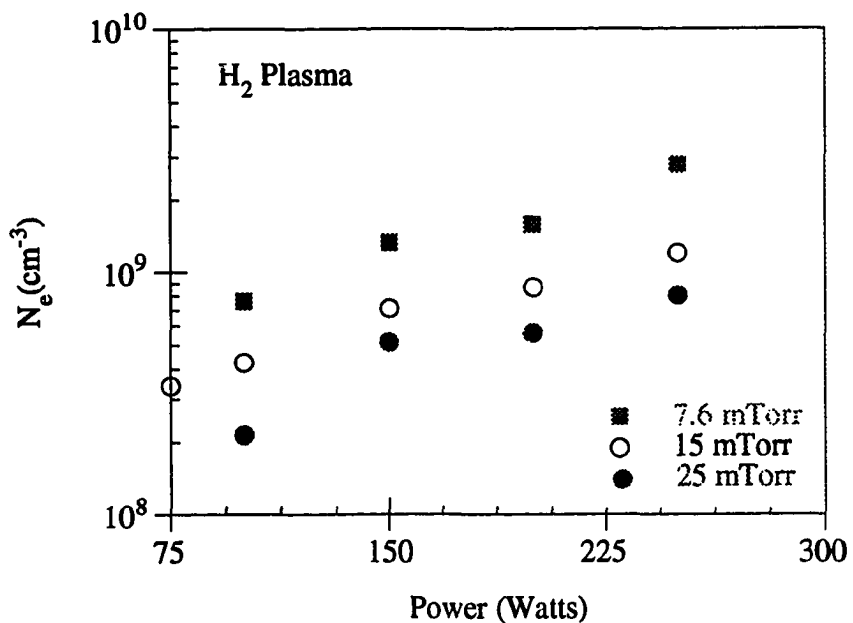


Figure 3.10: Variation of the plasma density with microwave power.

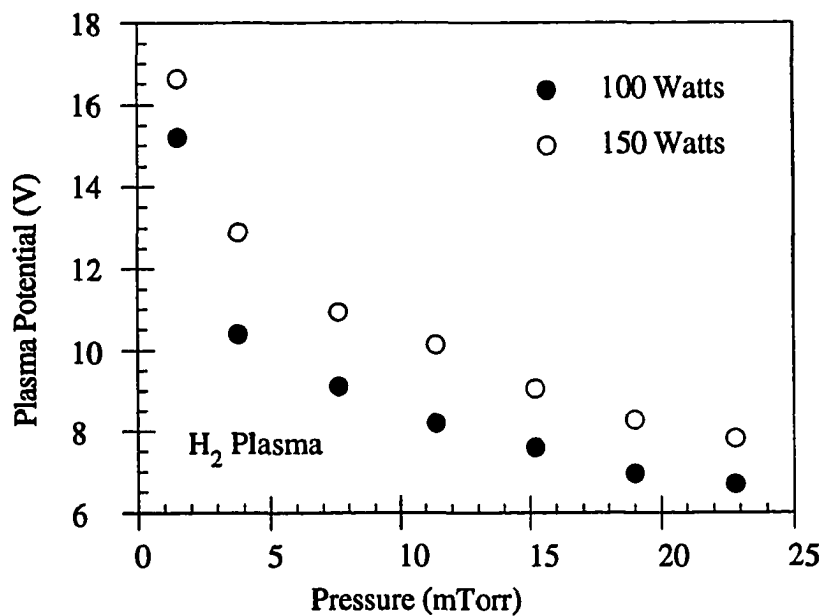


Figure 3.11: Variation of the plasma potential with chamber pressure.

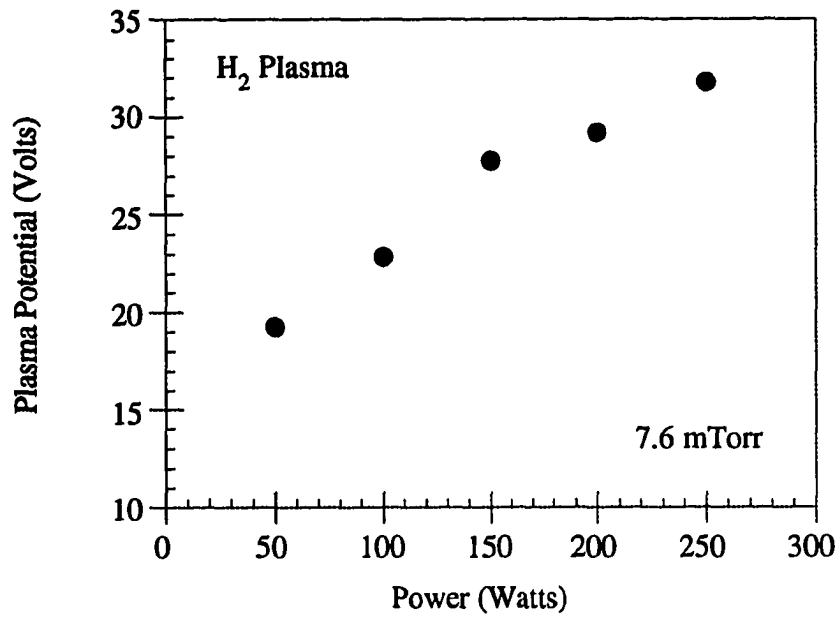


Figure 3.12: Variation of the plasma potential with incident microwave power.

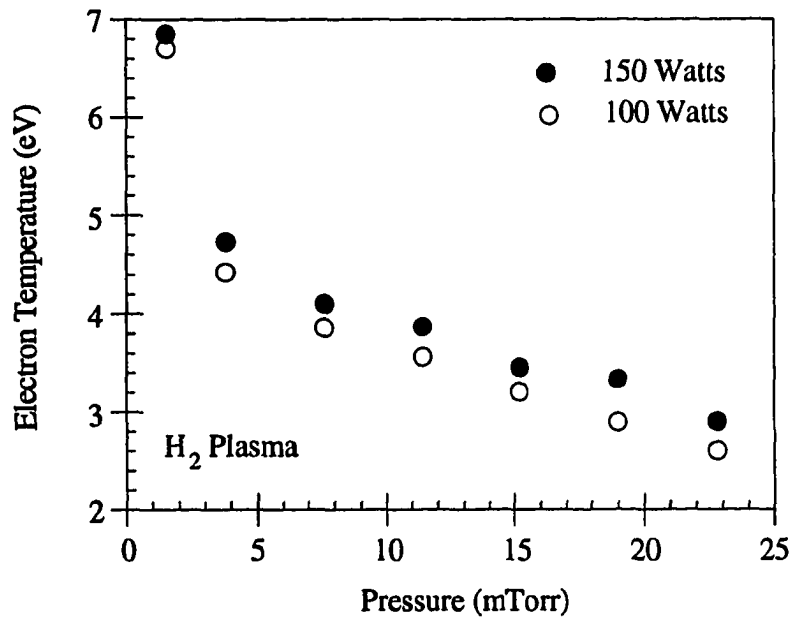


Figure 3.13: Variation of the electron temperature with chamber pressure.

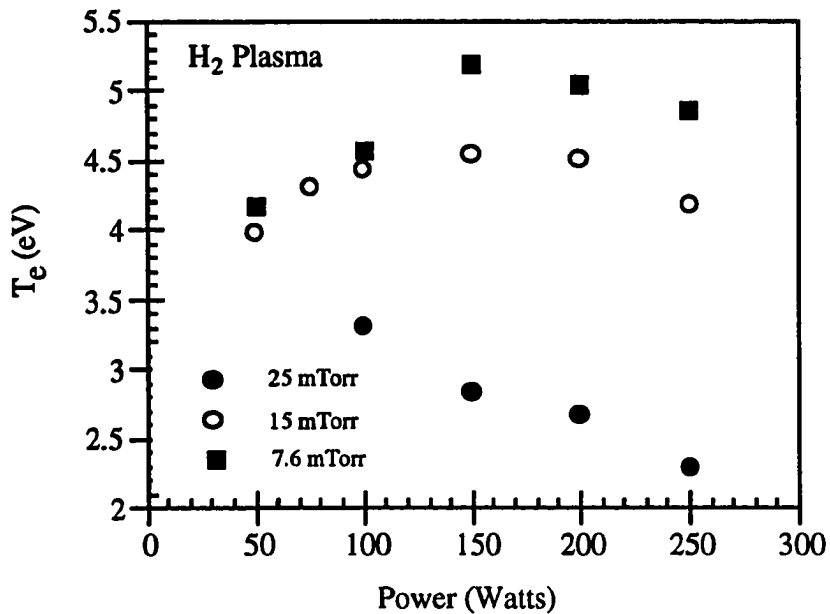


Figure 3.14: Variation of the electron temperature with incident microwave power.

Figure 3.12 being shifted up. Although the magnitude of the plasma potential is uncertain, the trends shown in these two figures are very distinct. The plasma potential decreases rapidly as the pressure is increased; and it increases approximately linearly with increased microwave power for the range shown in the figure.

The relationship between the measured electron temperature and the pressure is shown in Figure 3.13. The decrease in electron temperature with pressure is related to the mean free path of the electrons decreasing at higher pressures. The dependence of T_e on microwave power, shown in Figure 3.14, seems to depend on the pressure in some manner. At 15 and 25 mT, the electron temperature seems to have a maximum at around 150 Watts, while at 7.6 mT it simply decreases with increasing power.

Measurements on a helium plasma have been done as a function of pressure for the

purpose of comparison. The variation of the He plasma parameters with pressure is in some cases significantly different from the behavior of the H₂ plasma. One example of this is the current density in the helium plasma shown in Figure 3.15. The current density for a hydrogen plasma was shown to decrease linearly with pressure in Figure 3.7. The helium current density is also shown to decrease as the pressure is increased for pressures below 15 mT. However, for helium, the current density increases again at around 20 mT before being reduced due to the reduced mean free path at high pressures. The electron density in the helium plasma also behaves in a much different manner than in the hydrogen plasma. The dependence is shown in Figure 3.16. The maximum which occurs between 5 and 10 mT in a hydrogen plasma (Figure 3.9), is shifted out to about 25 mT in the helium plasma.

The dependence of the plasma potential on pressure in a helium plasma is shown in Figure 3.17. The dependence is very similar to the hydrogen plasma results shown in Figure 3.11. However, the magnitudes of the measured results for the helium plasma are larger. This indicates that there may be an increase in the ion energies for the helium plasma.

The behavior of the electron temperature for the helium plasma, shown in Figure 3.18, is also very similar to the hydrogen plasma result shown in Figure 3.13. The values measured for the helium plasma are again somewhat higher. Overall, the results from these plasma measurements indicate that the properties of a helium plasma are significantly different from those of a hydrogen plasma.

The uniformity of the plasma is very important for growing good quality films. A series of Langmuir probe measurements have been done at different positions across the film growth region in order to determine the plasma uniformity. The measurement positions are shown in Figure 3.19 and the results are given in Figure 3.20. A hydrogen plasma was used for this study. From these results, we can see that the plasma is uniform radially across the growth region to be used for the films grown in this work.

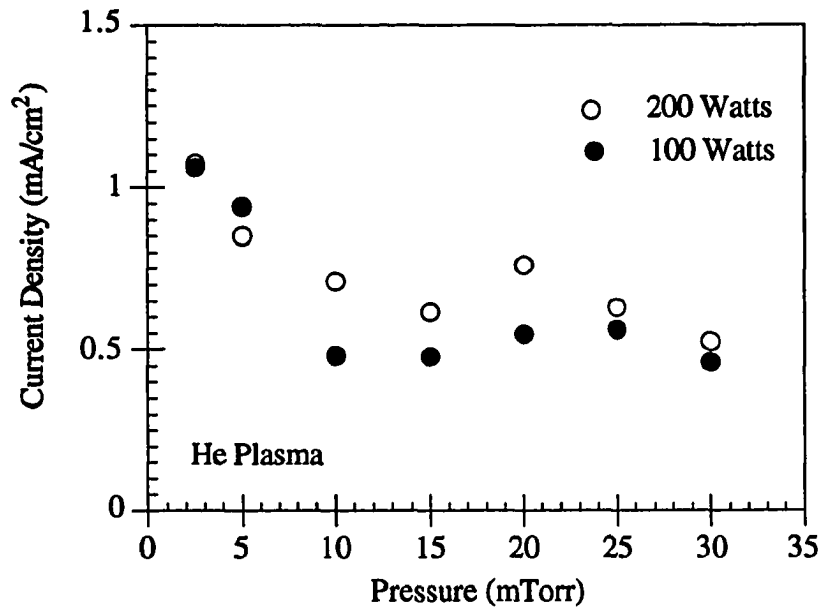


Figure 3.15: Variation of the current density with pressure in a helium plasma.

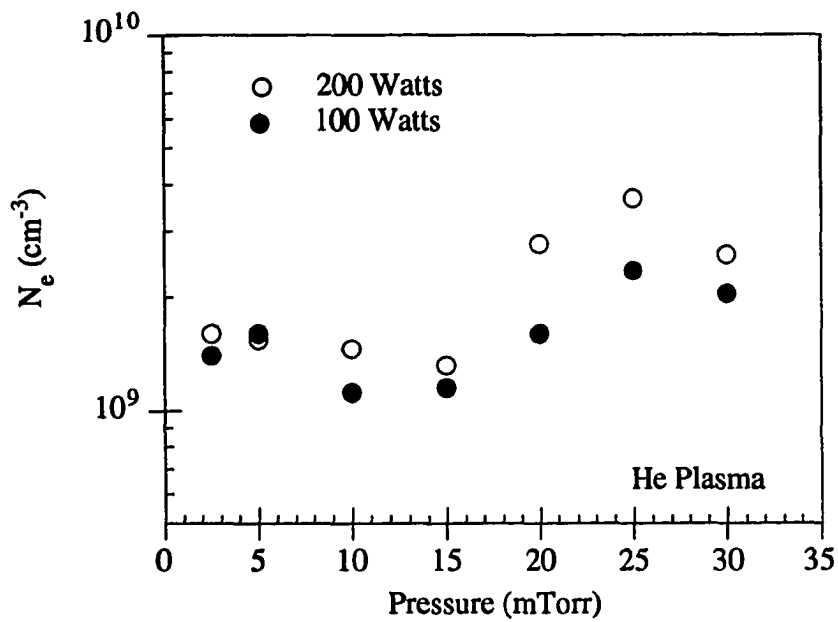


Figure 3.16: Variation of the electron density with pressure in a helium plasma.

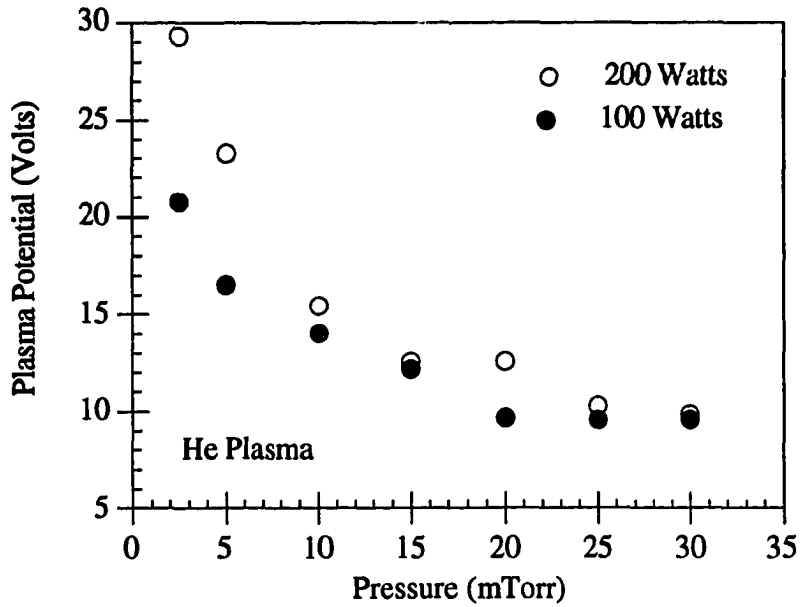


Figure 3.17: Variation of the plasma potential with pressure in a helium plasma.

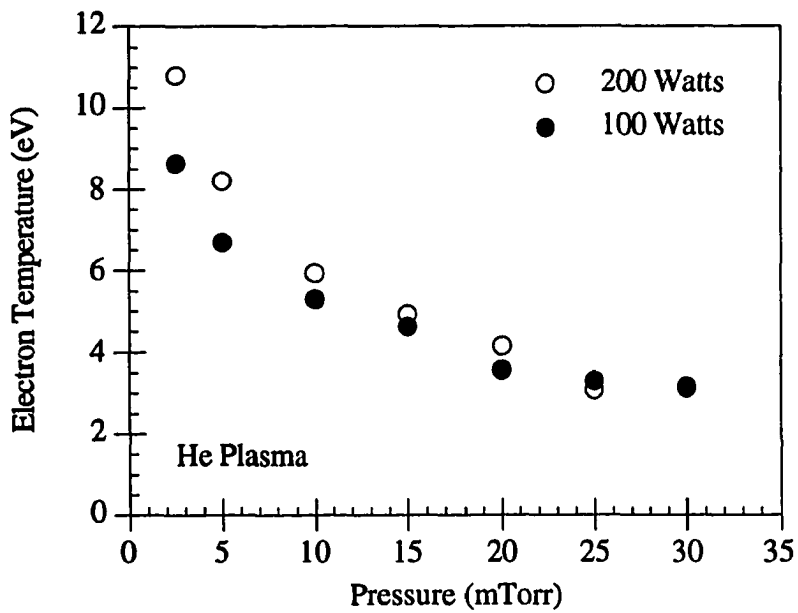


Figure 3.18: Variation of the electron temperature with pressure in a helium plasma.

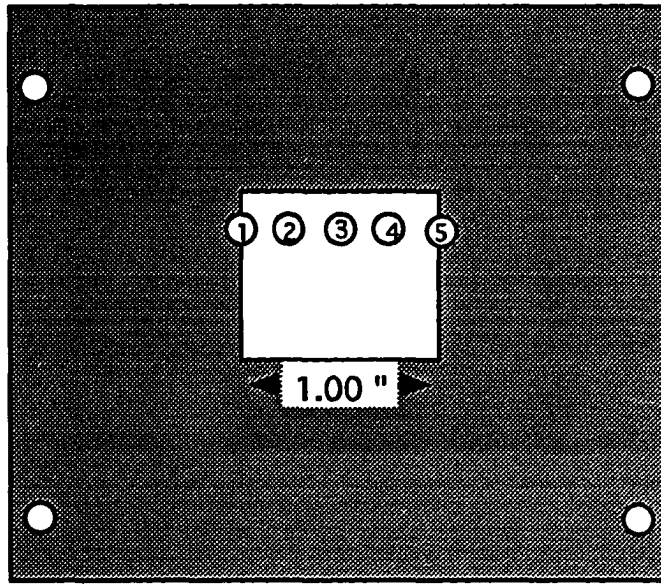


Figure 3.19: Measurement positions for plasma uniformity study.

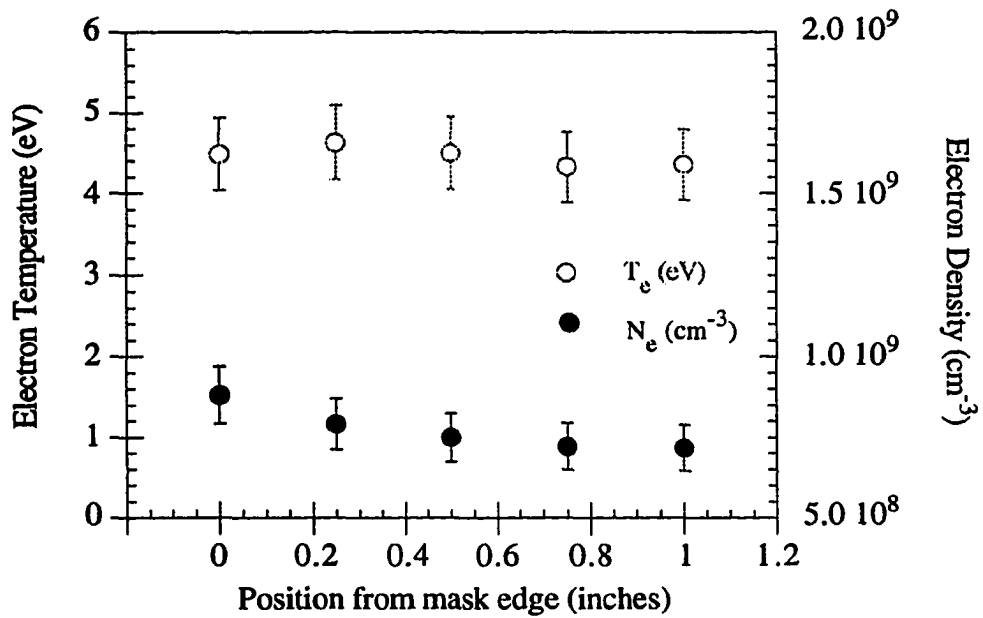


Figure 3.20: Uniformity of plasma parameters across the growth region. .

3.3 Wafer Temperature Measurements

The final aspect of the system that needs to be characterized is the temperature difference between the substrate and the sample holder during growth. At the pressures used during growth (7 mT to 25 mT), the thermal conductivity between the heater block and the wafer clamped to it is limited. This results in the wafer temperature being significantly lower than the heater temperature as shown in Figure 3.21.

The heater temperature is monitored by two type K thermocouples imbedded in the heater block. The wafer temperature is monitored by a 0.01" diameter type K thermocouple connected to the wafer surface with thermally conductive high temperature cement. The measurement was performed five times and the results were consistent to within $\pm 10^\circ\text{C}$. The wafer temperature during a typical run is shown in Figure 3.22.

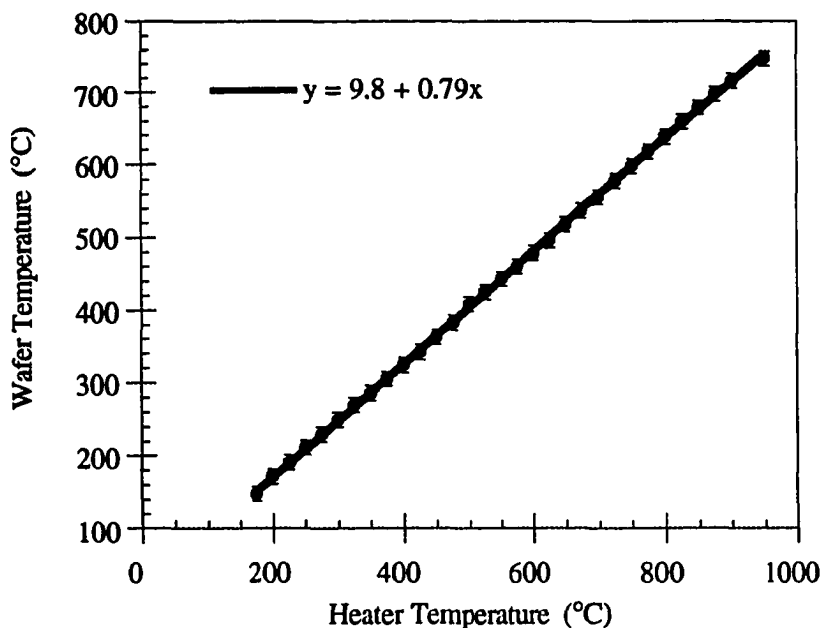


Figure 3.21: Relationship between the actual wafer temperature and the temperature of the inconel substrate holder.

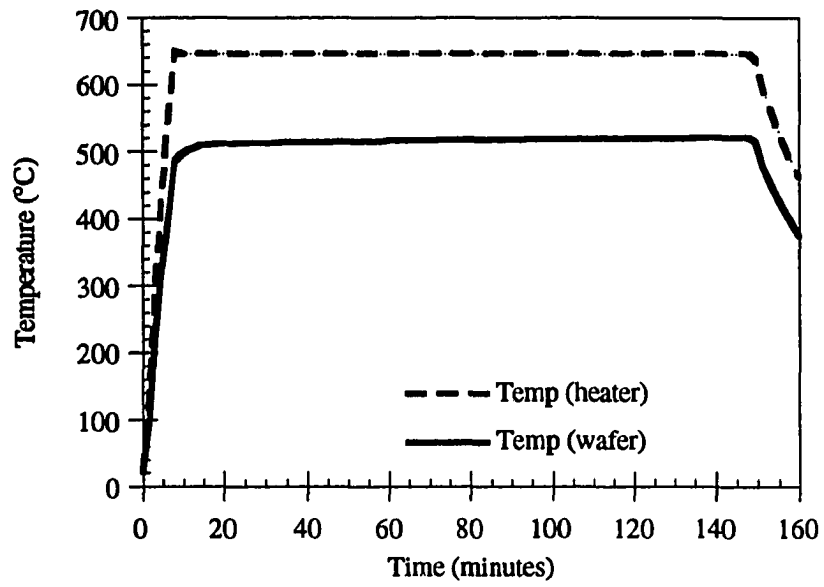


Figure 3.22: Heater and wafer temperatures during a typical growth run.

IV. MATERIAL CHARACTERIZATION TECHNIQUES

Several different techniques have been used to characterize the structural and electronic properties of the silicon films grown in this work. All of the characterization, with the exception of the spreading resistance profiles, was done at Iowa State University. The spreading resistance profiles were done by Solecon Laboratories in California.

4.1 UV Reflectance

UV reflectance has been used in to determine the crystalline quality of the films studied in this work. Figure 4.1 illustrates the differences in the spectra for crystalline, polycrystalline and amorphous silicon. The peaks at 280 nm (4.4 eV) and 365 nm (3.4 eV) in

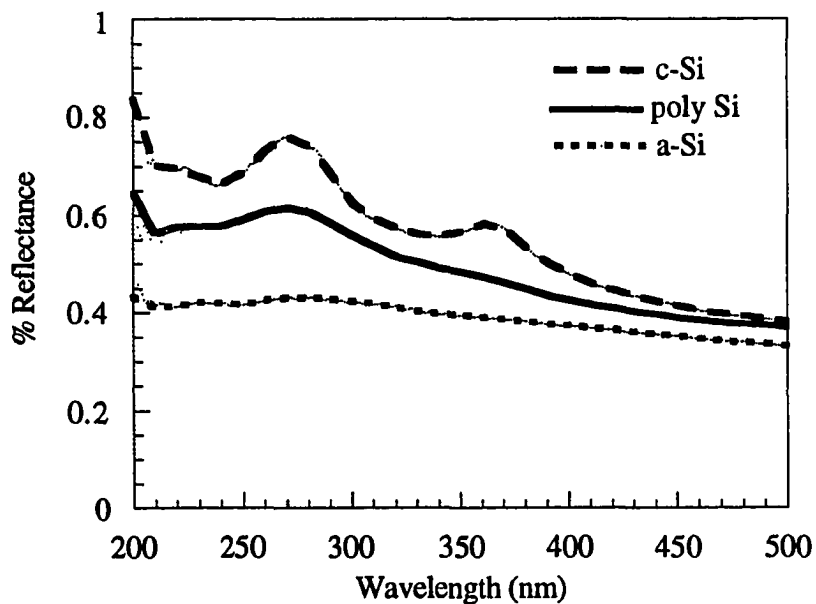


Figure 4.1: UV reflectance spectra for different types of silicon material.

the crystalline silicon spectra are the result of interband transitions [20]. As the amount of disorder in the lattice increases the peaks are reduced until finally they are not present at all in the amorphous sample. This method is quite valuable for obtaining a quick indication of the crystalline structure present in a film. It will be shown, in Chapter 6, to be an excellent tool for looking at the transition from polycrystalline to single crystal silicon films.

4.2 Raman Spectroscopy

Raman scattering is another very useful nondestructive technique for determining the crystal quality of silicon films. The basis of the Raman effect is the scattering of an incident photon by the solid with the subsequent creation or annihilation of a phonon. The energy and momentum conservation equations for such a process are shown in Equation 4.1 and Equation 4.2 respectively, where the subscripts (s, i and p) refer to scattered, incident and phonon, respectively.

$$h\omega_s = h\omega_i \pm h\omega_p \quad (4.1)$$

$$hk_s = hk_i \pm hq_p \quad (4.2)$$

The fact that a phonon may be either created or destroyed is indicated by the plus or minus sign in the equations. If a phonon is created (minus sign) the event is referred to as Stokes scattering and if a phonon is destroyed (plus sign) it is referred to as anti-Stokes scattering.

From this discussion, it is apparent that the Raman spectrum for a particular material will be determined by its allowed vibrational modes. For crystalline silicon, momentum

conservation limits the Raman scattering to only one allowed frequency at the center of the Brillouin zone (520 cm^{-1}). The Raman spectrum measured for a single crystal n-type silicon (100) wafer is shown in Figure 4.2.

Raman scattering measurements provide three quantities (Raman parameters) which contain information about the crystal quality of the film being measured. The intensity of the peak, the frequency of the Raman band, and the peak width all contain useful information. Of these three quantities, the intensity is the least useful. The Raman intensity is dependent on the structural perfection of the films and it is reduced in damaged and amorphous films. Due to the measurement procedure available, the uncertainty in the measured intensities is approximately 50%. For this reason, the intensity will not be used for film comparison in this work.

The frequency of the Raman band is useful because it is related to the bond length or lattice spacing. The frequency is shifted up from the normal position of 520 cm^{-1} when there is compressive stress in the film. The magnitude of the shift gives an indication of the amount of stress present. The peak is typically shifted to lower wavenumbers as the material becomes disordered. The measurement of the peak position is accurate to within less than 1 cm^{-1} .

The Raman peak width is the most useful parameter for looking at the crystal quality of the material. As the material becomes disordered, relaxation of the momentum conservation in the scattering process occurs. As a result of this, broadening of the Raman peak occurs. By looking at the change in peak width of a film with respect to the silicon wafer, the crystal quality of the film can be evaluated. For amorphous silicon, the phonon dispersion curve is relaxed due to the lack of long range order. This results in the Raman spectra resembling the phonon density of states. The Raman spectrum for an amorphous silicon film is shown in Figure 4.3. The apparatus used for the Raman measurements has previously been described in detail [21].

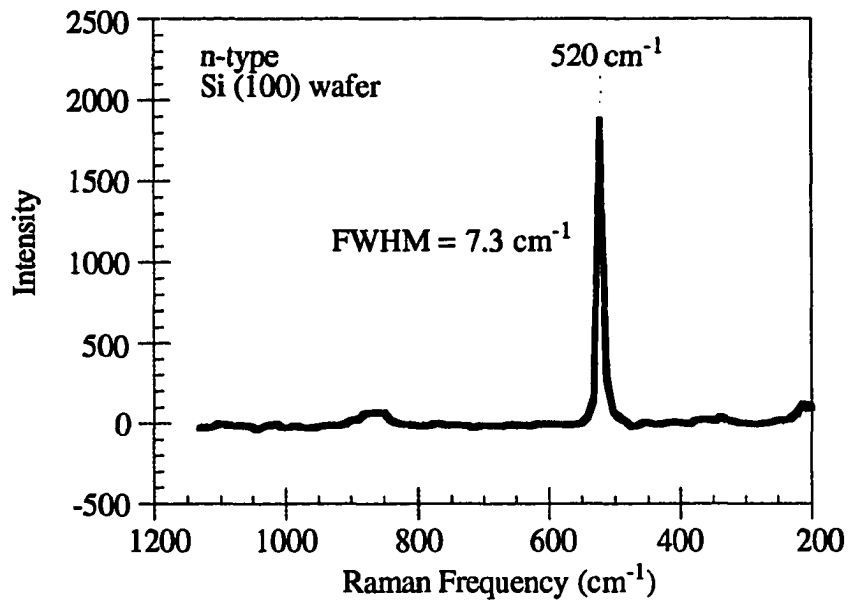


Figure 4.2: Raman spectra for an n-type silicon (100) wafer.

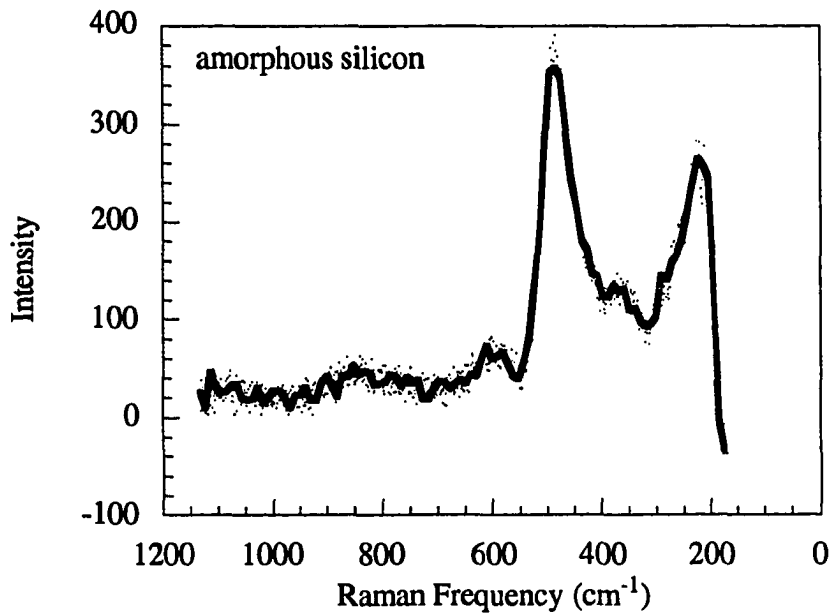


Figure 4.3: Raman spectra for an amorphous silicon film.

4.3 Spreading Resistance Profiling

Spreading resistance profiling (SRP) has been used to obtain profiles of the carrier concentration as a function of depth in the films. The procedure for the technique involves beveling a small angle on the sample and then stepping two probes down the beveled angle to measure the resistance. The exact procedure for SRP measurements is given in ASTM Standard F672 [22]. The measurements were done by Solecon Laboratories in San Jose California.

A typical SRP for an undoped polysilicon film grown on a heavily doped p-type silicon wafer is shown in Figure 4.4. From the figure it is evident that besides the carrier concentration, the SRP measurement also provides the film thickness and an indication of the abruptness of the film/wafer interface.

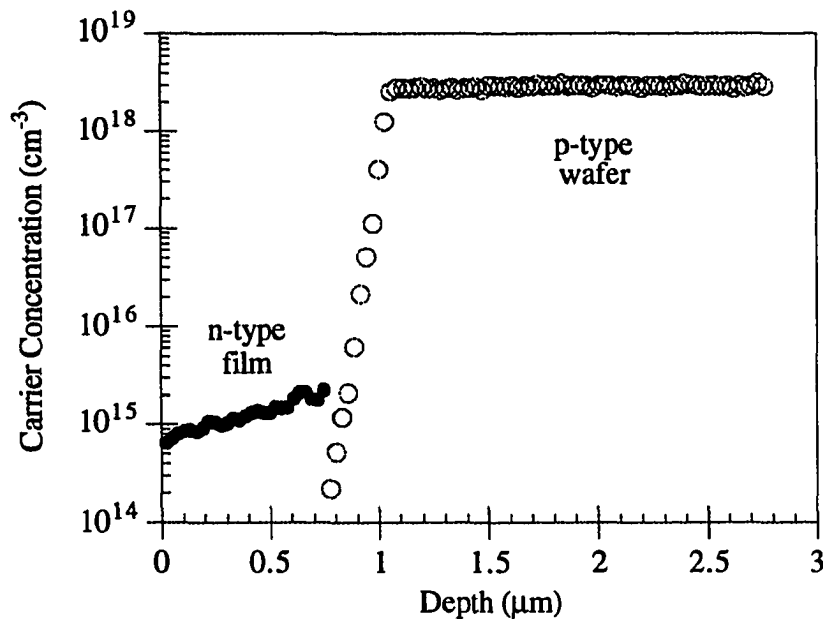


Figure 4.4: Spreading resistance profile for an undoped silicon film grown on a heavily doped p-type silicon (100) wafer.

4.4 Film Thickness

An accurate knowledge of the film thickness is very important to many of the other characterization techniques. Several different techniques have been attempted with varying degrees of success. Among these are the bevel and stain technique [23], profilometer step height measurement and the SRP measurement described in the previous section. Table 4.1 shows the results for a film measured by each of these three techniques.

Table 4.1: Thickness measurements on sample 037.

<u>Method</u>	<u>Thickness (μm)</u>
SRP	2.1 ± 0.25
Bevel and Stain	2.5 ± 0.60
Profilometer	2.4 ± 0.2

The agreement between the three measurement methods is reasonably good. The profilometer was chosen as the best method due to its ease of use and availability in comparison to the other methods. The instrument used was a Sloan Dektak Stylus profilometer. The uncertainty in the thickness measurements was less than $\pm 0.2 \mu\text{m}$. This uncertainty was dependent on the film roughness and the presence of wafer warp.

4.5 Four-Point Probe

The four-point probe technique provides a simple method for obtaining the sheet resistance of silicon films grown on silicon wafers. The method is applicable as long as the

film has the opposite conductivity from the wafer it is grown on. The arrangement for the measurement consists of four collinear probes. A current is passed between the two outside probes and the voltage drop is measured across the two inside probes by a high impedance voltmeter. The current levels which yield voltages between 5 and 30 mV are recorded and the I-V curve is plotted. The sheet resistance can then be calculated from

$$R_s = \frac{\rho}{t} = \frac{\pi}{\ln(2)} \frac{\Delta V}{\Delta I} \quad (4.2)$$

where $\Delta I/\Delta V$ is the slope of the I-V curve, t is the film thickness and s is the probe spacing [24]. This equation is only valid when the film thickness is small compared to the probe spacing ($t \leq s/2$). A more detailed explanation of the measurement procedure is given in ASTM Standard F374 [25]. After the sheet resistance has been determined, the resistivity of the film can be calculated ($\rho=R_s t$) using the film thickness which was measured by the profilometer. Finally, the graph of resistivity vs. carrier concentration on page 60 of Jaeger [26] can be used to estimate the concentration of free carriers in the film. The agreement between this procedure and SRP measurements has been found to be very good.

4.6 Van der Pauw

The van der Pauw method allows the determination of the resistivity of a flat arbitrarily shaped sample. The samples used for this measurement were 1 cm x 1 cm square pieces with small evaporated aluminum contacts in the corners. A detailed description of the exact procedures used for this measurement is given in ASTM F76 [27]. The resistivity of the sample is given by Equation 4.3,

$$\rho_{AV} = \frac{\rho_A + \rho_B}{2} \Omega \cdot \text{cm} \quad (4.3)$$

where

$$\rho_A = \frac{1.133f_A t}{I} [V_{21,34} - V_{12,34} + V_{32,41} - V_{23,41}]$$

and

$$\rho_B = \frac{1.133f_B t}{I} [V_{43,12} - V_{34,12} + V_{14,23} - V_{41,23}]$$

The notation $V_{AB,CD}$ refers to the potential difference measured between point C and point D, when the current enters at point A and leaves at point B.

The main conditions that must be satisfied for this technique to be valid are that the contacts are small and on the periphery, the sample thickness is uniform and there are no pinholes in the sample. This measurement has generally been found to give nearly identical results to the four-point probe measurements.

4.7 Hall Mobility

The Hall mobility measurement is actually a continuation of the van der Pauw resistivity measurement described in the previous section. After the resistivity measurement, the sample with the four contacts is placed in a DC magnetic field and the Hall voltage is measured as a function of this field. The Hall coefficient, Hall mobility, and carrier concentration can then be calculated from Equations 4.4, 4.5 and 4.6, respectively.

$$R_H = \frac{t \Delta V}{I \Delta B} \quad (4.4)$$

$$\mu_H = \frac{|R_H|}{\rho_{AV}} \quad (4.5)$$

$$n = -\frac{1}{qR_H} \quad (4.6)$$

A more detailed explanation of the procedure for determining the Hall mobility is given in ASTM F76 [27]. It is important to note that all the mobilities measured in this work are Hall mobilities. This differs from the conductivity mobility by r , the Hall scattering factor ($\mu_H = r \cdot \mu_n$), which is generally larger than 1.

4.7 Electron Microscopy

Scanning electron microscopy (SEM), transmission electron microscopy (TEM) and convergent beam electron diffraction (CBED) have all been used to evaluate the structural quality of the silicon films. The SEM work was done on a JEOL 6100 scanning electron microscope. The TEM and CBED work was done using a Phillips CM 30 transmission electron microscope.

The SEM was used to look at the surface morphology of the silicon films grown in this work. It was useful for looking at poor samples. However, as soon as a growth process was found which produced smooth samples, the SEM was of little use.

The TEM was used to look at the crystalline quality of silicon films grown on silicon wafers. TEM allows the observation of defects such as dislocations and stacking faults in the lattice. It also allows the observation of pre-growth surface roughening due to plasma exposure. Finally, high resolution TEM images can be used to verify the epitaxial nature of films.

The TEM results from this work were very interesting and it would have been nice to prepare several more samples. The main limitation for this technique is the time required for the sample preparation procedure. The samples must be less than approximately 3000 Å thick in order for enough electrons to pass through them to form an image. This thickness requirement results in a rather complicated preparation procedure. The sample is first cleaved into 4 x 10 mm sized pieces and then glued together into a 4 mm high stack using Gatan G-1 epoxy. A diamond saw is then used to cut off 400 μm thick samples. A core drill is then used on the sample to produce a cylinder which has a 3 mm diameter and is 400 μm thick. The 3 mm diameter is important because that is the sample holder size in the TEM. After the core drill, the sample is thinned to approximately 200 μm in a polisher. Once the sample is ≤ 200 μm, it is placed in a dimpler to thin the middle down until a small hole appears in the center. Generally, after one side of the sample is dimpled a copper grid is glued onto the sample for support. After a small amount of additional thinning in an ion mill, the sample preparation is complete. A more thorough explanation of the sample preparation procedure is given in the literature [28].

Convergent beam electron diffraction (CBED) has been used to verify the epitaxial nature of the silicon films. This is done by observing the electron diffraction pattern as the electron beam is moved across the interface from the wafer side to the film side. When the diffraction pattern is the same on both sides, the film has the same orientation as the wafer. CBED patterns contain more information than regular electron diffraction patterns because the spots themselves contain information about the symmetry in the lattice. In this case, the

extra information is not very important because the lattice structure is known. However, when the crystal structure is not known this is a very powerful technique.

V. WAFER CLEANING PROCEDURE

One of the major obstacles in growing epitaxial films at low temperatures is the removal of the native oxide. A clean, oxide free surface is required for epitaxial growth. In conventional CVD growth of epi silicon, a high temperature bake is performed to desorb the native oxide from the wafer, leaving a bare silicon surface for growth. This procedure is very effective, but a high temperature cleaning procedure is not desirable in a low temperature growth process. Most of the cleaning processes used in low temperature epitaxy research involve etching away the oxide with HF [5], rather than thermal desorption. The wafer cleaning procedure used in this work is a two step process consisting of a wet clean and a hydrogen plasma clean.

5.1 Wet Cleaning Procedure

The wet cleaning procedure used in this work is outlined in Table 5.1. A three minute rinse in deionized (DI) water is done between each of the steps. This cleaning procedure has been used in industry for more than 30 years.

Table 5.1: Procedure for Standard Clean

SC-1:	15 minutes at 80°C 100 ml NH ₄ OH + 100 ml H ₂ O ₂ + 500 ml DI H ₂ O
HF dip:	15 seconds in 50:1 HF
SC-2:	15 minutes at 80°C 100 ml HCl + 100 ml H ₂ O ₂ + 600 ml DI H ₂ O
HF dip:	30 seconds in 50:1 HF just before loading in reactor

The first step (SC1) is used for particle removal from the wafer surface. The exact chemistry of the particle removal is not well understood. The HF dip in the middle of the cleaning process is used to strip the native oxide. The last step of Standard Clean (SC-2) then grows a thin protective oxide layer on the wafer surface. This oxide layer limits further oxidation and hydrocarbon uptake. Removal of metallic contamination also takes place during SC 2. A second dilute HF dip is performed just prior to growth. This HF dip again removes the oxide layer and leaves the silicon surface terminated with hydrogen. This hydrogen layer passivates the silicon surface and prevents re-oxidation. The surface remains essentially oxide-free on the scale of hours following the HF treatment [29].

5.2 Hydrogen Plasma Cleaning

The ability of the HF treated surface to easily remain oxide-free in air for the amount of time required to load it into the growth chamber is very important. This hydrogen terminated surface is however, very susceptible to hydrocarbon contamination [30]. This becomes especially important when the wafer temperature is raised above 500°C in preparation for growth. In order to grow good quality silicon films, a method must be developed for removing the hydrocarbon contamination while at the same time maintaining the hydrogen passivation on the wafer surface. This has been done through the use of a hydrogen plasma clean. The removal of carbon and oxygen from a silicon surface by an ECR hydrogen plasma is shown in Figure 5.1 [31]. It may also be possible to eliminate the HF dip altogether by using the hydrogen plasma to remove the oxide layer. The etching of a thermally grown oxide layer in a hydrogen plasma is shown in Figure 5.2. This result indicates that the native oxide can easily be removed by a hydrogen plasma. The plasma conditions for the pre-growth cleaning procedure were; 7.6 mTorr, 75 Watts, No bias voltage

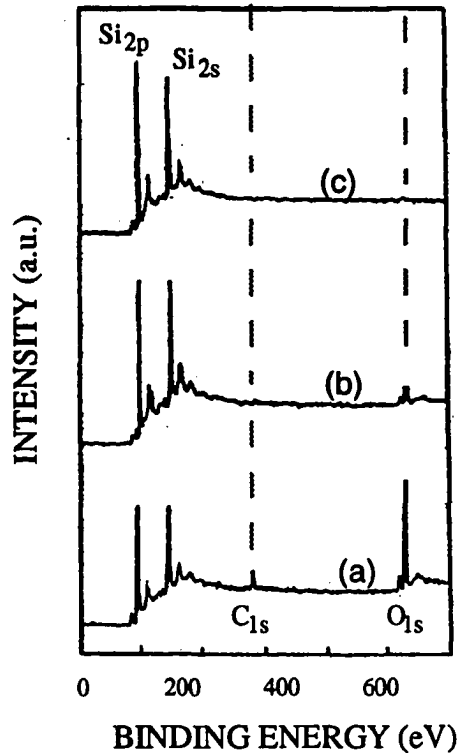


Figure 5.1: XPS spectra of (a) an as received silicon wafer, (b) the wafer after an ECR hydrogen plasma clean for 1 minute and (c) a 10 minute hydrogen plasma clean [31].

and 525°C. These conditions were chosen in order to maximize the plasma density while minimizing the amount of sputtering from the chamber walls.

The work done on optimizing the cleaning procedure has indicated that both the dilute HF dip and the hydrogen plasma clean are necessary for the growth of specular epitaxial silicon films. The effect of omitting the dilute HF dip prior to growth is illustrated in Figure 5.3. In this figure, the native oxide remaining on the wafer results in a very rough surface despite the hydrogen plasma clean which was done prior to growth. Attempts to grow films after an HF dip, but without a plasma clean, also resulted in rough films. Films which were

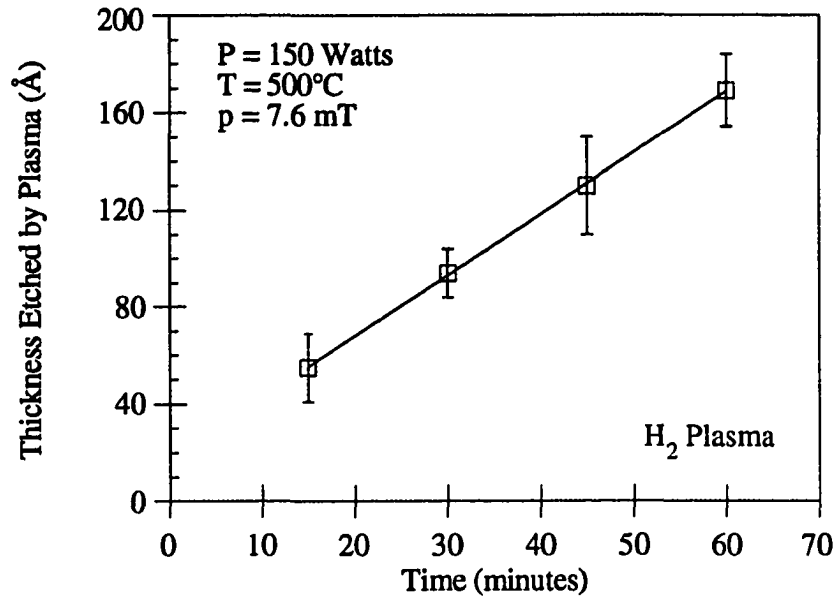


Figure 5.2: Hydrogen plasma etching of a thermally grown oxide.

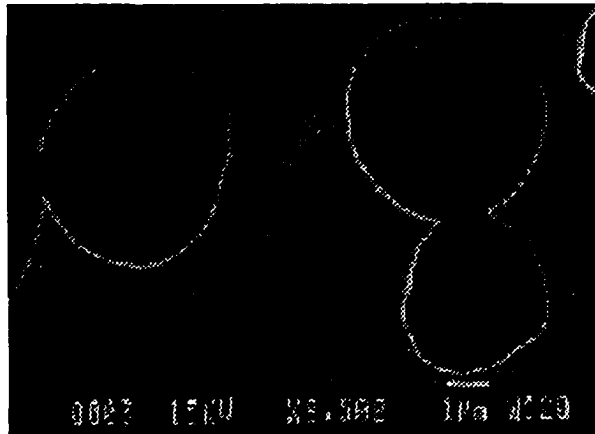


Figure 5.3: SEM image of a silicon film deposited without an HF dip prior to growth.

grown under identical conditions to the one shown in Figure 5.3 had no observable surface features when both an HF dip and a hydrogen plasma clean were done prior to growth.

VI. EPITAXIAL SILICON GROWTH AND CHARACTERIZATION

6.1 Growth Model

The starting point in the development of a low temperature growth process for epitaxial silicon is an understanding of the chemistry which results in good quality growth. Once the reaction is understood, a process can be developed which takes advantage of the strengths of the particular growth method being used. The most likely mechanism for silicon growth in an ECR plasma deposition system using SiH_4 diluted in H_2 is shown below.

- 1) $\text{SiH}_4 + \text{H}^* \Rightarrow \text{SiH}_3^* + \text{H}_2$
- 2) $\text{SiH}_3^* + \text{Surface Site} \Rightarrow \text{SiH}_3(\text{Surface})$
- 3) $\text{SiH}_3(\text{Surface}) \Rightarrow \text{SiH}(\text{Crystal}) + \text{H}_2$

In the first step a silane molecule interacts with an atomic hydrogen radical to form an SiH_3 radical and hydrogen gas. It is still uncertain whether SiH_3 or SiH_2 is the dominant species during the growth of epitaxial silicon. Most likely they both play some role, and the dominance of one over the other depends on the growth method being used. For ECR plasma deposition from a hydrogen and silane plasma, it is likely that SiH_3 is the species involved in growth. This is a reasonable assumption because the SiH_3 radical fits in nicely at the location where the hydrogen atom desorbed from.

The second step in the model involves the adsorption of the SiH_3 at a surface site. The previous work on low temperature growth of epitaxial silicon, as described in Chapter 1, has

indicated that the CVD growth rate is limited by the desorption of hydrogen from the wafer surface. At temperatures below 600°C this severely limits the growth rate. It is possible that the energy provided to the wafer surface by the ECR plasma bombardment will enhance the removal of hydrogen from the surface, thus allowing increased growth rates.

The final step in the model results in the incorporation of the silicon atom into the lattice leaving the wafer surface terminated with hydrogen. As mentioned in Chapter 1, if the surface mobility is low, the adsorbed molecules may interact before they are incorporated into the lattice. The resulting three dimensional growth causes the surface of the films to be rough. In conventional CVD, the surface mobility is primarily determined by the wafer temperature during growth. Since the growth rate is very small for low temperature CVD, the reduced surface mobility is not a problem. However, if large growth rates are desired at temperatures below 600°C, the low surface mobility will be a significant problem. The presence of the ECR plasma will again help solve this problem by providing energy to the wafer surface and enhancing the surface mobility.

In addition to utilizing the beneficial aspects of the ECR plasma deposition system, the development of a satisfactory growth process also involves overcoming the liabilities of such a system. The two main liabilities are: the possibility of ion bombardment causing damage to the crystal lattice, and the high vacuum (10^{-7} Torr) background conditions during growth as compared to the UHV systems ($<10^{-10}$ Torr) used in the majority of the previous research. The results from the Langmuir probe measurements indicate that the ion energy and flux can be effectively tuned to find the proper conditions for good quality films. The fact that the chamber has some O-ring sealed flanges and a base pressure of 10^{-7} Torr makes it much more representative of a production environment than the UHV growth systems. However, the constant flux of carbon and oxygen to the wafer surface during growth is much larger under HV conditions. This problem is magnified by the fact that at low growth temperatures the impurities are much more likely to stick to the surface. In order to reduce the

incorporation of carbon and oxygen in the film, the growth rate must be maximized. The presence of hydrogen in the plasma during growth also helps to remove carbon and oxygen, as seen in the previous chapter. The hydrogen is also believed to etch away the weaker non-crystalline silicon bonds on the surface and lead to better quality epitaxial silicon films.

In order to develop an optimized growth process, many different growth conditions have been investigated. Initially, the effects of varying the incident microwave power and the growth pressure were studied. These results will be described in the first two sections. The following sections will look at the effects of substrate biasing, growth temperature, SiH₄/H₂ ratio during growth, doping the films and the addition of helium to the plasma.

6.2 Microwave Power Effects

In Chapter 3, it was shown that all four of the important plasma parameters increase in magnitude as the incident microwave power is increased. From these results, it seems likely that varying the microwave power would have a dramatic effect on the properties of the resulting films. In order to study these effects, a series of films were grown in which the incident microwave power was varied from 100 to 200 Watts. The other growth parameters are shown in Table 6.1.

Table 6.1: Growth conditions for the microwave power variation study.

Temp:	525°C
Pressure:	12 mT
Bias:	0 Volts
H ₂ flow:	47 sccm
SiH ₄ flow:	3 sccm

This was the first study done after the system construction was complete, so it was also used to verify the accuracy of the measurement techniques to be used in the remainder of this work. This verification was accomplished by first measuring all the samples with the profilometer and four point probe as described in Chapter 4, and then sending them to Solecon Labs for spreading resistance profiles.

The variation of the growth rate with power is shown in Figure 6.1. When the uncertainty in the measurements is taken into consideration, there is not any observable effect of microwave power on the growth rate under these conditions. The excellent agreement between the profilometer and the SRP measurements for the film thickness is also shown in Figure 6.1. This is a very important result because an accurate knowledge of the film thickness is required for additional characterization. The SRP for the film grown at 100 Watts is shown in Figure 6.2.

The variation of the carrier concentration with power is shown in Figure 6.3. There is very little dependence observed, and the slight increase shown is not really significant. Since there is no observable advantage to using high power levels for film growth, the majority of the films studied in the remainder of the work were grown at 100 Watts.

The final result to be presented in this section is the dependence of the growth rate on microwave power for films grown at 25 mT. This dependence is shown in Figure 6.4. This dependence was discovered while attempting to grow p-type films at high pressures. These p-type films will be discussed in Section 6.5. It is not exactly clear why the strong dependence on power arises at higher pressures, when there was essentially none at 12 mT. It is possible that the reduced mean free path at higher pressures makes the generation of a larger number of the growth species (assumed to be SiH_3) necessary. The high mean free path at the lower pressure results in the atmosphere near the growth surface being saturated with the growth species. Because of this saturation, the increase in power and corresponding generation of SiH_3 has no effect on the growth rate.

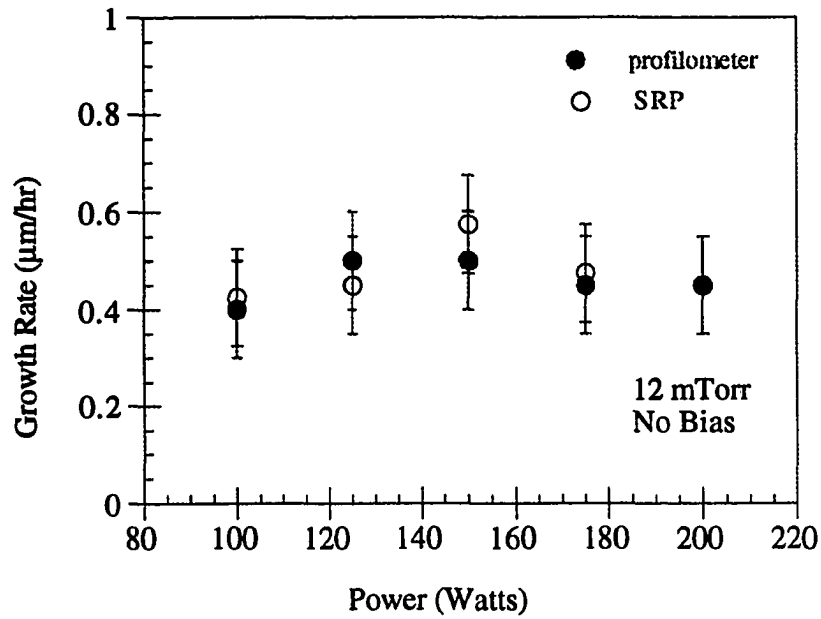


Figure 6.1: Growth rate as a function of microwave power for films grown at 12 mT.

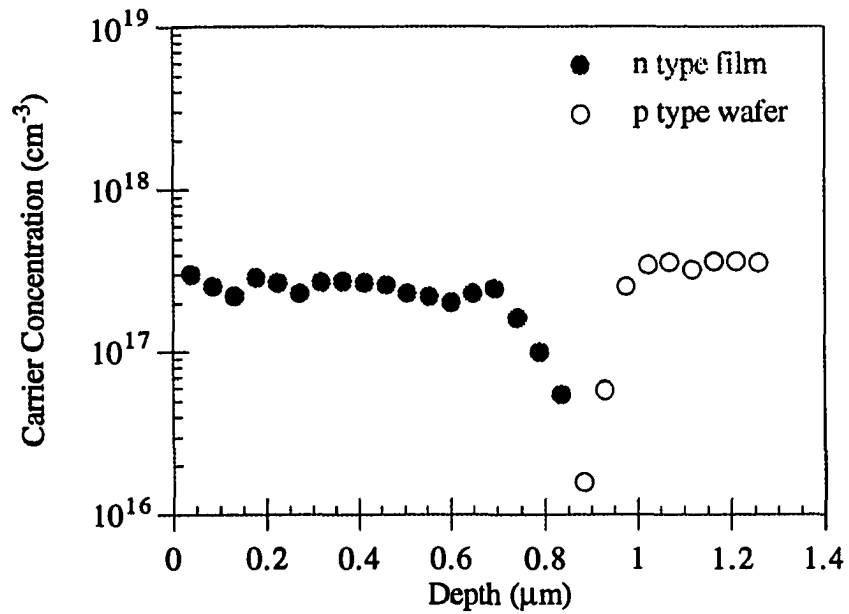


Figure 6.2: Spreading resistance profile for a silicon film grown at a microwave power of 100 Watts.

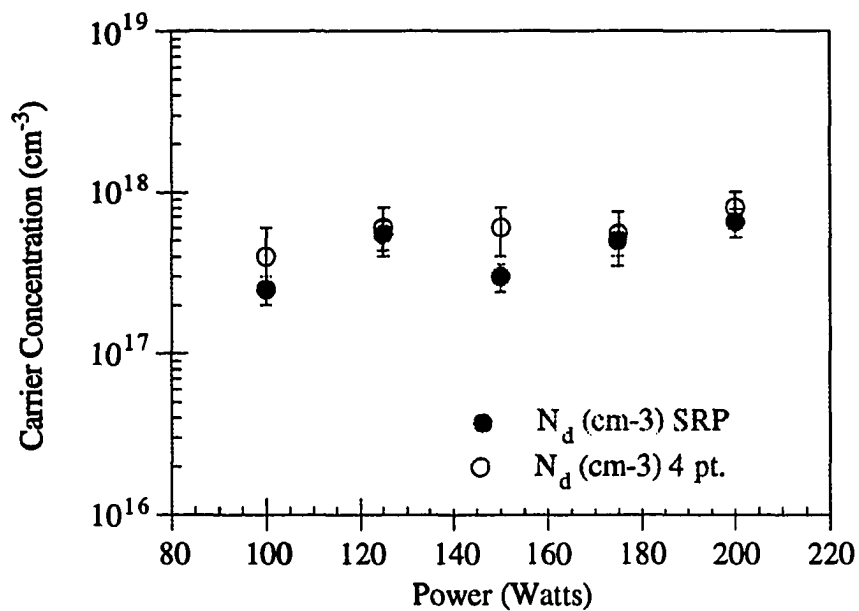


Figure 6.3: Carrier concentration as a function of incident microwave power.

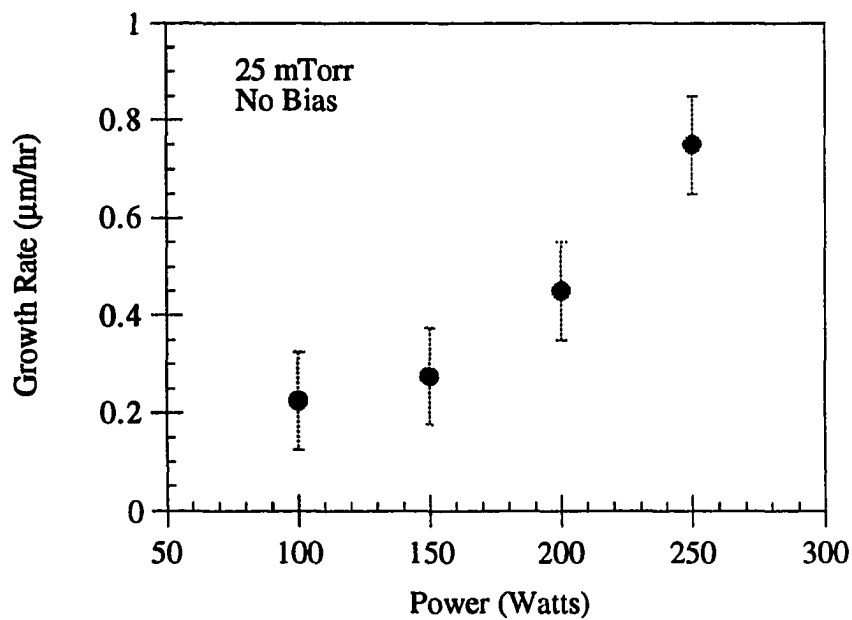


Figure 6.4: Growth rate as a function of microwave power for films grown at 25 mT.

6.3 Growth Pressure Effects

The variation of the plasma parameters with pressure was shown in Chapter 3. These results suggest that considerably different growth conditions can be achieved by varying the pressure. In order to determine a suitable pressure for epitaxial film growth, a series of films was grown at pressures between 2 and 30 mT. The other growth conditions are shown in Table 6.2.

Table 6.2: Growth conditions for the growth pressure variation study.

Temp:	475°C
Power:	100 Watts
Bias:	0 Volts
H ₂ flow:	10 sccm
SiH ₄ flow:	10 sccm

The film quality was found to be very dependent on the growth pressure. As the growth pressure was reduced below 10 mT, the resulting films became increasingly hazy. The films grown at pressures above 10 mT were specular, but the growth rate became very small at the higher pressures. The growth rate is shown in Figure 6.5. Obviously, changing the pressure allows the growth rate to be varied over a wide range. This provides flexibility to the growth process if good film quality can be maintained. Unfortunately, under the conditions used in this study, the film quality is poor at low pressures. The variation of the carrier concentration with pressure is shown in Figure 6.6. The decrease in free carriers in the films grown below 10 mT, along with the rough appearance, indicates that the films are highly defective. The films grown at pressures above 20 mT were too thin to get a four point probe measurement. The spreading resistance profile shown in Figure 6.7 is in good agreement with the four point probe measurement of the film grown at 6 mT. The ability to

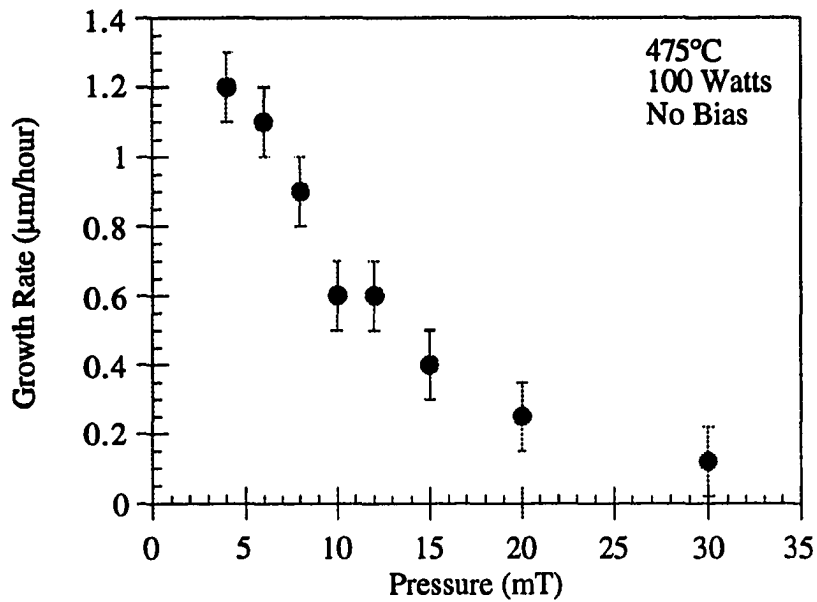


Figure 6.5: Growth rate as a function of pressure for ECR deposited silicon films.

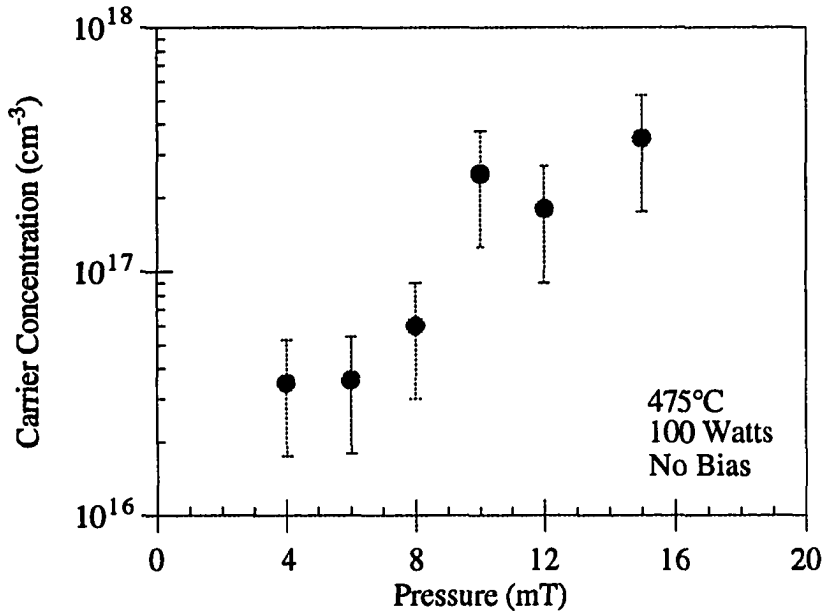


Figure 6.6: Carrier concentration as a function of growth pressure.

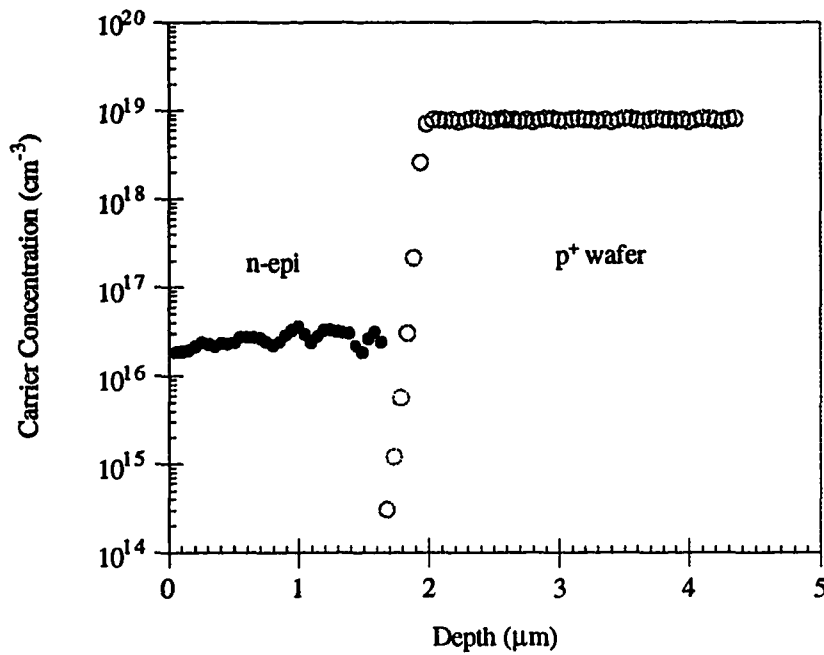


Figure 6.7: Spreading resistance profile for a silicon film grown at a pressure of 6 mT.

grow an undoped layer on a heavily doped substrate and achieve an abrupt interface is also shown by the SRP in Figure 6.7.

The results of this study indicate that under these growth conditions, a growth pressure of more than 10 mT is required for growing good quality films. It is quite likely that the pressure could be reduced if some of the other process variables were adjusted. However, since these conditions since appeared to be capable of producing acceptable films, a growth pressure of 12 mT was chosen, and the other process variables were optimized for that pressure.

6.4 Substrate Bias Effects

The fact that the plasma can be tuned by changing the pressure or microwave power was illustrated by the Langmuir probe measurements in Chapter 3. An additional method of controlling the plasma properties is by biasing the substrate with respect to the rest of the deposition chamber. This effectively allows the ion energy and flux to be adjusted to the desired level. The optimization of these parameters is an important step in the development of a suitable growth process.

In order to study the effects of substrate biasing, the films shown in Table 6.3 were grown. All the growth conditions for the films were identical, other than the bias applied to the substrate. The films were grown at 525°C, 12 mT, and 100 Watts. In certain cases it was not possible to perform some of the measurements on all the samples. For example, the -50 Volt sample was too rough and warped to get an accurate profilometer measurement, so it is not included in the growth rate results.

Table 6.3: Substrate bias study.

Sample #	111	123	118	122	116	120	121	117	127
Bias (Volts)	+10	0	-10	-15	-20	-22.5	-25	-30	-50

The first effect that is seen from this study is that the growth rate is dramatically affected by the presence of the bias voltage. This is shown in Figure 6.8. The fact that the growth rate is enhanced by negative biases and reduced for positive biases indicates that charged particles definitely play a large role in the film growth. The growth rate reduction at

positive biases is unfortunate because one way to reduce energetic ion bombardment damage is to positively bias the substrate. If an ultra high vacuum system was being used, and there was no need to maximize the growth rate, positively biasing the substrate would no doubt lead to the best quality films. However, since neither of those conditions apply in this work, the best option is to determine how much negative bias can be applied without sacrificing the material quality.

As a first test of the film quality, UV reflection was done on the films. These results are shown in Figure 6.9. The spectra for the films grown with biases of +10, 0 and -10 Volts are identical to that of a single crystal silicon wafer. As the bias is made more negative than -10 Volts, the peak heights decrease until at -50 Volts the spectra is that of polycrystalline silicon. These results apparently suggest that there is very little damage due to ion bombardment for positive biases and negative biases down to -10 Volts. As the bias is made more negative than -10 Volts, the ions have sufficient energy to begin to damage the crystal lattice. Finally, as the bias is reduced down to -50 Volts, the ion energy is sufficient to make the film polycrystalline. These results indicate that UV reflection measurements can give a very good indication of the crystalline quality of the silicon films.

Raman spectroscopy measurements have also been done on the same films for comparison to the UV reflectance results just described. The Raman results are shown in Figure 6.10. The results show very good agreement with UV reflectance. The broadening of the peak width, shown in Figure 6.10a, indicates a transition to more disordered material for biases more negative than -50 Volts. The FWHM of the peak for +10, 0 and -10 Volts is consistent with that of a crystalline silicon wafer. Figure 6.10b shows a shift in the peak position for large negative biases. This is an indication of compressive stress in the films as mentioned previously in Chapter 4.

The electronic properties of the films also show the transition from crystalline to polycrystalline material. Figure 6.11 shows the sharp increase in resistivity that occurs as the

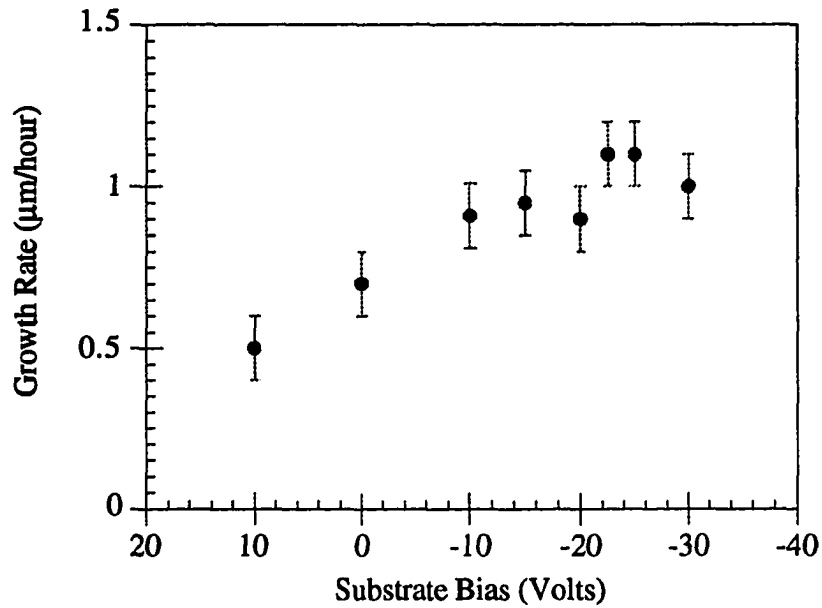


Figure 6.8: Substrate bias effects on the growth rate of ECR deposited silicon films.

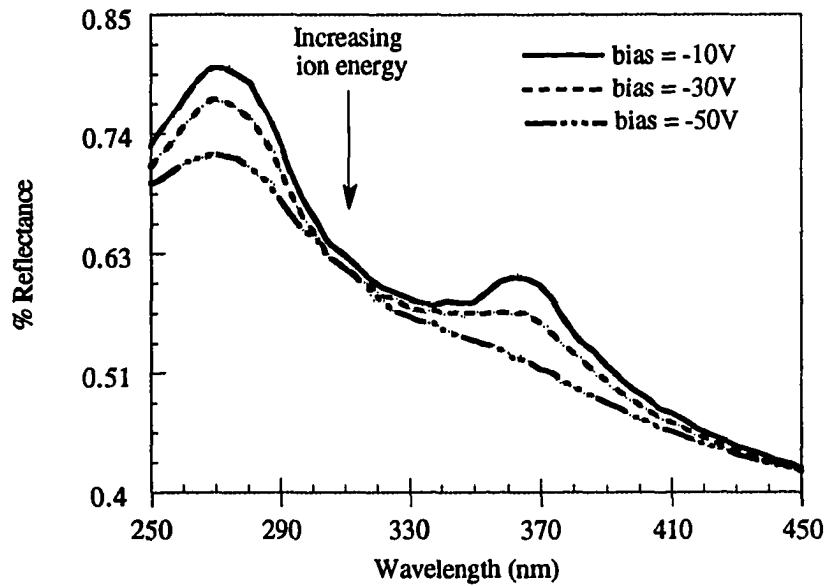
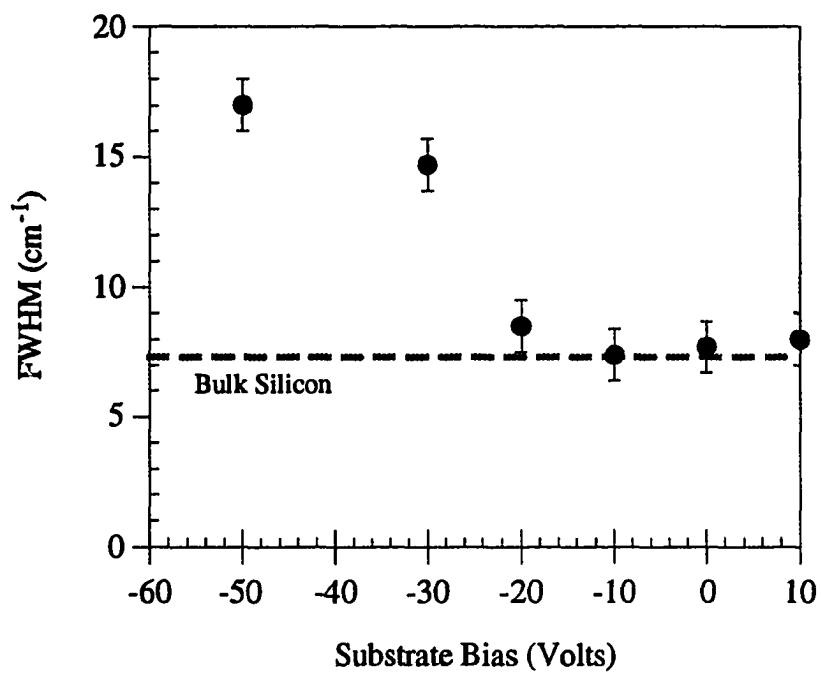
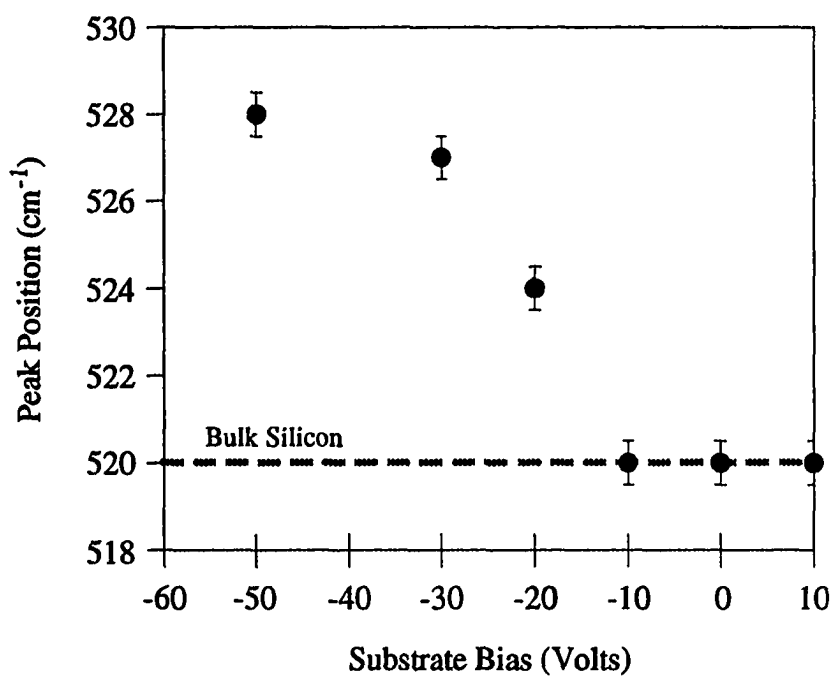


Figure 6.9: UV reflectance measurement showing the transition from crystalline to polycrystalline silicon films caused by ion bombardment damage.



a)



b)

Figure 6.10: Raman measurements showing a) the increase of the full width at half maximum (FWHM) and b) the shift in the peak position as a function of the substrate bias.

ion bombardment begins to damage the lattice, and Figure 6.12 shows the corresponding decrease in Hall mobility. This transition occurs for biases more negative than -10 Volts, just as was found from both UV reflectance and Raman measurements. While the change in material quality is easily seen from the sharp decrease in Hall mobility in Figure 6.12, it is more informative to look at the deviation of the Hall mobility from the mobility of bulk silicon ($\Delta \mu = \mu_H - \mu_{\text{Bulk}}$). This parameter gives a good indication of the material quality, and is easier to use since the films being compared in this work frequently have dramatically different resistivities. The value of μ_{Bulk} is obtained by using the free carrier concentration determined in the Hall measurement in the mobility expression given in the literature [32]. The plot of $\Delta \mu$ vs. substrate bias shown in Figure 6.13, again shows the sharp degradation in material quality for biases more negative than -10 Volts.

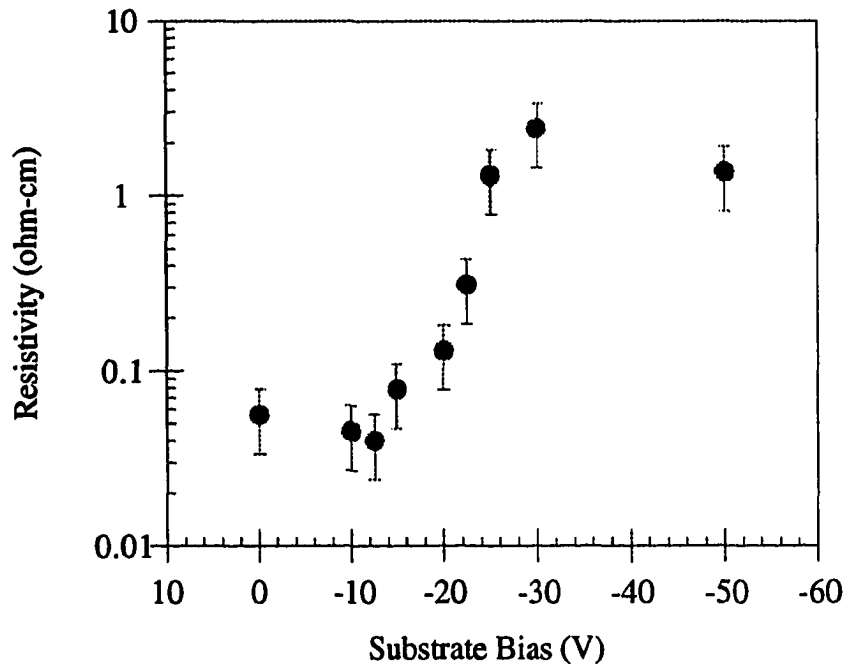


Figure 6.11: Resistivity of ECR deposited silicon films as a function of substrate bias.

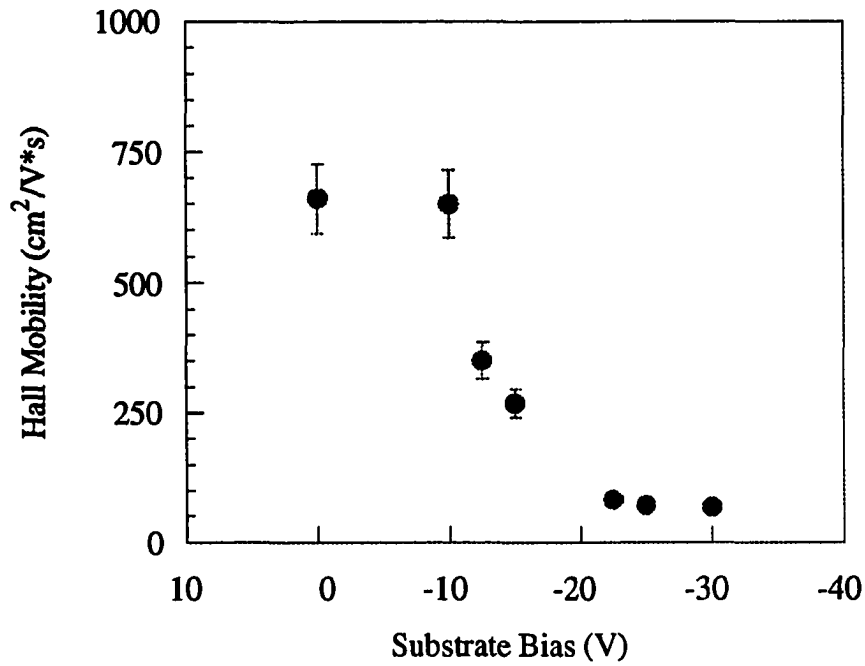


Figure 6.12: Hall mobility of ECR deposited silicon films as a function of substrate bias.

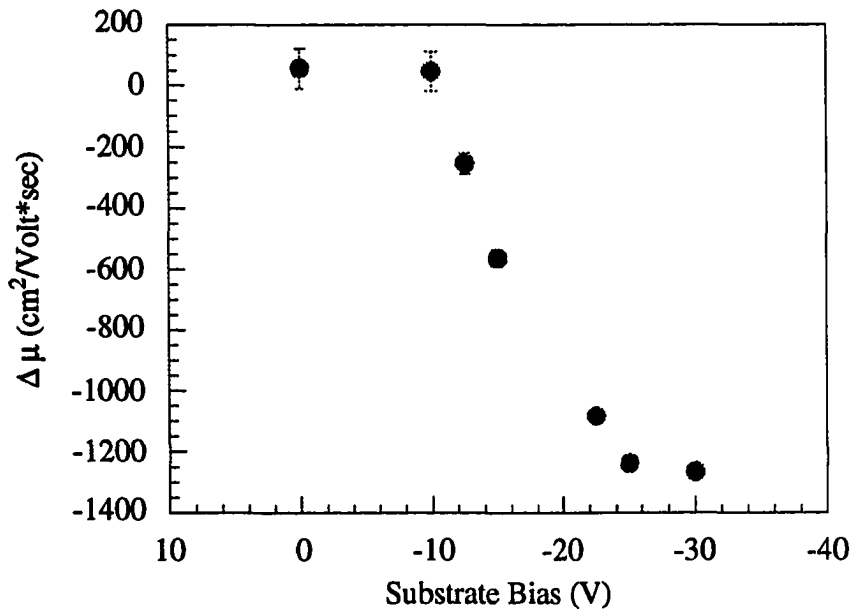


Figure 6.13: Deviation of the Hall mobility from the bulk mobility ($\Delta \mu = \mu_H - \mu_{Bulk}$) as a function of substrate bias for ECR deposited silicon films.

6.5 Growth Temperature Effects

One of the main goals of this work is to grow good quality epitaxial silicon films at the lowest temperature possible in this deposition system. As the temperature is reduced, the material quality is expected to degrade due to the decrease in surface mobility, the increase in carbon and oxygen contamination, and the decrease in the desorption rate of hydrogen from the surface. In order to study the effect of reducing the growth temperature, a TEM study was done on two films grown at different temperatures. Following the TEM study, two sets of films were deposited under very different conditions. The first samples were undoped films grown under similar conditions to the films in the previous section. The second set of samples were doped p-type and grown at a much higher pressure and power.

6.5.1 TEM Study

The first step taken in the study of the growth temperature was the growth of two films under identical conditions except that one was grown at a substrate temperature of 475°C and the other at 525°C. These two temperatures were chosen because at the time they were the lower and upper temperature limits for specular film growth. The electronic properties measured for the films were very similar. The mobilities of the films were not measured. The films were 1.2 - 1.5 μm thick and had resistivities between 0.06 and 0.1 ohm-cm. The hydrogen plasma clean in each case was done at the same temperature as the growth. Transmission electron microscope images for the two films are shown in Figure 6.14. The imaging conditions were the same in both cases. The fact that the dislocations in the 475°C film originate at the interface indicates that the plasma clean does not effectively remove carbon and oxygen from the wafer surface at the lower temperature. The film grown at 525°C did not have any observable defects. These results suggest that it may be possible to grow good quality films by performing the plasma clean at 525°C and then reducing the

a)

b)

Figure 6.14: TEM images of epitaxial silicon films grown at a) 475°C and b) 525°C.

temperature for film growth. In practice this is accomplished by turning down the temperature controller to the desired growth temperature just as the film growth begins. It then takes 2-5 minutes for the wafer temperature to drop from 525°C to the reduced growth temperature. This procedure has resulted in the growth of specular films at much lower temperatures. Another noteworthy result from the images in Figure 6.14 is the absence of surface roughening at the interface due to the hydrogen plasma exposure. The epitaxial nature of the films was verified using convergent beam electron diffraction (CBED). This was done by observing that there was no change in the diffraction pattern as the beam was moved from the wafer into the film. The CBED pattern for the (011) zone axis of the film is shown in Figure 6.15. High resolution TEM imaging was also used to verify that the films were epitaxial, but unfortunately the pictures did not turn out.

6.5.2 Undoped Films

As previously mentioned, these films were grown under similar conditions to the films in the substrate biasing study in Section 6.4. The films were grown on 0.005-0.02 ohm-cm p-type silicon (100) wafers. The wafer preparation procedure outlined in the previous chapter was used. Films were grown at temperatures between 325-525°C. The other growth conditions are shown in Table 6.4.

The substrate bias of -10 Volts was chosen in order to increase the surface mobility by increasing the energy of the incoming ions. In the previous chapter it was determined that

Table 6.4: Growth conditions for undoped films.

Pressure:	12 mT
Power:	100 Watts
Bias:	-10 Volts
SiH ₄ flow:	10 sccm
H ₂ flow:	32 sccm

Figure 6.15: Convergent beam electron diffraction pattern for an epitaxial silicon film grown at 525°C.

the bias could not be made more negative than -10 Volts without introducing damage. The growth rate for all the temperatures investigated was the same (0.8 $\mu\text{m}/\text{hour}$).

The properties of the films change dramatically as the substrate temperature is varied. The change in the crystal structure is shown in the Raman results in Figure 6.16. At a growth temperature of 325°C, the material shows both the polycrystalline peak at 520 cm^{-1} and the broad peak at 480 cm^{-1} which is characteristic of a-Si. This indicates that either there are two different phases present in the region of the sample which was measured (10x400 μm), or possibly the grain size is just slightly larger than amorphous material. In either case, this growth temperature is definitely right at the transition between amorphous and polycrystalline material. At a growth temperature of 375°C, the width of the peak at 520 cm^{-1} indicates that the film is polycrystalline. The 520 cm^{-1} peak for the film grown at 475°C is very nearly identical to the peak measured for a crystalline silicon wafer. The FWHM for the wafer was 7.4 cm^{-1} , as shown in Section 6.4. The fact that the peaks for all three temperatures are at 520 cm^{-1} indicates that there is no stress in the films.

The reflectance results shown in Figure 6.17 also show the increase in crystalline quality as the growth temperature is increased. The spectra for the 325°C film has only a slight bump at 280 nm. This is again an indication that the film has very little crystal structure. The films grown at 475°C and 525°C both have spectra that are not distinguishable from that of a single crystal silicon wafer.

The electronic properties of the films show the same improvement with increasing growth temperature, as seen in the Raman and UV reflection. The increase in resistivity as the growth temperature is reduced, shown in Figure 6.18, is an obvious result of the reduced grain size. This also results in the free carrier concentration being very low for the films grown at low temperatures as seen in Figure 6.19. The error bars in both of these graphs reflect the uncertainty in the thickness measurement using the profilometer. The final uncertainty in the carrier concentration is taken to be 50%, due to the rather crude method by

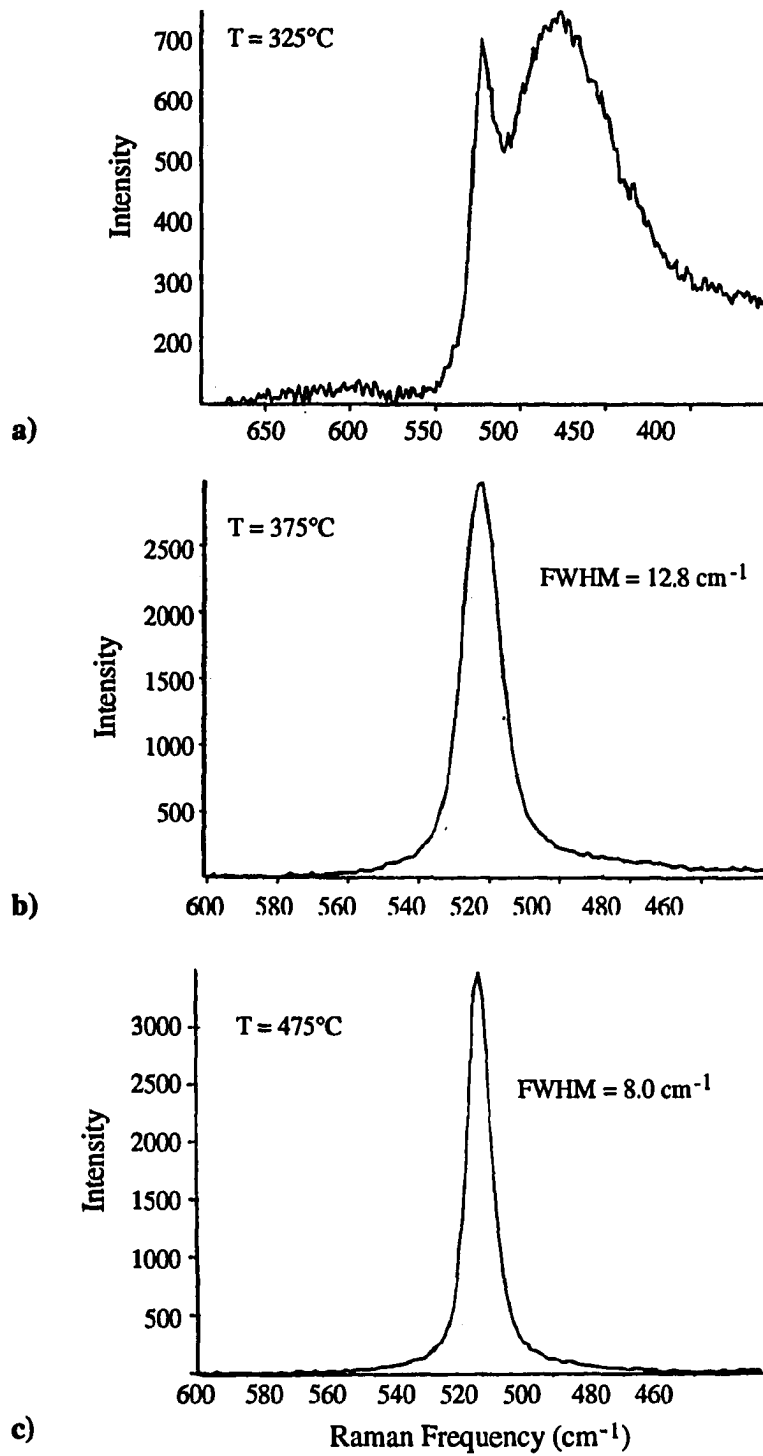


Figure 6.16: Raman spectra showing the transition to improved crystal quality with growth temperature; a) 325°C , b) 375°C and c) 475°C .

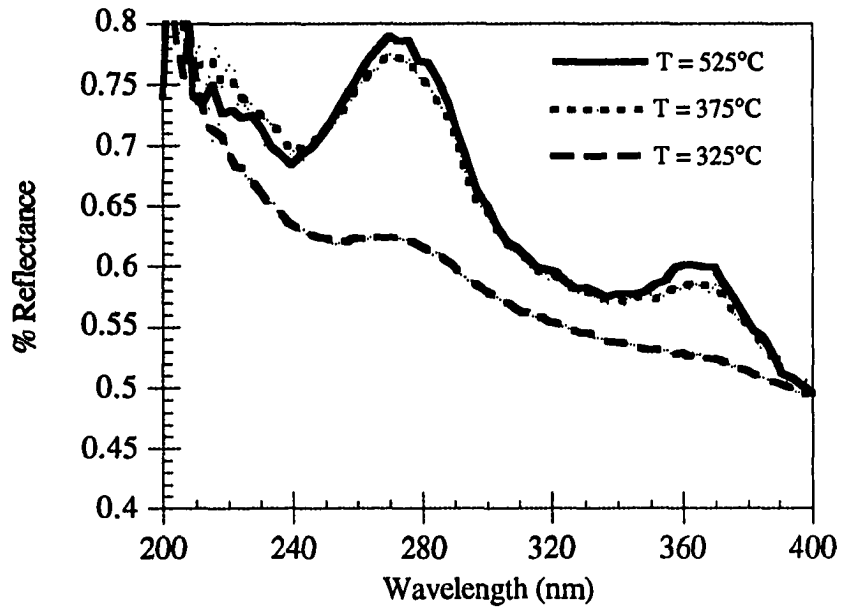


Figure 6.17: Reflectance spectra showing the improved crystal quality with increased growth temperature. The result for the film grown at 525°C is identical to the spectra seen for a single crystal silicon wafer.

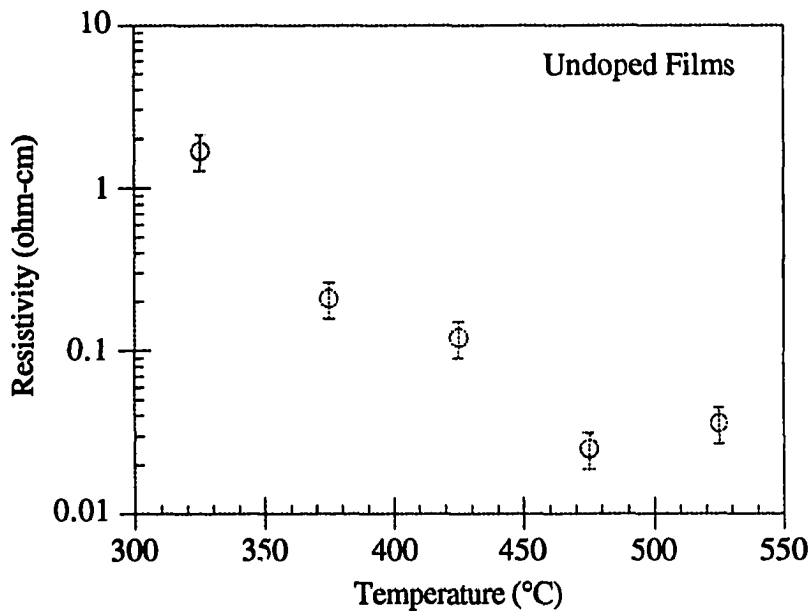


Figure 6.18: Resistivity variation as a function of growth temperature.

which it is determined.

Measurements of the Hall mobilities of these samples show that the films grown at 475°C and 525°C have mobilities comparable to bulk silicon. The deviation of the measured mobility from that of bulk silicon for the same resistivity is shown in Figure 6.20. The sharp decrease in mobility for films grown at temperatures below 475°C again indicates the material is becoming polycrystalline. The error bars in this graph correspond to an estimated 20% error in the result from Hall measurement. This error is primarily due to uncertainty in the magnetic field measurement.

6.5.3 P-type Films

These films were planned and measured by Randy Bartels and myself as part of his summer research project in the NSF program. They were grown under very different conditions than previously used, primarily because they were the only ones that resulted in p-type films. The growth conditions for the films are shown in Table 6.5. The dopant gas used for these films was 1000 ppm B₂H₆ diluted in hydrogen. When the usual growth pressure and power (12 mT, 100 Watts) were used, the films turned out n-type despite the presence of the diborane. The only condition which was found to consistently produce p-type films was growth at higher pressure. The main problem with this was that the growth rate was always

Table 6.5: Growth Conditions for p-type films.

Pressure:	25 mT
Bias:	-10 Volts
SiH ₄ Flow:	10 sccm
H ₂ Flow:	32 sccm
1000 ppm B ₂ H ₆ Flow:	10 sccm

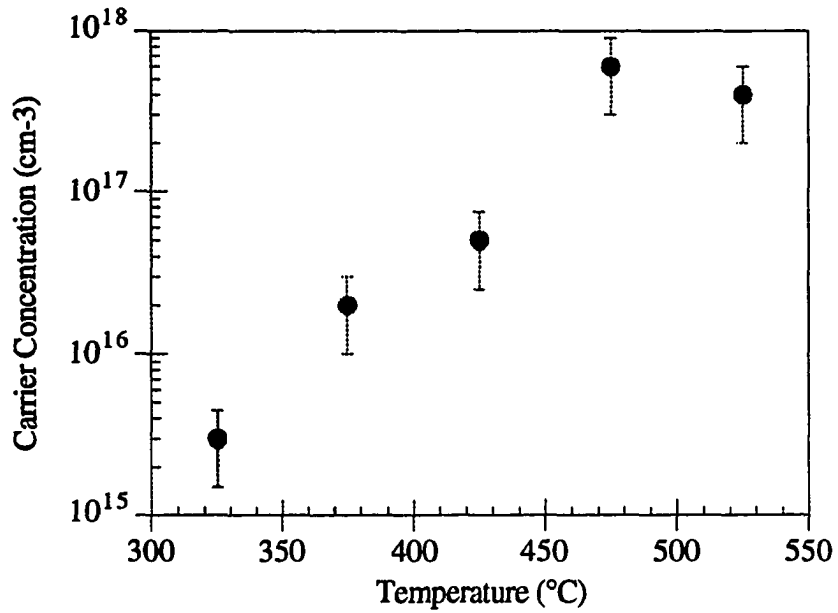


Figure 6.19: Free carrier concentration in undoped films as a function of growth temperature.

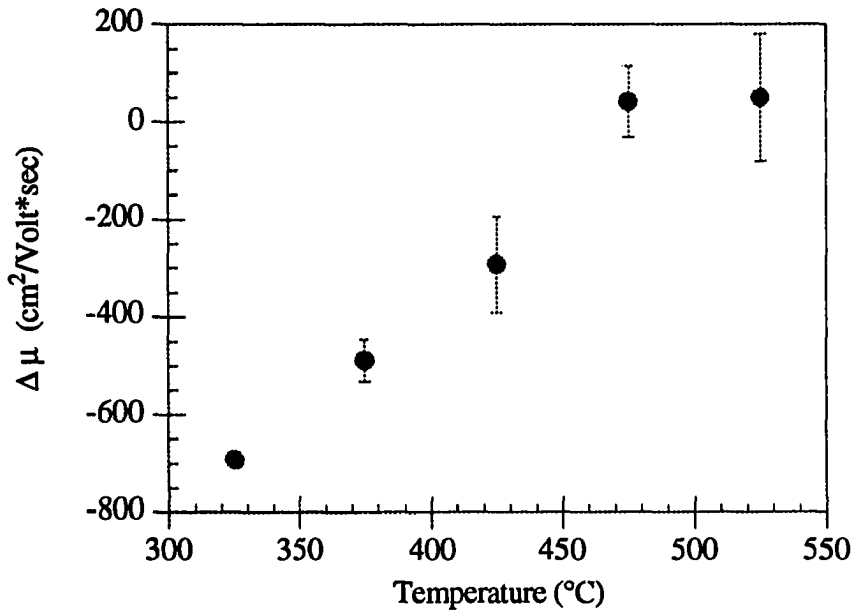


Figure 6.20: Deviation of the Hall mobility from the bulk mobility as a function of growth temperature ($\Delta \mu = \mu_{\text{Hall}} - \mu_{\text{Bulk}}$).

extremely small ($<1000 \text{ \AA}/\text{hour}$) at the pressures required, as seen in Section 6.2. In order to increase the growth rate, the power was increased to 200 Watts. This resulted in a more acceptable growth rate of $4000 \text{ \AA}/\text{hour}$.

The results from the measurements of the electronic properties of the films provided some interesting results. The resistivity of the films is plotted versus the growth temperature in Figure 6.21. From this graph it is apparent that the resistivity of the p-type films varies in the opposite direction from the undoped films, which decreased with increasing growth temperature. An explanation for this behavior is that the boron tends to congregate along the grain boundaries in the low temperature films and cause them to be more conductive. The exponential increase in the free carrier concentration at low temperatures, shown in Figure 6.22, definitely indicates that either more boron is incorporated, or more of it is electrically active in the low temperature films. Figure 6.23 shows the variation of the mobility as the

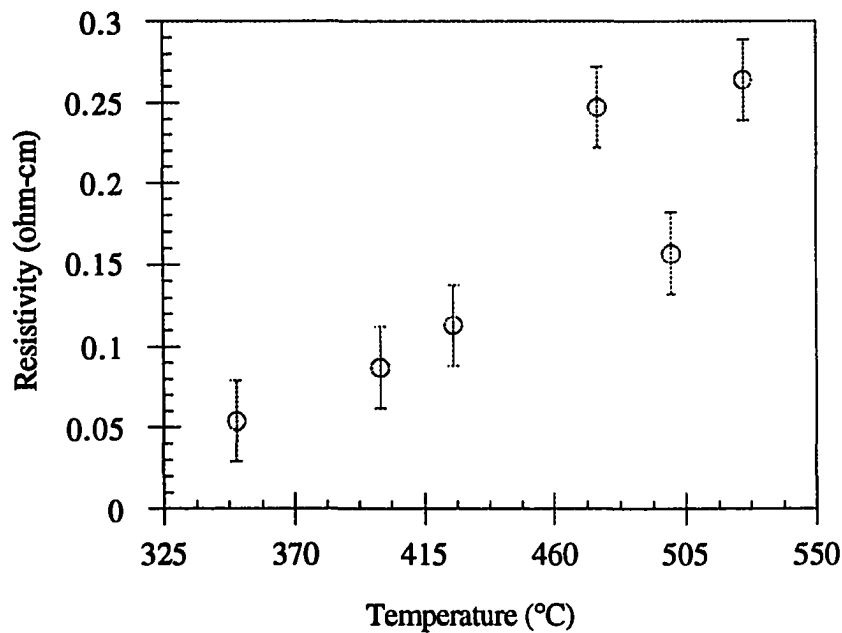


Figure 6.21: Resistivity of p-type films as a function of growth temperature.

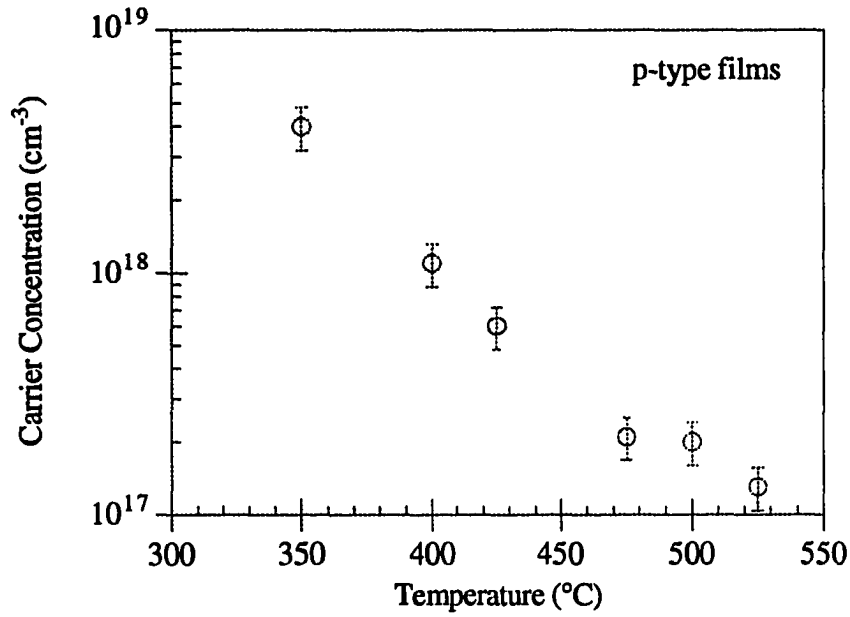


Figure 6.22: Free carrier concentration in p-type films as a function of growth temperature.

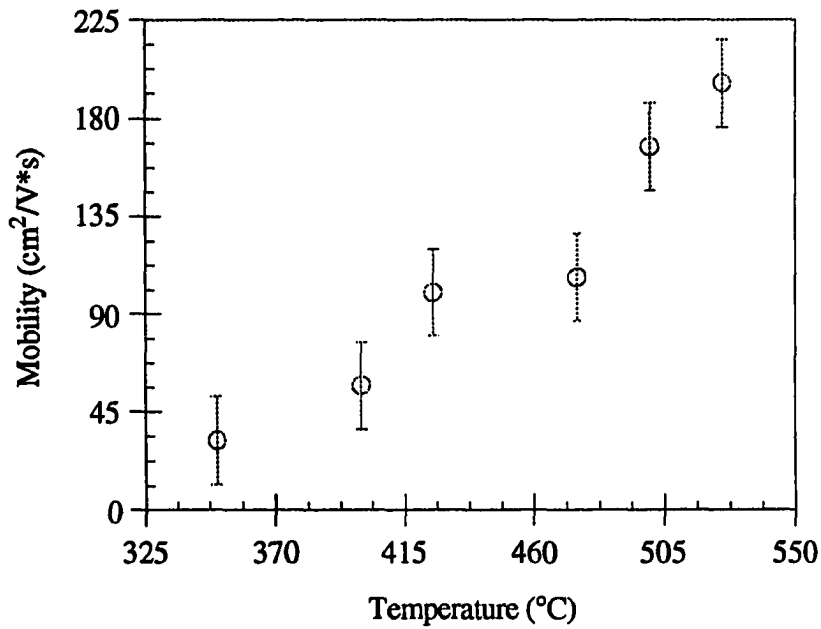


Figure 6.23: Hall mobility in p-type films as a function of growth temperature.

temperature is increased. The mobility is seen to grow approximately linearly with the deposition temperature. This result was expected since the crystalline quality is improving as the growth temperature is increased. However, all of the films have mobilities that are between 90 and 130 $\text{cm}^2/\text{Volt}\cdot\text{sec}$ lower than the bulk value for the corresponding resistivity. This is a good indication that these growth conditions are not suitable for growing high quality epitaxial p-type films. The solution to this problem lies in changing the dilution level of the diborane, and that will be discussed in Section 6.7.

6.6 Effect of the $\text{H}_2:\text{SiH}_4$ Ratio

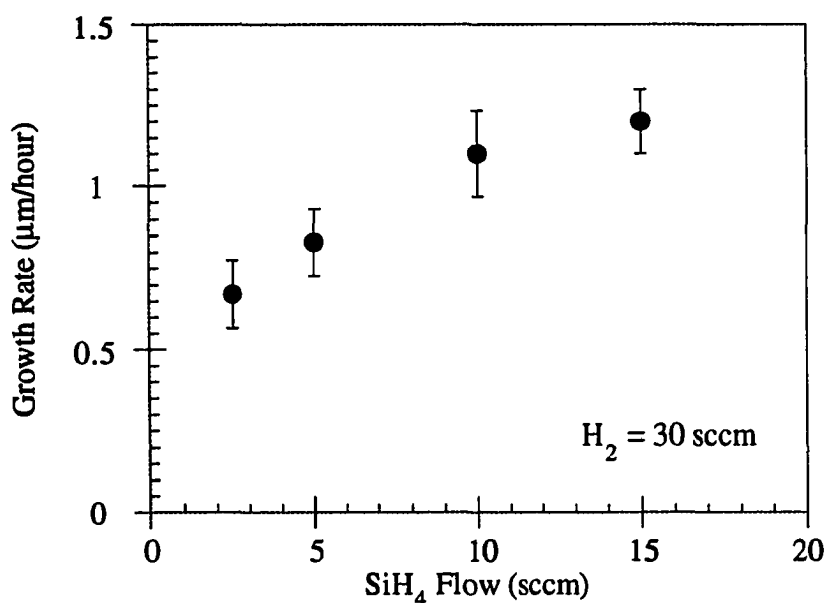
In order to grow good quality material, the proper ratio of hydrogen to silane must be determined. A pure hydrogen plasma is known to etch away silicon as well as removing carbon and oxygen from the surface. This results in there being an optimized ratio of hydrogen to silane. When the $\text{H}_2:\text{SiH}_4$ ratio is too high, the growth rate is suppressed due to the etching of silicon by the hydrogen in the plasma. As the $\text{H}_2:\text{SiH}_4$ ratio is decreased, eventually there is not enough hydrogen to etch away the non-crystalline silicon bonds forming on the surface. This will result in the degradation of the film quality for $\text{H}_2:\text{SiH}_4$ ratios below some level. In order to study the effect of changing the $\text{H}_2:\text{SiH}_4$ ratio, a set of films were grown. All the growth conditions for these films were identical, except the SiH_4 flow was varied. Table 6.6 shows these growth conditions.

The reduction in the growth rate for increased hydrogen dilution is shown in Figure 6.24. From this graph, it would seem that the answer to optimizing the growth rate is simply to use a pure silane plasma. However, the beneficial effects of higher hydrogen dilution become apparent when the electronic properties of the films are measured. Figure 6.25 shows the increase in resistivity that occurs as the hydrogen dilution is decreased. The

Table 6.6: Growth conditions for H₂:SiH₄ ratio effect study.

Sample #	SiH ₄ flow (sccm)	Common Growth Parameters	
198	2.5	H ₂ flow:	30 sccm
199	5	Temperature:	525°C
200	10	Bias:	-10 Volts
201	15	Pressure:	12 mT
		Power:	100 Watts

resistivity measurements by the two different techniques are in very good agreement. The increase in resistivity at low hydrogen dilution levels is in agreement with the idea that more of the non-crystalline silicon bonds remain under these conditions. The fact that indeed the material is becoming polycrystalline is seen by looking at the mobilities of the films. Figure 6.26 shows the deviation of the measured film mobilities from the mobility of bulk silicon of the same resistivity. This graph shows that there is an optimum H₂:SiH₄ ratio for growing high quality epitaxial silicon films in this system.

**Figure 6.24:** Growth rate as a function of SiH₄ flow for ECR deposited silicon films on p⁺-Si (100) wafers. The flow rate of hydrogen in each case is 30 sccm.

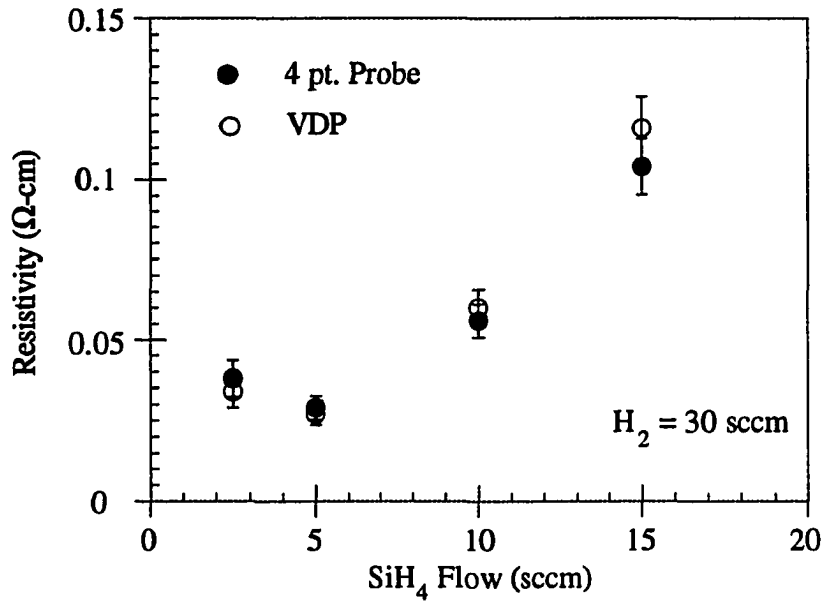


Figure 6.25: Resistivity as a function of SiH₄ flow for ECR deposited silicon films on p⁺-Si (100) wafers. The flow rate of hydrogen in each case is 30 sccm.

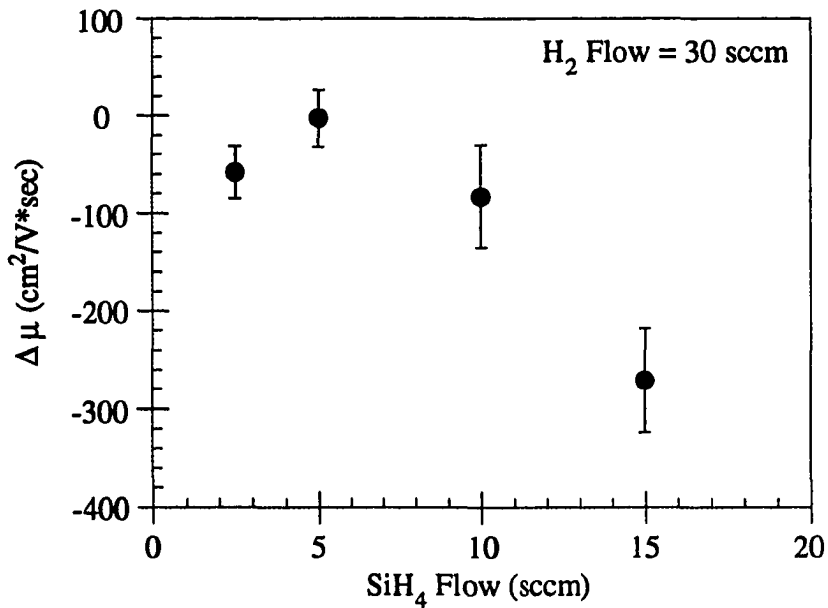


Figure 6.26: Deviation from bulk silicon mobility as a function of SiH₄ flow for ECR deposited silicon films on p⁺-Si (100) wafers. The flow rate of hydrogen in each case is 30 sccm.

6.7 Growth of Doped Films

The growth of doped films will be of great importance for future work involving devices. There are obviously many things that could be studied regarding the effects of the addition of the dopant gas during growth. The detailed study of doped films will be left for the time when the specific device structures desired are known. The results in this section verify that both n-type and p-type crystalline silicon films can be grown in this system.

Table 6.7: Growth conditions for n-type films.

	<u>undoped</u>	<u>PH₃ Doped</u>
Temp:	525°C	525°C
Power:	100 Watts	100 Watts
Pressure:	12 mT	12 mT
Bias:	0 Volts	0 Volts
H ₂ flow:	47 sccm	30 sccm
SiH ₄ flow:	3 sccm	3 sccm
PH ₃ in H ₂ : (100 ppm)	0 sccm	17 sccm

The doping levels in the films were primarily determined by the dilution level of the dopant gas. The growth conditions for phosphorous doped films are shown in Table 6.7. The large hydrogen:silane ratio during growth is a result of the high dilution level of the phosphine (100 ppm). At least 10-15 sccm of hydrogen is always passed into the source region of the chamber through the plasma manifold. This causes the plasma in the source region to be primarily composed of hydrogen and reduces the amount of silane that diffuses back into the source region. When enough 100 ppm PH₃ (in hydrogen) to effectively dope the film is added to this plasma hydrogen, there is a large amount of hydrogen in the chamber. This large flow of H₂ is too much for the turbo pump on the system to handle, so the silane flow rate has to be reduced in order to keep the growth pressure at 12 mT. The net

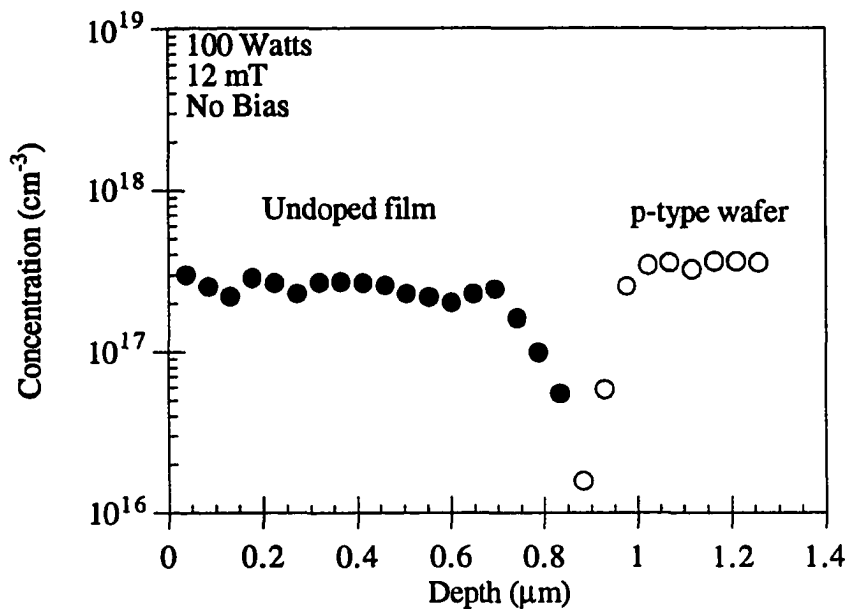
result is a high $H_2:SiH_4$ ratio. The effect of the phosphorous doping is shown in Figure 6.27. The two films shown in this figure were grown under identical conditions. The presence of the PH_3 is shown to increase the carrier concentration by an order of magnitude.

The growth of p-type films using 10 ppm diborane in hydrogen has already been discussed in Section 6.5. The process required high pressure and power, and still resulted in a low growth rate and poor quality films. In order to grow p-type films under conditions closer to those found to produce the best undoped films, the 10 ppm diborane was replaced with 1% B_2H_6 in hydrogen. The new growth conditions for p-type films are shown in Table 6.8. These conditions were found to be very effective for growing heavily doped p-type films with abrupt junctions. This is illustrated by the SRP shown in Figure 6.28. This

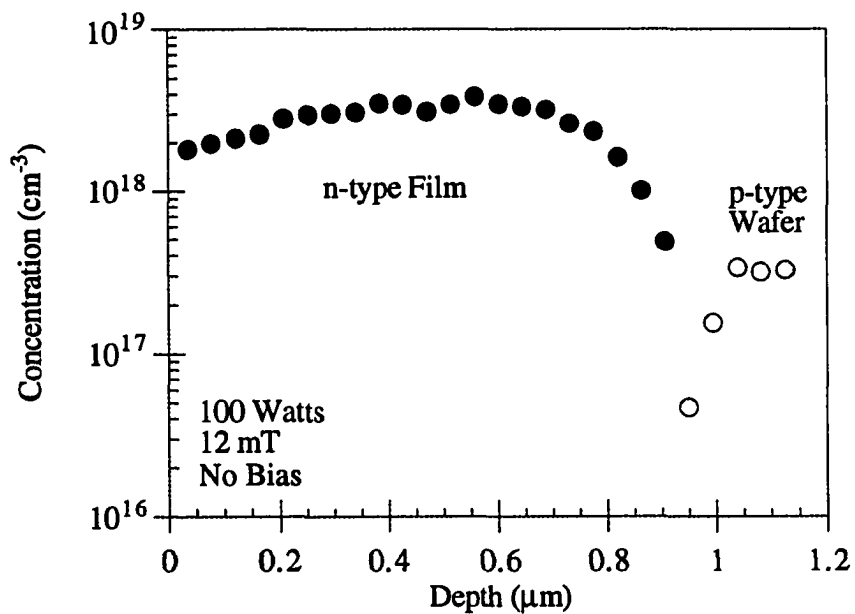
Table 6.8: Growth conditions for p-type films.

	<u>undoped</u>	<u>B_2H_6 Doped</u>
Temp:	525°C	525°C
Power:	100 Watts	100 Watts
Pressure:	12 mT	12 mT
Bias:	-10 Volts	-10 Volts
H_2 flow:	32 sccm	22 sccm
SiH_4 flow:	3 sccm	3 sccm
B_2H_6 in H_2 : (1%)	0 sccm	10 sccm

figure shows the effect of adding the diborane after growing an undoped film. The hydrogen flow was held at 32 sccm after the 1% diborane was turned on by reducing the plasma hydrogen flow to 22 sccm. This allowed the growth conditions to remain constant other than the addition of the diborane. This growth process resulted in much better films than the earlier high pressure method. The films were specular and the growth rate was approximately $0.8 \mu\text{m}/\text{hour}$. Reflection measurements confirmed that the crystalline quality of the films was good.



a)



b)

Figure 6.27: SRP measurements for a) an undoped silicon film and b) a phosphorous doped film grown under the same conditions.

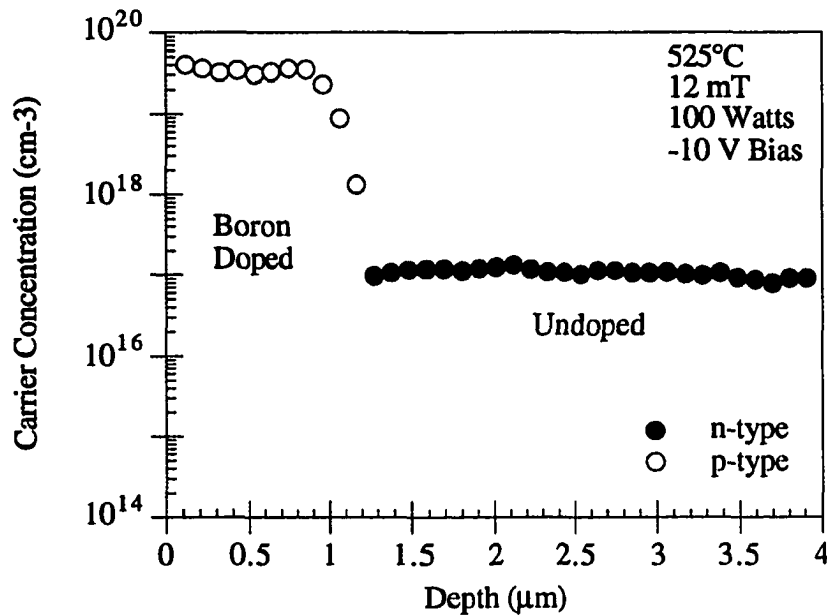


Figure 6.28: SRP measurement showing the extremely abrupt interface between an undoped film and a heavily doped p-type film.

6.8 Helium Dilution Effects

The presence of helium in the plasma has been found, both by our group [33] and other authors [34], to increase the growth rate of amorphous silicon films. The exact mechanism for this growth rate enhancement is still not completely clear. Optical emission spectroscopy (OES) measurements have been done to compare silane and hydrogen plasmas to silane and helium plasmas [35]. These results have investigated the effect of helium dilution on the SiH* emission. They have found the emission intensity of SiH* to be consistently larger for the helium diluted plasmas. It is safe to assume that the increase in SiH* is accompanied by an increase in the amount of SiH₂ and SiH₃* being generated in the plasma. This increase in

the species responsible for growth results in the growth rate enhancement mentioned previously.

The increased production of silane fragments may be caused by the metastable state of helium which has an energy of 19.8 eV. This state is thought to be very efficient at transferring energy to the silane, which has an activation energy less than 5 eV[36]. The Langmuir probe measurements in Chapter 3 indicated that the electron temperature and plasma density are higher for a helium plasma than a hydrogen plasma. These properties are also likely to play a role in the enhanced growth rate.

In order for helium dilution to be useful for the work done here, it must provide both a substantial increase in the growth rate and also produce good quality crystalline silicon films. The effect of adding helium to the plasma has been studied by comparing films grown with and without helium present. The films were grown under conditions which were previously determined to produce good quality material. The growth conditions for the film grown without helium were; 12 mT, 100 Watts, -10 Volts bias, 525°C, 10 sccm SiH₄ and 32 sccm H₂. The only difference for the second film was that an additional 10 sccm of helium was present during growth. The resulting properties of the films are shown in Table 6.9.

The addition of helium has obviously altered the resulting films properties. The growth rate has been increased significantly as anticipated. Both films appeared smooth, and there was no haze present on either film. The higher resistivity in the second film may be the

Table 6.9: Helium dilution effects.

Helium flow (sccm)	Growth rate (μm/hour)	Resistivity (ohm-cm)	Mobility (theory) (cm ² /Volt•sec)	Mobility (Hall) (cm ² /Volt•sec)
0	0.8	0.048	607	656
10	1.5	0.095	776	603

result of reduced oxygen incorporation at the higher growth rate. The mobility is reduced in the film grown in the presence of helium. This mobility reduction is even more significant when it is compared to the theoretical value of mobility for the measured resistivity. Despite this reduction, the value of $603 \text{ cm}^2/\text{Volt}\cdot\text{sec}$ is still one of the highest measured for films grown in this system, and in some cases the enhanced growth rate may be important enough to sacrifice some of the material quality.

VII. CONCLUSIONS

The development of a process for the low temperature ($< 600^{\circ}\text{C}$) growth of epitaxial silicon is an important technological issue. In this dissertation, a process has been developed and optimized for epitaxial silicon growth in a high vacuum electron cyclotron resonance plasma deposition system. This process development consisted of several different components which were described in the previous chapters. The first components were the construction and characterization of the ECR system. This was followed by the determination of the useful material characterization techniques, and the development of a suitable wafer cleaning procedure. Finally, the effects of varying several different process variables were systematically studied.

The system construction took place between the Fall of 1992 and the Fall of 1993. In addition to the construction of the deposition chamber and gas handling system, this involved putting in ventilation ducts, and running water and nitrogen lines into the room. Safety and compactness were emphasized in the design and construction of the laboratory.

The system was carefully characterized before film growth was started. First, the magnetic field profiles were measured for all the possible magnet settings, and one arrangement of magnet currents and three stub tuner settings was found which resulted in very stable growth conditions. Next, the behavior of the plasma was investigated using Langmuir probe measurements. The results of these measurements were used to help determine the best conditions both for the hydrogen plasma clean and for film growth. The most important thing the Langmuir probe measurements provided was a general understanding of how the plasma was affected when the pressure or microwave power was changed. Finally, the wafer temperature was calibrated as a function of the heater

temperature in order to get an accurate measurement of the substrate temperature during growth.

The wafer cleaning procedure prior to growth was found to be extremely critical for the growth of good quality epitaxial silicon films. The cleaning procedure used in this work consisted of two parts. First, a standard RCA clean followed by a dip in dilute HF was done. This procedure left the wafer surface passivated with hydrogen. The second part to the cleaning procedure was a hydrogen plasma clean done at 525°C. This cleaning procedure was found to effectively prepare the wafer surface for epitaxial growth.

The first process parameter which was studied was the incident microwave power. This was found to have almost no effect in the range studied for films grown at 12 mT. However, when the growth pressure was increased to 25 mT, the growth rate was shown to increase rapidly with increasing microwave power. This study was also used to verify that excellent agreement could be achieved between the four-point probe and profilometer measurements done at Iowa State, and the SRP measurements done by Solecon Laboratories.

The second process parameter studied was the growth pressure. The growth rate was found to increase rapidly as the pressure was reduced. This result was anticipated from the increase in the current density at low pressures seen in the Langmuir probe measurements. The results from the film characterization indicated that the best quality crystalline films were grown at pressures above 10 mT. This led to the choice of 12 mT as the growth pressure used in the majority of the rest of the work done.

The study of the effects of substrate biasing provided some of the most interesting results found in this work. Substrate biasing was used to control the energy of the incident ions during growth. As the bias was made more negative, the ions eventually gained enough energy to begin to damage the crystalline lattice. This resulted in a transition in the film structure from single crystal material to polycrystalline material for biases more negative than -10 Volts. This transition was verified independently by Raman spectroscopy, UV

reflectance, resistivity and Hall mobility measurements. The Hall mobilities measured for the films grown at 0 and -10 Volts were consistent with bulk silicon ($656 \text{ cm}^2/\text{Volt}\cdot\text{sec}$ for a free carrier concentration of $2 \times 10^{17} \text{ cm}^{-3}$). The -10 Volt growth process used in this study produced the best quality films of any grown in this system. The -10 Volt bias was superior to no bias because there was a significant growth rate enhancement due to the negative bias. These results were presented at the First World Conference on Photovoltaic Energy Conservation on December 7, 1994 in Hawaii [36].

The study of growth temperature effects also provided interesting results. This study was especially important since reducing the growth temperature is the major goal of this work. It was determined that good quality epitaxial silicon films could be grown at temperatures as low as 475°C . The effect of the growth temperature on the crystal quality was especially evident from the transition shown by the Raman results in Figure 6.16. The transition was also evident from the UV reflectance and the measurements of the films electronic properties.

The effect of the ratio of hydrogen to silane present in the system during growth was also found to be significant. This result was not unexpected since the hydrogen is thought to provide beneficial etching during growth. The results of this study indicated that the presence of either too much or too little hydrogen during growth results in the deterioration of the film quality. Mobilities consistent with bulk silicon were again obtained when the conditions were optimized.

The growth of doped films will be important to any future device work to be done using this growth process. The growth of both n-type and p-type epitaxial silicon films on silicon wafers has been demonstrated. The interface between the film and the heavily doped wafer it was grown on has been shown, from spreading resistance profiles, to be very abrupt.

The final study done in this work looks at the effects of adding helium to the plasma during growth. The reason for the addition of helium was the possibility of an increased

growth rate. The results found here indicate that the presence of helium does indeed significantly increase the growth rate. The optimized growth rate without helium is 0.8 $\mu\text{m}/\text{hour}$ and with helium the growth rate is increased to 1.5 $\mu\text{m}/\text{hour}$. However, the quality of the resulting films was also found to be somewhat lower, as indicated by a reduced Hall mobility (603 $\text{cm}^2/\text{Volt}\cdot\text{sec}$). In some cases the enhanced growth rate may be worth the reduction in material quality.

Overall, the major goals of this research project have been successfully accomplished. A new ECR plasma deposition laboratory has been constructed, and the low temperature growth of epitaxial silicon films has been systematically studied. While this system is not necessarily scalable for production, the results from this work are very relevant to any plasma assisted growth process for epitaxial silicon. The flexibility of the ECR plasma deposition system allows many of the important process parameters to be tuned, and is therefore a very useful tool for process development and research.

REFERENCES

- [1] H.M. Liaw and J. Rose, in *Epitaxial Silicon Technology*, edited by B. Baliga (Academic Press Inc., New York, 1986).
- [2] D. Mui, S. Fang and H. Morkoc, *Appl. Phys. Lett.* **59**, 1887 (1991).
- [3] B. Myerson, *Appl. Phys. Lett.* **48**, 797 (1986).
- [4] B. Myerson, F. LeGoues, T. Nguyen and D. Harama, *Appl. Phys. Lett.* **50**, 113 (1987).
- [5] B. Myerson, F. Himpsel and K. Uram, *Appl. Phys. Lett.* **57**, 1034 (1990).
- [6] T. Donahue and R. Reif, *J. Appl. Phys.* **57**, 8 (1985).
- [7] S. K. Ghandhi, *VLSI Fabrication Principles* (John Wiley and Sons, New York, 1983).
- [8] J.H. Comfort and R. Reif, *J. Electrochem. Soc.* **136**, 2386 (1989).
- [9] J.H. Comfort and R. Reif, *J. Electrochem. Soc.* **136**, 2398 (1989).
- [10] M. Liehr, C. M. Greenlief, S. R. Kasi and M. Offenbergl, *Appl. Phys. Lett.* **56**, 629 (1990).
- [11] R. Knox, V. Dalal and O. Popov, *J. Vac. Sci. Technol. A* **9**, 474 (1991).
- [12] B. Moradi, R. Knox and V. Dalal, *J. Vac. Sci. Technol. A* **12**, 251 (1994).
- [13] H. Tae, S. Hwang, S. Park, E. Yoon and K. Whang, *Appl. Phys. Lett.* **64**, 1021, (1994).
- [14] C. Khattak and K. Ravi, *Silicon Processing for Photovoltaics II* (Elsevier Science Publishing Co., New York, 1987).
- [15] O. Popov, *ECR Plasma Sources and their use in Thin Film Deposition*, currently unpublished.
- [16] P. Lorrain and D. Corson, *Electromagnetic Fields and Waves*, 2 ed. (Freeman and Company, San Francisco, 1970).
- [17] R. S. Crandall, B. P. Nelson, P.D. Moskowitz, and V. M. Fthenakis, NREL Safety Analysis Report, July 1992.
- [18] Kettani and Hoyaux, *Plasma Engineering* (John Wiley and Sons, New York, 1973).

- [19] F. Chen, in *Plasma Diagnostic Techniques*, edited by R. Huddleston and S. Leonard (Academic, New York, 1965).
- [20] G. Harbeke, in *Polycrystalline Semiconductors*, edited by Harbeke (Springer-Verlag, New York, 1985), p. 160.
- [21] B. Moradi, Ph.D. Dissertation, Iowa State University, 1993.
- [22] ASTM Standard F672, *1988 Annual Book of ASTM Standards* (Am. Soc. Test. Mat., Philadelphia, 1988).
- [23] ASTM Standard F110, *1988 Annual Book of ASTM Standards* (Am. Soc. Test. Mat., Philadelphia, 1988).
- [24] D. K. Schroder, *Semiconductor Material and Device Characterization* (John Wiley and Sons, New York, 1990), pp. 2-20.
- [25] ASTM Standard F374, *1988 Annual Book of ASTM Standards* (Am. Soc. Test. Mat., Philadelphia, 1988).
- [26] R. C. Jaeger, *Introduction to Microelectronic Fabrication* (Addison-Wesley, New York, 1993), p. 60.
- [27] ASTM Standard F76, *1988 Annual Book of ASTM Standards* (Am. Soc. Test. Mat., Philadelphia, 1988).
- [28] R. Anderson, S. Klepeis, J. Benedict, W. Vandygrift, and M. Orndorff in *Microscopy of Semiconducting Materials 1989*, edited by A. Cullis and J. Hutchison (Institute of Physics, New York, 1989), pp. 491-500.
- [29] N. Huashita, M. Kinoshita, I. Aikawa, and T. Ajioka, *Appl. Phys. Lett.* Vol. **56**, 451 (1990).
- [30] S. Kasi, M. Liehr, P. Thiry, H. Dallaporta, and M. Offenbergl, *Appl. Phys. Lett.* **58**, 1378 (1991).
- [31] M. Ishii, K. Nakashima, I. Tajima and M. Yamamoto, *Appl. Phys. Lett.* **58**, 1378 (1991).
- [32] G. Baccarani and P. Ostoja, *Solid-State Electronics* **18**, 579 (1975).
- [33] J. Knights, R. Lujan, M. Rosenblum, R. Street, D. Biegleson, J. Reimer, *Appl. Phys. Lett.* **38**, 331 (1981).
- [34] R. Patel, D. Olsen, J. Shirck and N. Tran, in *Material Research Society Proceedings*, **70**, 55 (1986).
- [35] T. Bell, K. Perkins and P. Perkins, *J. Phys. Chem.* **88**, 116 (1984).
- [36] S. DeBoer and V. Dalal in *Proceedings of the First World Conference on Photovoltaic Energy Conversion*, 1994.

ACKNOWLEDGMENTS

I would like to thank the many people that have played a very important part in the completion of this project. I am very grateful to my major professor, Dr. Vikram Dalal, for giving me the wonderful opportunity to build my own laboratory, and for having the confidence in me to let me do independent work. I would also like to thank Dr. Stanley Burns, Howard Shanks, Dr. Gary Tuttle and Dr. Scott Chumbley for serving on my committee. I would also like to thank Dr. George Chumanov for the Raman measurements and Dr. Scott Chumbley for his help with the TEM work.

I would like to thank William Catron for the financial support provided during the past two years and the Department of Education for financial support during my first two years at the Microelectronics Research Center.

I am very grateful to Dr. Ralph Knox for the many times he provided advice, and for his friendship during my stay at the MRC. I could never have built the lab without his knowledge and experience in a wide variety of areas. I would also like to thank Michael Thomas, Mark Leonard, Sanjeev Kaushal, Russ Bruhn, Greg Baldwin and my father for their help in building the lab, and for their friendship.

Special thanks are due to Mike Stoops for his advice during the construction of the system and for the late nights at the machine shop. Thanks also go to my sister, Kathi Stoops, for letting Mike spend the late nights helping me, and for making our time in Ames special. I would like to thank my mom and dad for their support and guidance during my many years in school.

Finally, I would like to thank my wife, Jennifer DeBoer, for her support, patience and love during my years in graduate school. The completion of this work is an accomplishment we share together.

APPENDIX A. ELECTRON MOTION IN A STATIC MAGNETIC FIELD

Free electrons in the plasma generation region spiral around the static magnetic field lines, due to the Lorentz force.

$$\dot{\mathbf{F}} = q(\dot{\mathbf{v}} \times \dot{\mathbf{B}}) \quad (\text{A-1})$$

If we assume that $\dot{\mathbf{B}} = B_o \hat{\mathbf{a}}_z$, this can be written as shown in Equation A-2.

$$m \frac{d^2x}{dt^2} \hat{\mathbf{a}}_x + m \frac{d^2y}{dt^2} \hat{\mathbf{a}}_y + m \frac{d^2z}{dt^2} \hat{\mathbf{a}}_z = qB_o \left(v_y \hat{\mathbf{a}}_x - v_x \hat{\mathbf{a}}_y \right) \quad (\text{A-2})$$

By equating components, we get the results shown in Equation A-3.

$$m \frac{d^2x}{dt^2} = qB_o v_y \quad m \frac{d^2y}{dt^2} = -qB_o v_x \quad m \frac{d^2z}{dt^2} = 0 \quad (\text{A-3})$$

Now by integrating with respect to t, we get Equation A-4.

$$\frac{dx}{dt} = \frac{qB_o y}{m} + C_1 \quad \frac{dy}{dt} = -\frac{qB_o x}{m} + C_2 \quad \frac{dz}{dt} = C_3 \quad (\text{A-4})$$

The result in Equation A-4 can be put back into Equation A-3 to get separated differential equations. For example, the equation for x is

$$\frac{d^2x}{dt^2} + \omega_o^2 x = x_o \omega_o^2 \quad (\text{A-5})$$

where $\omega_o = \frac{qB_o}{m}$ and $x_o = \frac{C_2}{m\omega_o}$. The solution to this equation is

$$x = x_o + R \cos(\omega_o t + \phi) \quad (\text{A-6})$$

where R and F are the constants of integration. By taking the derivative of Equation A-6 we get the x-component of the velocity.

$$v_x = \frac{dx}{dt} = -R\omega_o \sin(\omega_o t + \phi) \quad (\text{A-7})$$

This result can then be substituted back into Equation A-4 in order to get

$$y = y_o - R \sin(\omega_o t + \phi) \quad (\text{A-8})$$

and

$$v_y = \frac{dy}{dt} = -R\omega_o \cos(\omega_o t + \phi) \quad (\text{A-9})$$

where $y_o = \frac{C_1}{m\omega_o}$. Now if we square and add Equations A-6 and A-8 we see that the motion of the electron in the plane perpendicular to the magnetic field is circular with radius R.

$$(x - x_o)^2 + (y - y_o)^2 = R^2 \quad (\text{A-10})$$

From Equations A-7 and A-9 we can solve for the radius.

$$R = \frac{\sqrt{v_x^2 + v_y^2}}{\omega_o} = \sqrt{v_x^2 + v_y^2} \left(\frac{m}{qB_o} \right) \quad (\text{A-11})$$

Since the velocity of the electron in the z-direction (parallel to the magnetic field) is constant, the electron spirals around the z-axis with a frequency of

$$\omega_o = \frac{qB_o}{m} \quad (\text{A-12})$$

and a radius given by Equation A-11 above.

APPENDIX B. MAGNET DESIGN

Table B.1: Materials required for construction of magnets.

3/16" OD soft Cu tubing
12 Gauge magnet wire (Rated at 200°C)
Aluminum spools
Stainless steel support rods
Aluminum support frame

Calculation of magnetic field

The magnets are arranged in a Helmholtz coil configuration as shown below. In this set-up the distance between the coils (d), is the same as the effective radius of the coils (a). This arrangement gives a uniform B-field in the z -direction.

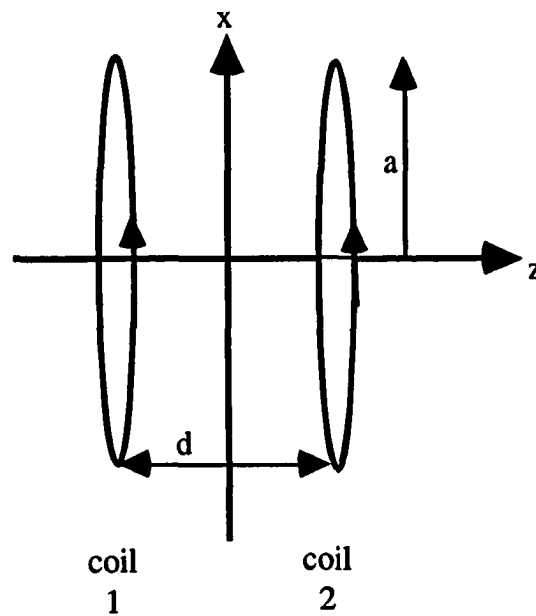


Figure B.1: Helmholtz coil arrangement.

The field between the coils is given by

$$B = \frac{NI\mu_0}{d\left(\frac{5}{4}\right)^2} \quad (\text{B-1})$$

where

N = number of turns per coil = 972 turns

I = current in coil = 20 Amps (max),

d = distance between coils = effective radius of coil = 5" = 0.127m

This results in a maximum B-field of 1375 Gauss. The ECR condition requires 870 Gauss, so this design is high by a safe amount.

Materials Calculations

Since the average radius is 5", the amount of wire needed per coil is

$$L_w = 2\pi\left(\frac{5}{12} \text{ ft}\right)(972 \text{ turns}) = 2545 \text{ ft}$$

the resistance per coil is

$$R = \frac{2545 \text{ ft}}{517 \text{ ft}/\Omega} = 4.92 \Omega$$

the power that must be dissipated per coil for $I = 20$ Amps is about 2 kW. We are using 20 Amps in all our calculations because that is the maximum amount we can safely run through the 12 gauge wire. The power supply for each coil must be able to supply 100 V and 20 Amps.

The amount of Cu tubing per coil is (7 layers)(6 turns/layer)(2.62 ft/turn) = 110 ft.

Construction Procedure

The magnet wire was cut into 450 ft. sections. The wire was then wrapped onto the spools 6 wires at a time. After each 3 layers of wire a layer of copper tubing was spiraled on.

Swagelock fittings were used for connecting the copper tubing.

A rotometer was put in the water line so that the magnet power supplies could not be turned on if the cooling water was not flowing through the magnets. The design of the support structure for the magnets is shown below.

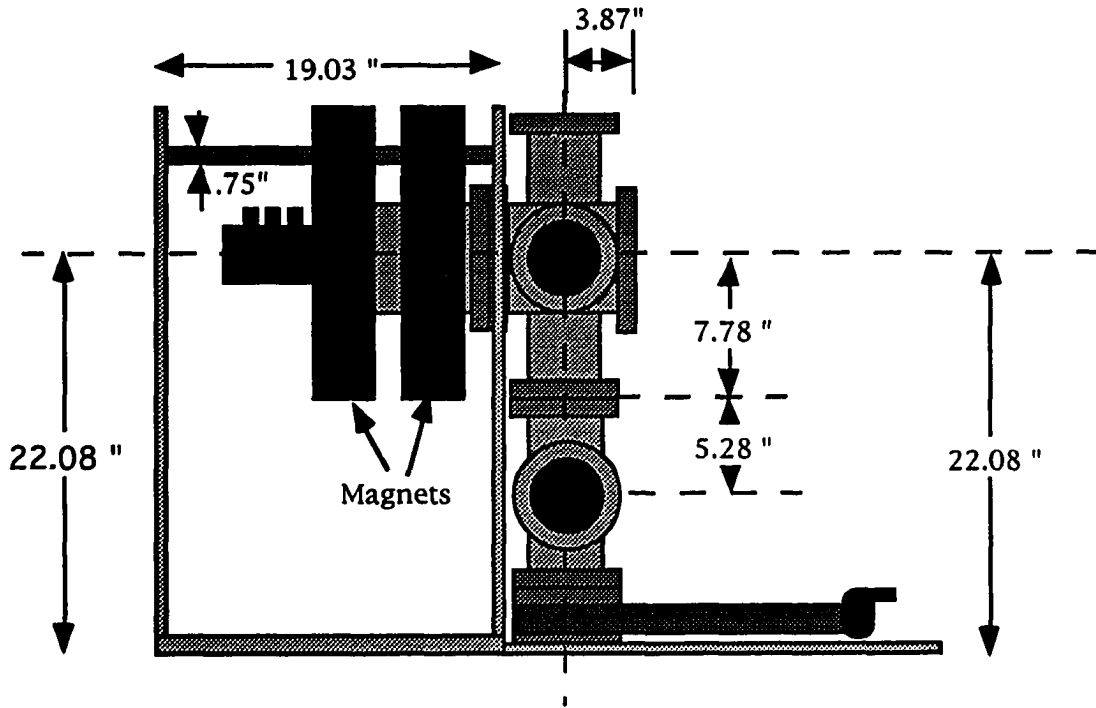


Figure B.2: Diagram of the support structure constructed for the magnets.

APPENDIX C. STANDARD OPERATING PROCEDURE

Film Growth

- 1) Cleave wafer (2 samples per wafer).
- 2) RCA clean followed by a 30 second 50:1 HF dip.
- 3) Fill out the gas log book.
- 4) Put on dust-free gloves.
- 5) Place sample on heater and tighten screws evenly with fingers.
- 6) Close gate valve over turbo pump.
- 7) Vent chamber. Remove pressure release kwik flange. Leave N₂ on until heater is lowered into system. Slide shutter in front of sample.
- 8) Turn off N₂. Replace kwik flange. Open roughing valve.
- 9) Connect power line and thermocouple probe. Swing cooling fan over top of heater. Press the **M** button on the temperature controller. Verify the thermocouple is down in the hole.
- 10) When Baratron turns on, close the roughing valve and open the gate valve.
- 11) Turn on the safety N₂.
- 12) Turn the key switch on.
- 13) Flip the all cylinders switch on. Turn on the desired manifold switches.
- 14) Verify the MFC's are all set to off, and then turn on the switches for the gases that will be used in the run. This pumps out the lines back to the MFC's.
- 15) Turn on the ion gauge and wait until the pressure falls below 10⁻⁶ Torr. Then turn ion gauge off and zero the Baratron gauge.
- 16) Turn the gas switches on the control board off except for H₂.
- 17) Set the H₂ MFC to the desired level (32 sccm) and switch it to manual. Adjust pressure with the gate valve to approx. 50 mTorr.

- 18) Turn on both magnet power supplies. If they stay at 0 V, 0 Amps the water is off. Do Not adjust the current levels (10.8 Amps Front, 13.5 Amps Rear) or the 3-stub tuner, these have been optimized.
- 19) Turn on the forward and reflected power meters. Left meter is reflected (0-10V = 0-150 Watts) and right meter is forward power (0-10V = 0-300 Watts).
- 20) Turn the line knob on the microwave generator from the 0 to the 1 position. The white light will come on and the green ready light will come on.
- 21) Push the green button to turn the microwaves on. The black knob adjusts the power level. The reflected power should drop down near zero (10-50 mV). If P_r does not pressure to the desired level with the gate valve.
- 22) Push the arrow up button on the temperature controller to set the desired temperature. Wait for the temperature to stabilize after reaching the set point (5 min.). The order of the steps reflects the fact that a low power H_2 plasma is generally run during temperature ramp up (with the shutter covering the sample).
- 23) When turning on additional gases, first turn on the switch on the gas control board, then switch the MFC to manual (this eliminates blasts of gas entering the system since the lines were previously pumped out).
- 24) When the shutter is open, close the shutter gate valve to avoid contamination. Never leave the shutter open when B_2H_6 or PH_3 is in the chamber.

Cool Down Procedure

- 1) Turn off the microwaves, magnets and microwave power meters.
- 2) Turn off all gases except H_2 and use gate valve to adjust the pressure to approximately 50 mTorr.
- 3) Change the set point on the temperature controller to $< 20\text{ }^\circ\text{C}$ (Takes 1.5 hours to cool from $650\text{ }^\circ\text{C}$ to $100\text{ }^\circ\text{C}$).
- 4) Open the shutter gate valve and push the shutter in.

Sample Removal

- 1) Turn off: H_2 switch, Final solenoid switches, All cylinders and the key switch.
- 2) Once the system pressure is $<10^{-5}$ Torr, close the gate valve and turn on the vent N_2 .
- 3) Remove the over-pressure release kwik flange when the system is up to atm. pressure. Leave the N_2 flowing while the sample is being removed.

- 4) **Disconnect the heater power line and the thermocouple connection. Lift the sample holder out of the chamber.**
- 5) **Immediately put the blank ASA cap flange on the system, turn off the N₂, replace the over-pressure kwik flange and open the roughing valve.**
- 6) **When the Baratron comes on scale, close the roughing valve and open the gate valve over the turbo pump.**
- 7) **Remove the sample from the holder and put the holder back in the chamber by repeating Steps 2-4.**

**APPENDIX D. PAPER ACCEPTED FOR PUBLICATION
IN APPLIED PHYSICS LETTERS**

Low Temperature Epitaxial Silicon Film Growth Using High Vacuum Electron Cyclotron Resonance Plasma Deposition

Scott J. DeBoer and Vikram L. Dalal
Dept. of Electrical and Computer Engineering, Iowa State University, Ames, Iowa 50011

George Chumanov
Dept. of Chemistry, Iowa State University, Ames, Iowa 50011

Randy Bartels
Dept. of Electrical and Computer Engineering, Oklahoma State University, Stillwater,
Oklahoma

Abstract

In this paper, we report on the growth technique and electrical properties of epitaxial Si films grown at low temperatures using an electron-cyclotron-resonance plasma deposition technique. We have used standard high vacuum apparatus to grow high quality films at 450-525 °C. A critical step in achieving high quality films is an in-situ hydrogen plasma cleaning of the wafer before growth. We have systematically studied the influence of ion bombardment during growth by biasing the substrate, and find that the films are crystalline for substrate bias voltages less negative than about -15 V, but become polycrystalline as the magnitude of the negative bias is increased. The crystallinity of the film was measured using Raman spectroscopy. The undoped films are n-type with carrier concentrations in the 10^{16} - 10^{17} cm⁻³ range. The Hall mobilities measured for the films are comparable to values obtained in bulk Si crystals. We can achieve abrupt profiles in carrier concentrations between the heavily doped substrate and the epi layer, with no evidence of diffusion.

Low temperature epitaxial growth of silicon is of significant current interest due to its potential for making devices with small feature sizes.⁽¹⁾ A low growth temperature (400-700 °C) prevents the deleterious effects of auto-doping from the substrate and lateral diffusion from contacts. To achieve such a low temperature growth, various techniques, such as ultrahigh vacuum chemical vapor deposition (UHV-CVD)^(1,2), very low pressure CVD⁽³⁾, plasma enhanced CVD⁽⁴⁾ and low pressure UHV electron-cyclotron-resonance (ECR) CVD⁽⁵⁻⁸⁾ have been used. The advantages of ECR-CVD are the low particulate production in the reactor, enhanced growth rate at low temperatures and the ability to control plasma potentials, and hence ion bombardment of the substrate, during growth. In this paper, we report on a systematic study of conditions leading to the growth of very high quality Si films using a controlled, low pressure ECR plasma of silane and hydrogen at low temperatures (450-525 °C).

The growth apparatus is similar to the one used in previous work by Mui et al⁽⁸⁾, and Tae et al.⁽⁶⁾ However, unlike these previous authors, we did not use a UHV system, but merely a standard high vacuum system equipped with O-rings, which is much more representative of a production environment. The system has previously been described in detail.⁽⁹⁾ The base pressure in the system, pumped with a turbo-pump, is in the range of $5-9 \times 10^{-8}$ Torr. These vacuum conditions require the growth rate to be maximized in order to reduce the incorporation of impurities as previously described by Comfort and Reif.⁽³⁾ Most of the current techniques for growing epitaxial silicon films below 600 °C require UHV conditions due to their extremely low growth rates ($< 1 \text{ \AA}/\text{sec}$).^(2, 5-8) In contrast, the enhanced surface mobility of radicals due to ion bombardment in the ECR plasma allows typical growth rates of more than $3.5 \text{ \AA}/\text{sec}$ to be achieved. The growth rate in this type of system is very sensitive to the process conditions, especially the pressure, and silane to hydrogen ratio. The system is a remote plasma type, with the electron resonance point being approximately 15 cm

away from the substrate. We used hydrogen as the plasma gas, with a typical flow rate of 30 sccm. Silane was introduced close to the substrate at a flow rate of 10 sccm, thus giving a dilution ratio of H_2/SiH_4 of 3:1. We found the H_2/SiH_4 ratio to be a very important parameter in determining the film quality. Further reduction of the dilution ratio leads to rough polycrystalline films while increasing the ratio leads to a reduction in the growth rate. We have deposited specular films at pressures between 6 and 50 mT and at temperatures between 425 and 600 °C. The upper limit to the growth temperature regime has previously been attributed to the rapid desorption of hydrogen, leaving the surface unprotected from contamination during growth.⁽¹⁰⁾ The substrate was introduced into the chamber by using a virtual load lock system, where the system was flooded with nitrogen during the few seconds it took to load the substrate into the chamber. The chamber was equipped with a shutter, so that the system could be plasma cleaned before the growth of the epitaxial layer without depositing on the substrate. This same plasma cleaning was also found to be useful between the growth of doped and undoped layers, so as to minimize any cross-contamination between multiple layers of a device.⁽¹¹⁾

We monitored the electron temperatures, plasma densities and plasma potentials next to the substrate by using Langmuir probe measurements. A single disk Langmuir probe was used to collect the data. The measurement procedure has been outlined previously.⁽¹²⁾ Typical results for the plasma parameters are shown in Figure 1. It is clear that as the pressure is decreased there is an increase in both the electron temperature and the ion bombardment energy, which can be roughly estimated by the plasma potential shown in Figure 1a. The maximum observed in the plasma density in Figure 1b is consistent with previous results⁽¹³⁾ and has been found to be the optimum condition for hydrogen plasma removal of surface contamination. Our substrate can be biased with respect to the chamber walls during growth,

allowing us to control the energy of the incident ions. We have studied the influence of this bias voltage on the structural and electrical properties of silicon films.

Before introducing the Si wafers into the system, they were cleaned with a standard RCA process which leaves a thin protective oxide on the surface of the wafer. Just prior to the introduction of the wafers into the chamber, they were dipped into a 50:1 H₂O:HF solution. This etch was used to remove the thin oxide layer and to leave the wafer surface passivated with hydrogen. If this HF dip was not used, the films turned out to be polycrystalline with rough surfaces. This observation is consistent with the model proposed by Meyerson⁽¹¹⁾ that H passivation is the critical step in achieving successful low temperature epitaxial growth of Si. We have varied the dilution and the duration of the HF dip, and found no significant effect on film quality, so long as the resulting surface was hydrophobic.

After introduction of the wafers into the reactor and pumping down and heating cycles, the wafers were etched using a hydrogen plasma from the ECR source. This hydrogen plasma etch was found to be important in achieving reproducible growth of high quality films. This fact is not surprising, since hydrogen plasmas produced by ECR sources have been shown to be effective gettering agents for surface contaminants such as O and C.⁽¹³⁾ Since we are only using a high vacuum system, such contaminants are likely to be present, and the in-situ hydrogen plasma etch effectively removes them from the surface, and from the reactor walls. In contrast to previous results⁽⁶⁾, our transmission electron microscope (TEM) images have shown that no surface roughening is present due to the plasma exposure. This may be a result of the higher growth pressure, and corresponding lower ion energy, used in this work.

The films reported in this work were all grown with a substrate temperature of 525 °C at a reactor pressure of 12 mT. The substrate was biased using a dc source, and this bias voltage

was systematically varied for different runs. The thicknesses of the films in this work were 1.5 - 2.0 μm . The crystallinity of the films was measured using both TEM measurements, and Raman spectroscopy. In Figure 2a, we show the typical Raman spectra of a Si (100) wafer, and in Figure 2b, the Raman signal for an ECR grown polycrystalline Si film is shown. Note that for poly Si films, there is a shift in the peak position, and there is a significant broadening of the peak, leading to an increase in full width at half maximum (FWHM). In Figure 3, we show the influence of varying substrate bias voltage on both FWHM and peak position of the Raman signal. It is apparent from this figure that increasing the magnitude of the negative bias voltage leads to an abrupt change in the crystallinity of the film at about -15V bias voltage, or about -25V total voltage difference between the plasma sheath and the substrate. For greater bombardment energies, the films are polycrystalline, as indicated by the increasing FWHM and the shift in the peak position of the Raman signal. This result is consistent with the earlier result reported by Nagai et al. ⁽⁵⁾

To confirm that indeed, the films were becoming polycrystalline, we measured Hall mobilities in the material. In Figure 4, we show the resistivity and electron mobilities as a function of substrate bias voltage. All of the undoped films were n-type. For substrate biases between 0 and -10V the resistivities shown in Figure 4a correspond to carrier concentrations of about $2 \times 10^{17} \text{ cm}^{-3}$. Once again, we find that at about -15 V substrate bias, there is an abrupt increase in resistivity of the film, and a corresponding reduction in Hall mobilities, confirming the interpretation of the Raman results. The Hall mobilities measured for our crystalline films correspond very well to the bulk mobility value of $600 \text{ cm}^2/\text{V}\cdot\text{s}$ reported in the literature ⁽¹⁴⁾ for n-type silicon with $N_D = 2 \times 10^{17} \text{ cm}^{-3}$. This is another indication of the good crystalline quality of our films.

We measured the carrier concentration using spreading resistance profile (SRP) measurements. In Figure 5, we show the carrier concentration of an epitaxial film using the SRP technique. The low doping concentration (few 10^{16} cm^{-3}), and the abrupt junction edge between the substrate and the epi layer are noteworthy features.

In summary, we report on the growth of high quality epitaxial Si films using ECR plasma deposition in a high vacuum reactor. By using plasma cleaning of the wafer before growth, we can remove the contaminants present in such reactors. We have systematically measured the effects of ion bombardment on the electronic and structural properties of the films, and find that ion bombardment voltages greater than about 25 V cause damage to the film, and result in polycrystalline films. The high vacuum ECR plasma deposition technique is shown to produce films with excellent electron mobilities and low donor densities, and also produces layers with abrupt interfaces. We can also achieve high growth rates of 3-5 Å/sec.

This work was supported in part by a fellowship from the Catron foundation for Scott DeBoer, and in part by a grant from NREL. We thank Ralph Knox, Mike Stoops and Mark Leonard for many interesting discussions and their help in constructing the ECR reactor. We also thank Professor Therese Cotton of Iowa State University for her help in the Raman work.

- (1) B. Meyerson, *Appl. Phys. Lett.* **48**, 797, (1986).
- (2) B. S. Meyerson, *IBM J. Res. Develop.* **34**, 806, (1990).
- (3) J. Comfort and R. Reif, *J. Electrochem. Soc.* **136**, 2386, (1989).
- (4) J. Comfort and R. Reif, *J. Electrochem. Soc.* **136**, 2398, (1989).
- (5) I. Nagai, T. Takahagi, A. Ishitani, H. Kutoda and M. Yoshikawa, *J. Appl. Phys.* **64**, 5183, (1988).
- (6) H. S. Tae, S. Hwang, S. Park, E. Yoon and K. Whang, *Appl. Phys. Lett.* **64**, 1021, (1994).
- (7) H. Yamada and Y. Torii, *J. Appl. Phys.* **64**, 702, (1988).
- (8) D. S. Mui, S. F. Fang and H. Morkoc, *Appl. Phys. Lett.* **59**, 1887, (1991).
- (9) S. J. DeBoer and V. L. Dalal, *First World Conference on Photovoltaic Energy Conversion*; (1994), To be published.
- (10) B. Meyerson, F. Himpsel and K. Uram, *Appl. Phys. Lett.* **57**, 1034, (1990).
- (11) H. Ugur, S. Varol, S. Ugur and I. Karabay, *J. Non-Cryst. Solids* **137 &138**, 761, (1991).
- (12) R. D. Knox, V. L. Dalal and O. A. Popov, *J. Vac. Sci. Technol. A* **9**, 474, (1991).
- (13) M. Ishii, K. Nakashima, I. Tajima and M. Yamamoto, *Appl. Phys. Lett.* **58**, 1378, (1991).
- (14) G. Baccarani and P. Ostoja, *Solid-State Electronics* **18**, 579, (1975).

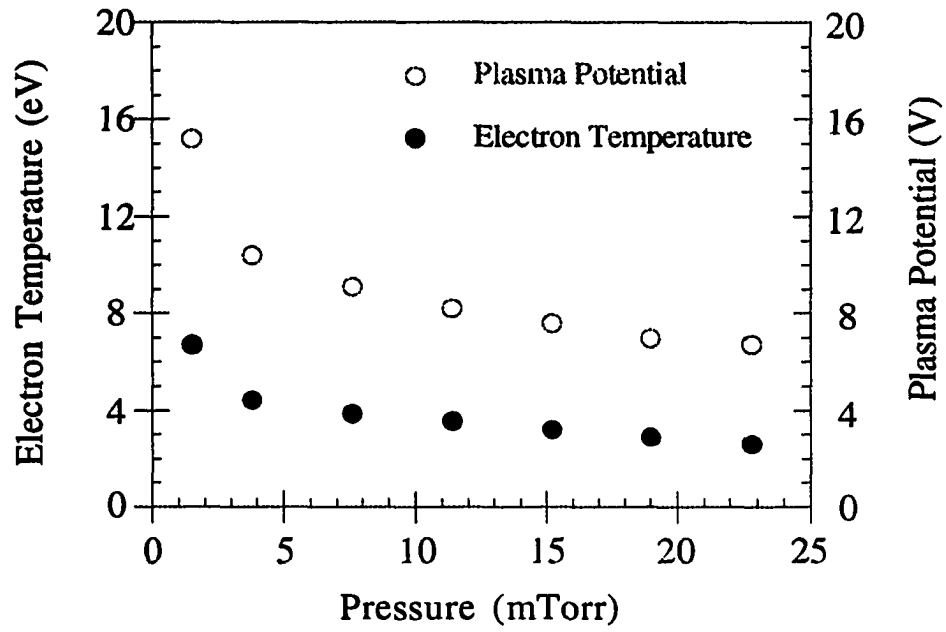
Figure 1: Langmuir probe measurements showing the variation of important plasma parameters with pressure: (a) plasma potential and electron temperature and (b) plasma density.

Figure 2: Typical Raman spectra of: (a) Si (100) wafer, (b) poly Si film. The intensity, peak position and FWHM are all indications of the film quality.

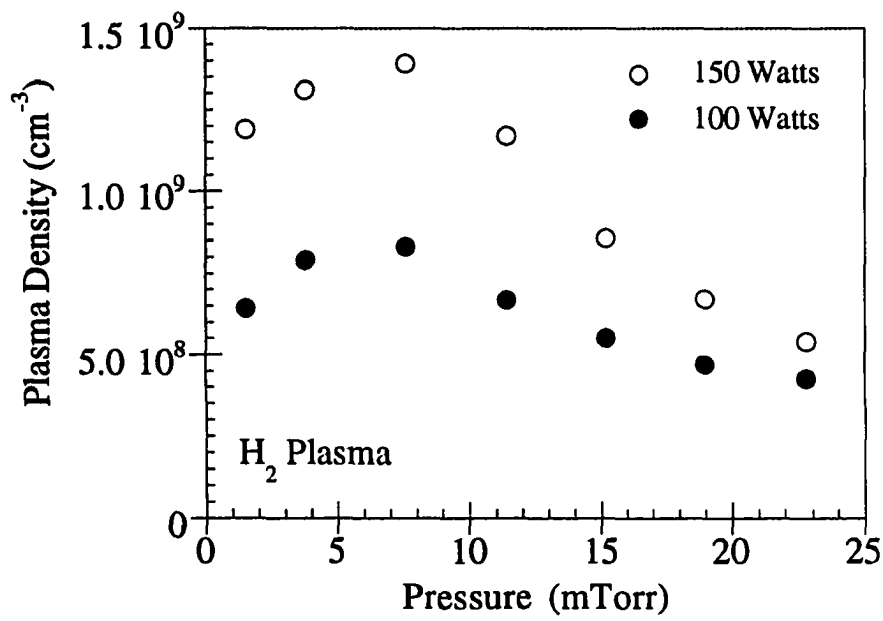
Figure 3: Raman results for a systematic study of substrate bias effects in ECR-CVD grown films. The sharp transitions in both (a) the FWHM and (b) the peak position indicate the conditions under which growth changes from crystalline to polycrystalline.

Figure 4: Variation of: (a) the resistivity and (b) Hall mobility of Si films as a function of substrate bias.

Figure 5: Typical spreading resistance profile for an undoped epitaxial silicon film grown using ECR-CVD at 525 °C.

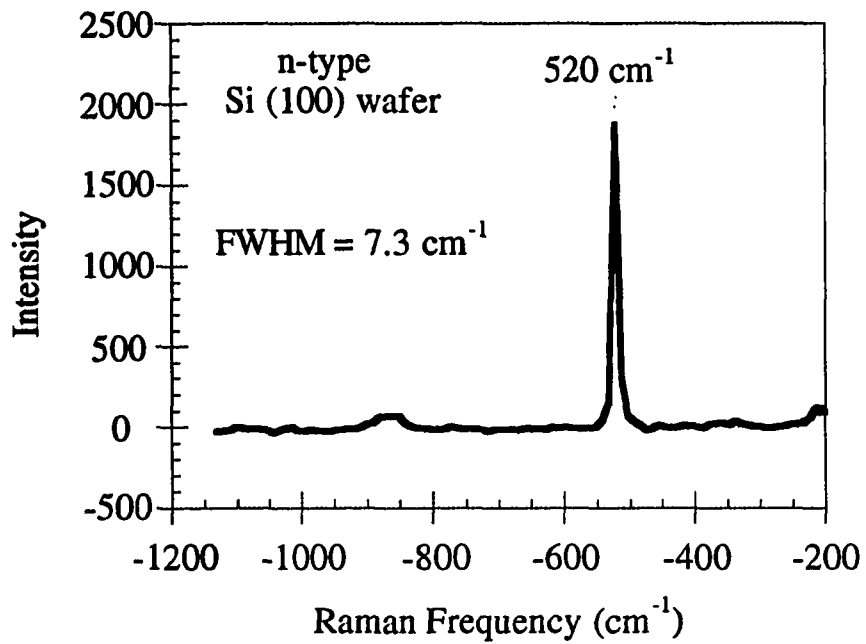


(a)

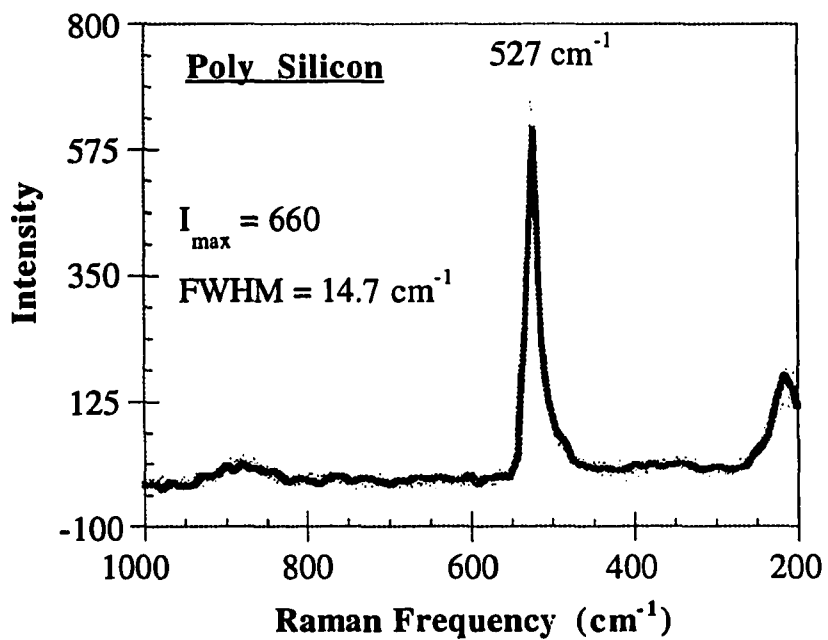


(b)

Fig. 1

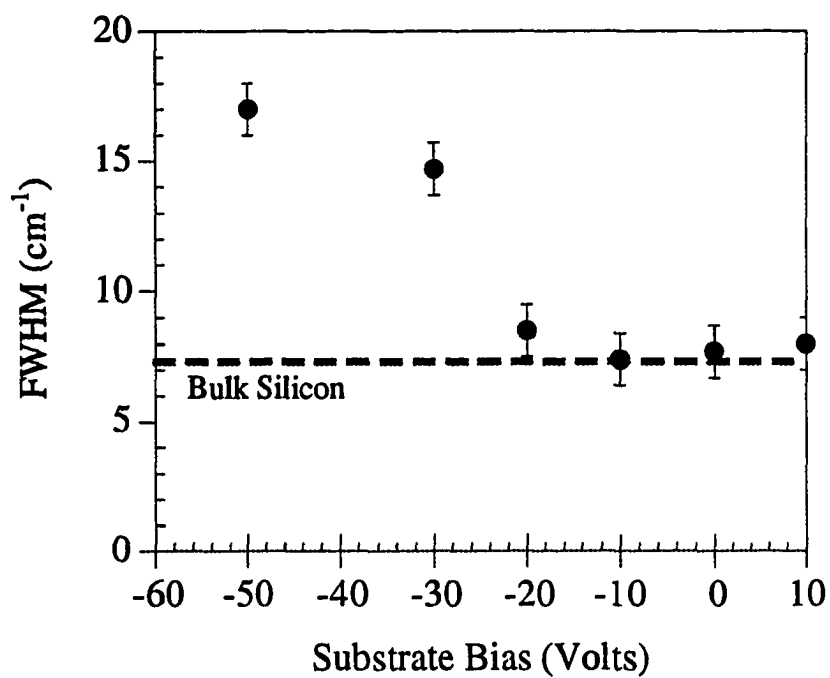


(a)

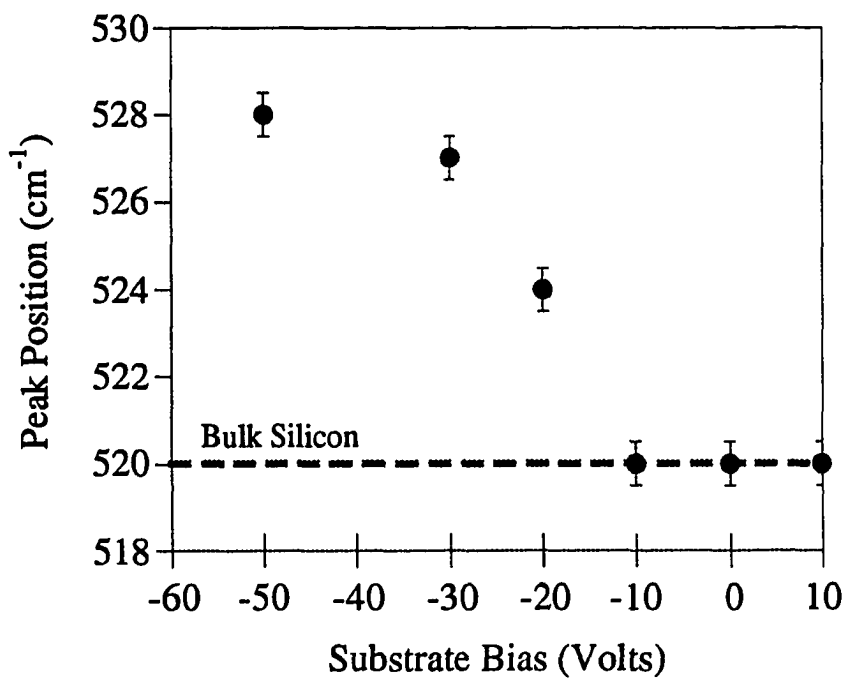


(b)

Fig. 2

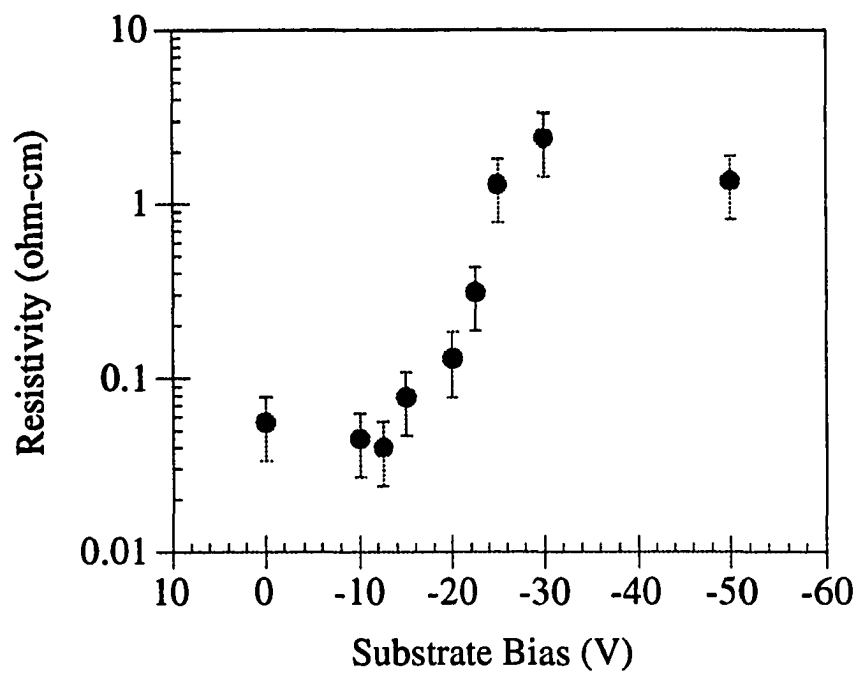


(a)

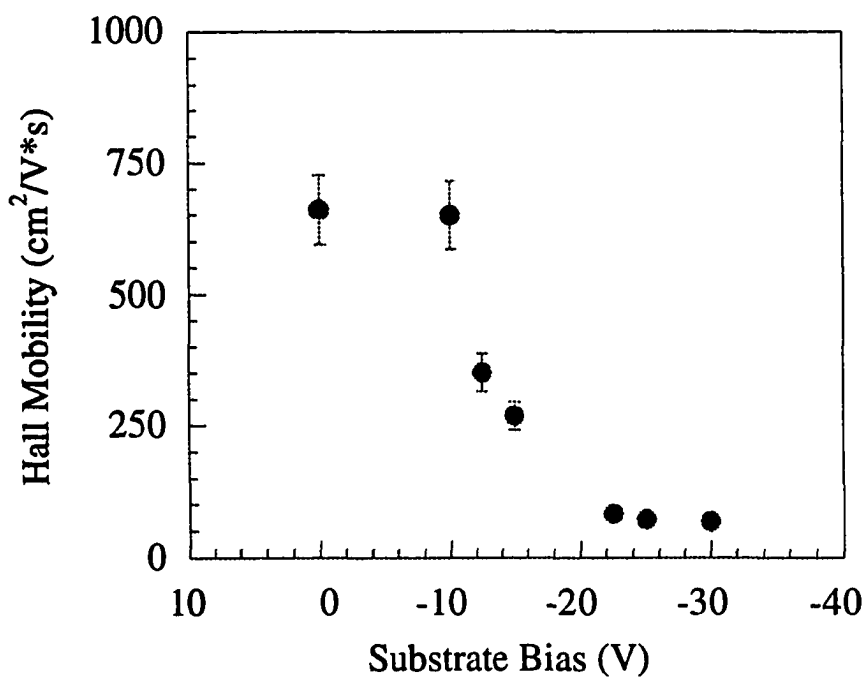


(b)

Fig. 3



(a)



(b)

Fig. 4

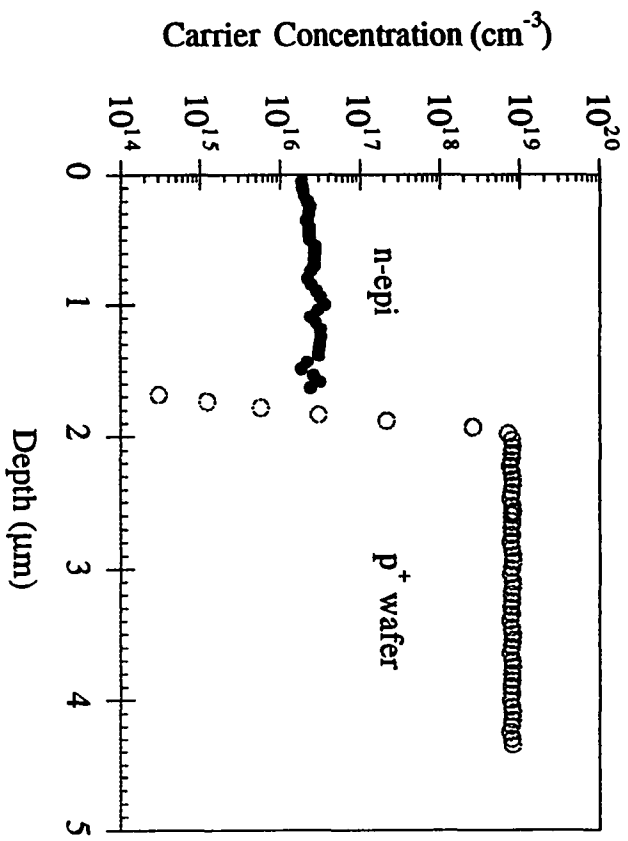


Fig. 5